NACA

RESEARCH MEMORANDUM

INVESTIGATION OF A THIN WING OF ASPECT RATIO 4 IN THE AMES 12-FOOT PRESSURE WIND TUNNEL. V - STATIC LONGITUDINAL STABILITY AND CONTROL THROUGHOUT THE SUBSONIC SPEED RANGE OF A SEMISPAN MODEL OF A SUPERSONIC AIRPLANE

By Ben H. Johnson, Jr., and Francis W. Rollins

Ames Aeronautical Laboratory
Moffett Field, Calif.

NATIONAL ADVISORY COMMITTEE FOR AERONAUTICS

WASHINGTON
December 8, 1949

NATIONAL ADVISORY COMMITTEE FOR AERONAUTICS

RESEARCH MEMORANDUM

INVESTIGATION OF A THIN WING OF ASPECT RATIO 4 IN THE AMES 12-FOOT PRESSURE WIND TUNNEL. V - STATIC LONGITUDINAL STABILITY AND CONTROL THROUGHOUT THE SUBSONIC SPEED RANGE OF A SEMISPAN MODEL OF A SUPERSONIC AIRPLANE

By Ben H. Johnson, Jr., and Francis W. Rollins

SUMMARY

Wind-tunnel tests have been made of a semispan model of a hypothetical supersonic airplane to determine the static longitudinal-stability and -control characteristics of the airplane throughout the range of subsonic Mach numbers up to 0.95. The semispan model had a long slender fuselage and a wing and horizontal tail of aspect ratio 4 and taper ratio 0.5. The midchord lines of the wing and of the horizontal tail were normal to the plane of symmetry. The profile of the wing and of the tail was a sharp-edged, faired, symmetrical double wedge with a thickness-chord ratio of 0.042. Tests were made with the horizontal tail mounted in the extended wing-chord plane and alternately 69.6 percent of the wing mean aerodynamic chord above the extended wing-chord plane. At a constant Reynolds number of 2,000,000 measurements were made with various stabilizer angles of the lift, drag, and pitching moment of the model at Mach numbers from 0.20 to 0.95. With the wing flaps deflected for maximum lift, similar measurements were made at a Mach number of 0.20 with Reynolds numbers up to 10,000,000. Measurements were made of the dynamic pressure at the two locations of the horizontal tail and of the character and location of the wing wake for the range of Mach numbers and Reynolds numbers noted above.

At zero lift, the Mach number for drag divergence, defined as the Mach number at which the slope of the drag coefficient with respect to Mach number equals 0.10, was about 0.92 for either location of the horizontal tail. The angle of attack for a constant lift coefficient decreased slightly with increasing Mach number but no marked or abrupt compressibility effects were evident at lift coefficients less than 0.6.

The contribution of the horizontal tail to the static longitudinal stability at low lift coefficients decreased with increasing Mach number,

primarily due to an increase with Mach number of the rate of change of effective downwash angle with angle of attack. For the model with the horizontal tail in the extended wing-chord plane, this decrease in the contribution of the horizontal tail to the static longitudinal stability was aggravated by the reduction with increasing Mach number in the dynamic-pressure ratio at the tail. With the horizontal tail mounted in the extended wing-chord plane, static longitudinal stability existed about the quarter point of the wing mean aerodynamic chord at all lift coefficients for Mach numbers less than 0.87. At Mach numbers between 0.87 and 0.95, the model was neutrally stable or unstable at lift coefficients less than 0.30. With the horizontal tail mounted above the extended wing-chord plane, the results indicated static longitudinal stability at all lift coefficients for all Mach numbers for which data were obtained. For both positions of the tail, either an all-movable stabilizer or a constant-chord elevator provided sufficient longitudinal control to balance the airplane at all test Mach numbers.

INTRODUCTION

As a part of a general program to determine the subsonic characteristics of wing plan forms suitable for flight at supersonic speeds, a series of tests of a thin sharp-edged wing having an aspect ratio of 4 and a taper ratio of 0.5 have been conducted. The midchord line of the wing was normal to the air stream. Results of these tests have been reported in references 1 through 4. Results of tests at transonic speeds of a wing of identical plan form and similar profile have been reported in reference 5.

The purpose of the present report is to summarize the wing data in terms of the static longitudinal-stability and -control characteristics throughout the subsonic speed range of a hypothetical airplane employing this wing. The airplane was represented by a semispan model comprising the wing, a slender pointed fuselage, and a horizontal tail geometrically similar to the wing. Force and moment characteristics of the wing, of the wing-fuselage combination, and of the complete model with two different tail heights are presented for Mach numbers up to 0.95 and a Reynolds number of 2,000,000. With the flaps on the wing deflected for maximum lift, similar data are presented for a Mach number of 0.20 and Reynolds numbers up to 10,000,000. The dynamic pressure at the horizontal tail and the location of the wing wake are presented for the wing-fuselage combination for the same ranges of Reynolds number and Mach number. The tests of the wing-tail-fuselage combinations were conducted with various horizontal-stabilizer settings to investigate the longitudinal control afforded by an all-movable horizontal tail. Data for an identical horizontal tail with a constant-chord elevator (reference 6) have been used with the wing-fuselage data to calculate the longitudinal-control characteristics of the model with a fixed stabilizer and an elevator.

The effective downwash angle at the tail, the Mach number at the tail, and the tail efficiency factor are presented herein.

COEFFICIENTS AND SYMBOLS

The following coefficients are used in this report:

C_L lift coefficient $\left(\frac{\text{lift}}{qS}\right)$

C_D drag coefficient $\left(\frac{\text{drag}}{qS}\right)$

C_m pitching-moment coefficient about an axis normal to the plane of symmetry passing through the quarter point of the wing mean aerodynamic chord $\left(\frac{\text{pitching moment}}{qSc'}\right)$

$\frac{\Delta H}{q}$ total-pressure-loss coefficient $\left(\frac{H_o-H}{q}\right)$

The following symbols are used in this report:

a speed of sound, feet per second

b twice the span of the semispan wing, feet

c local wing chord, feet

c' wing mean aerodynamic chord, chord through centroid of the wing semispan plan form $\left(\frac{\int_o^{b/2} c^2 dy}{\int_o^{b/2} c\, dy}\right)$

H local stagnation pressure in the region of the horizontal tail, pounds per square foot.

H_o free-stream stagnation pressure, pounds per square foot

i_t angle of the stabilizer setting with respect to the wing-chord plane, degrees

l_t tail length, distance from quarter point of the wing mean aerodynamic chord to the quarter point of the horizontal-tail mean aerodynamic chord, feet

M Mach number (V/a)

M_t Mach number at the position corresponding to the centroid of the semitail area

n normal-acceleration factor of the airplane

q free-stream dynamic pressure $(\frac{1}{2}\rho V^2)$, pounds per square foot

q_t dynamic pressure at the position corresponding to the centroid of the semitail area, pounds per square foot

R Reynolds number $\left(\frac{\rho V c'}{\mu}\right)$

S area of the semispan wing, square feet

S_t area of the horizontal semitail, square feet

u local airspeed in the tunnel-floor boundary layer, feet per second

V airspeed, feet per second

y distance from the plane of symmetry, feet

α_t effective angle of attack of the horizontal tail, degrees

α angle of attack of the wing-chord plane, degrees

δ tunnel-wall boundary-layer thickness, inches

δ^* displacement thickness of the boundary layer $\left[\int_1^{\delta} (1-u/V)dy\right]$, inches

δ_e elevator deflection, measured in a plane perpendicular to the elevator hinge axis, positive downward, degrees

δ_f trailing-edge flap deflection, measured in a plane perpendicular to the flap hinge axis, positive downward, degrees

δ_n leading-edge flap deflection, measured in a plane perpendicular to the flap hinge axis, positive downward, degrees

ϵ effective average angle of downwash, positive when the air is deflected downward, degrees

η efficiency of the horizontal tail

μ viscosity of air, slugs per foot-second

ρ mass density of air, slugs per cubic foot

MODEL AND APPARATUS

The tests were conducted in the Ames 12-foot pressure wind tunnel, which is a closed-throat variable-density wind tunnel with a low-turbulence level closely approximating that of free air.

The steel semispan model wing used for this investigation was the one used in the tests reported in reference 1 and represented a wing of aspect ratio 4 and taper ratio 0.50. The midchord line of the wing was perpendicular to the plane of symmetry. The wing profile was a faired double wedge having a thickness-chord ratio of 0.042. The horizontal tail was identical in plan form and profile to the wing and had an area equal to one quarter of the wing area. Dimensions of the semifuselage and its location with respect to the wing are given in figure 1. The semifuselage was fitted tightly to the wing and tail without fillets at the intersections. For a portion of the tests, the rear part of the fuselage was modified as shown in figures 1(b) and 2(c) to study the effects of such a modification on the pitching-moment characteristics of the model.

The wing was equipped with a full-span, constant-chord, leading-edge plain flap and a 60.9-percent-span, constant-chord, trailing-edge plain flap. The area of the leading-edge flap was 15 percent of the total area of the semispan wing and that of the trailing-edge flap was 12 percent of the total area of the semispan wing. The unsealed gaps between the flaps and the wing were 0.015 inch with the flaps undeflected.

The horizontal tail was mounted in the extended wing-chord plane (figs. 1(a) and 2(a)) and alternately 13 inches (0.696c') above the extended wing-chord plane (figs. 1(b) and 2(b)). To mount the tail above the fuselage, a bracket with a fairing body to enclose the fittings at the point of attachment of the tail surface was added to the fuselage. With the tail mounted in either position, provision was made to vary the angle of the stabilizer by pivoting it about its 50-percent-chord line.

As shown in figure 2, the semispan model was mounted with the wing perpendicular to the floor which served as a reflection plane. The gap between the model and the tunnel floor was maintained between 0.010 inch and 0.150 inch. No attempt was made to remove the tunnel-floor boundary layer which, at the location of the model, had a displacement thickness δ^* of 0.5 inch. The velocity characteristics of the wing-fuselage wake at the longitudinal location of the horizontal tail were measured with a rake consisting of 61 total-pressure tubes and 3 static-pressure tubes. The rake was mounted from the tunnel floor with the total-pressure tubes at a position corresponding to the centroid of the semitail area.

CORRECTIONS TO DATA

The data have been corrected for the effects of tunnel-wall interference, of constriction due to the tunnel walls, and of model-support tare forces. The method of reference 7 was used in computing the corrections to the data for tunnel-wall interference. The following corrections were added:

$$\Delta\alpha = 0.363\ C_L$$

$$\Delta C_D = 0.0056\ C_L^2$$

$$\Delta C_m = 0$$

Corrections to the data for the constriction effects of the tunnel walls have been evaluated by the method of reference 8. The magnitudes of these corrections as applied to Mach number and to dynamic pressure (measured with the tunnel empty) are illustrated by the following table:

Corrected Mach number	Uncorrected Mach number		$\frac{q_{corrected}}{q_{uncorrected}}$	
	Wing alone	Wing and fuselage	Wing alone	Wing and fuselage
0.95	0.937	0.917	1.005	1.036
.92	.915	.896	1.003	1.027
.90	.897	.881	1.002	1.023
.85	.848	.838	1.002	1.016
.80	.799	.792	1.001	1.012
.70	.700	.696	1.001	1.008
.50	.500	.499	1.001	1.005
.20	.200	.200	1.001	1.005

The theoretical choking Mach number for the wing-fuselage combination was 0.96.

Tare corrections due to the air forces exerted on the turntable were obtained from force measurements made with the model removed from the tunnel. Possible interference effects between the model and the turntable were not evaluated. The magnitude of the measured tare-drag coefficient, based on the wing area, was independent of Mach number and varied with Reynolds number as follows:

Reynolds number	$C_{D_{tare}}$
2,000,000	0.0063
6,000,000	.0057
10,000,000	.0056

The rake of total-pressure tubes and static-pressure tubes used to measure the dynamic pressure at the horizontal tail was calibrated throughout the complete range of Mach numbers, of Reynolds numbers, and of angles of attack of the rake.

TESTS

Lift, drag, and pitching-moment data have been obtained for the model and its components in the following combinations: (1) the wing alone; (2) the wing and the fuselage; (3) the wing, the fuselage, and the tail mounted in the extended wing-chord plane; (4) the wing, the fuselage, and the supporting bracket for mounting the tail above the fuselage; and (5) the wing, the fuselage, and the tail mounted above the fuselage.

At a Reynolds number of 2,000,000 the model was tested at Mach numbers from 0.20 to 0.95. The range of angles of attack for these tests was from -6° to beyond the stall, except at the higher Mach numbers where the range was reduced by the limitations of wind-tunnel power and of model strength. At a Mach number of 0.20 the effect of leading-edge and trailing-edge flap deflection ($\delta_n = 30^\circ$ and $\delta_f = 50^\circ$) was investigated at Reynolds numbers of 2,000,000, 6,000,000, and 10,000,000. This combination of flap deflections was selected upon the basis of reference 2 wherein it was shown to be the optimum for maximum lift of the wing alone.

To determine the longitudinal control which would be provided by an all-movable stabilizer, the model was tested with the angle of the stabilizer varied in 2° increments from -10° to 4° for the model with the tail mounted in the extended wing-chord plane and from -6° to 4° for the model with the tail mounted above the fuselage.

The velocity distribution in the wing-fuselage wake was investigated at a position corresponding longitudinally to the midchord of the horizontal tail (3.508 wing mean aerodynamic chord behind the quarter point of the wing mean aerodynamic chord) and corresponding laterally to the location of the mean aerodynamic chord of the tail (0.428 wing mean aerodynamic chord from the plane of symmetry). The extent of the survey was sufficient to permit the determination of the dynamic pressure at either position of the horizontal tail for a range of angle of attack, of Mach number, and of Reynolds number.

An index of the figures presenting the results of this investigation is given in the appendix.

RESULTS AND DISCUSSION

Force and Moment Characteristics

The lift, drag, and pitching-moment characteristics of the model and its components are presented in figures 3 through 26.

Wing alone.- The effects of Reynolds number and of Mach number on the lift, drag, and pitching-moment characteristics of the wing have been reported in reference 1. Data from that reference for a Reynolds number of 2,000,000 at Mach numbers from 0.20 to 0.94 are reproduced herein in figure 3. The data of this figure indicate no large or erratic effects of compressibility up to a Mach number of 0.94. The wing lift-curve slope was 0.062 at a Mach number of 0.20 and increased to 0.095 at a Mach number of 0.94. The total movement of the aerodynamic center at zero lift was only about 7 percent of the wing mean aerodynamic chord over the test Mach number range.

The force and moment characteristics of the wing with various combinations of leading-edge and trailing-edge flap deflections have been reported in reference 2. The data of this reference indicate that a leading-edge flap deflection of 30° and a trailing-edge flap deflection of 50° were optimum for maximum lift. Data obtained with this combination of flap deflections are presented herein in figure 4 for a Mach number of 0.20 and Reynolds numbers from 3,000,000 to 10,000,000. These data show that deflection of the flaps increased the maximum lift of the wing from 0.76 to 1.40 and that the aerodynamic characteristics of the wing with the flaps deflected were little affected by increase of Reynolds number to 10,000,000.

The variation with angle of attack of the lift coefficient of the wing with the gaps sealed and faired is presented in figure 5 for a Reynolds number of 1,000,000 for Mach numbers up to 0.94. Since the wing and tail were geometrically similar and the mean aerodynamic chord of the tail was one-half that of the wing, these data may be considered to represent the lift characteristics of the isolated tail and may be applied as the characteristics of the tail on the model at a Reynolds number of 2,000,000, based on the wing mean aerodynamic chord, if corrections are made for the downwash and reduction in the dynamic pressure at the tail.

Wing-fuselage combination.- The force and moment characteristics of the wing-fuselage combination with the flaps neutral are shown in figures 6, 7, and 8. Comparison of these data with those of figure 3 reveals that addition of the fuselage caused an increase in the drag, a reduction in

the maximum lift at Mach numbers less than 0.80, and a forward movement of the aerodynamic center at low lift coefficients. The lift, drag, and pitching-moment characteristics of the wing-fuselage combination with the wing flaps deflected are presented in figure 9. Comparison of these data with those of figure 4 indicates that the addition of the fuselage caused a decrease in the maximum lift coefficient from 1.40 to 1.34 and an increase of 1° in the angle of attack for zero lift. The characteristics of the wing-fuselage combination were little affected by a change in Reynolds number from 6,000,000 to 10,000,000, but an increase from 2,000,000 to 6,000,000 resulted in a sizable decrease in the drag.

Wing, fuselage, and horizontal tail in the extended wing-chord plane.- Lift, drag, and pitching-moment characteristics of the complete semispan model with the horizontal tail mounted in the extended wing-chord plane are presented in figures 10, 11, and 12 for Mach numbers up to 0.95 and stabilizer angle settings from 4° to -10°. At a Mach number of 0.20, the aerodynamic center was shifted from 14 percent to 41 percent of the wing mean aerodynamic chord due to the addition of the tail. (See fig. 12(a).) As the Mach number was increased, the stabilizing effect of the horizontal tail was diminished to the extent that at a Mach number of 0.95 the horizontal tail made little or no contribution to the stability of the model at lift coefficients between ±0.3. As will be discussed later, this decrease in the contribution of the tail to the stability was due to an increase in $\partial\epsilon/\partial\alpha$ and to a decrease in the dynamic-pressure ratio at the tail as the Mach number was increased. With a stabilizer angle setting of 0° and in a range of lift coefficients of about ±0.30, the complete model was neutrally stable about the quarter point of the wing mean aerodynamic chord at a Mach number of about 0.87 and longitudinally unstable at higher Mach numbers. At lift coefficients greater than 0.30 stability existed at all test Mach numbers. The all-movable stabilizer provided sufficient longitudinal control to balance the airplane model at all Mach numbers up to 0.95 and at all angles of attack up to the stall. The value of $(\partial C_m/\partial i_t)_{C_L=0}$ was approximately -0.036 at a Mach number of 0.20 and increased slightly with increasing Mach number. (See fig. 12.)

The lift, drag, and pitching-moment characteristics of the complete semispan model with the wing flaps deflected are presented in figures 13, 14, and 15 for a Mach number of 0.20 and Reynolds numbers of 2,000,000, 3,000,000, and 10,000,000. At lift coefficients from zero to the maximum the complete model was longitudinally stable about the quarter point of the mean aerodynamic chord.

Wing, fuselage, and horizontal tail above the extended wing-chord plane.- To investigate the improvement in longitudinal stability and control afforded by raising the horizontal tail above the wing wake, tests were conducted with the model tail mounted 13 inches (0.696 wing mean aerodynamic chord) above the extended wing-chord plane.

Mounting the tail above the fuselage necessitated a supporting bracket with a streamlined body to serve as a fairing for the fittings by which the stabilizer was attached. The force and moment characteristics of the wing and fuselage with the bracket and the fairing body are presented in figures 16, 17, 18, and 19. These data indicate no noticeable effects of the bracket on the characteristics of the wing–fuselage combination except a slight increase in the minimum drag. (See fig. 17.)

Lift, drag, and pitching-moment characteristics of the complete semispan model with the horizontal tail mounted above the extended wing-chord plane are presented in figures 20, 21, and 22 for Mach numbers up to 0.95 and for stabilizer settings from 4° to −6°. Comparison of the drag data of figure 21 with those of figure 11 indicates a slight increase in the minimum drag which may be attributed to the addition of the tail bracket and the fairing body and not to the raising of the horizontal tail. The model with the high tail was longitudinally stable at all lift coefficients below the stall and at all Mach numbers, as can be seen from figure 22. At a Mach number of 0.20, addition of the horizontal tail shifted the aerodynamic center from 14 percent to 53 percent of the wing mean aerodynamic chord. The contribution of the horizontal tail to the longitudinal stability decreased with increasing Mach number. As will be discussed later, this reduction in the contribution of the tail to the stability was due primarily to an increase in $\partial\epsilon/\partial\alpha$ with increasing Mach number. The all-movable stabilizer retained effectiveness in longitudinal control at all Mach numbers and all lift coefficients.

There was a marked change in the pitching-moment coefficient at zero lift as a result of raising the tail above the fuselage. Whereas with the tail in the extended wing-chord plane, zero pitching moment occurred at zero lift with a stabilizer angle of 0°, with the tail raised above the extended wing-chord plane a stabilizer setting of approximately 2° was required to produce zero pitching moment at zero lift. To investigate the cause of this shift in the zero-lift pitching-moment coefficient the Reynolds number was increased from 2,000,000 to 12,000,000 while the Mach number remained 0.20. This increase had no effect on the pitching-moment coefficient at zero lift. Visual observation, by means of tufts, of the flow at the afterend of the fuselage and on the tail-supporting bracket revealed a sizable stream angle in the region of the tail due to the rapid convergence of the rear end of the fuselage. This convergence was reduced by modifying the afterpart of the fuselage as shown in figure 1(b). The results of tests with the modified fuselage are shown in figure 23. These data show that, for the model with the tail mounted above the extended wing-chord plane, modification of the fuselage caused a decrease in the zero-lift pitching-moment coefficient greater than the increase accompanying the raising of the tail on the original fuselage.

The lift, drag, and pitching-moment characteristics of the complete semispan model with the high tail and the original fuselage and with the wing flaps deflected are presented in figures 24, 25, and 26. Raising

the tail above the fuselage had little effect on the lift and drag of the model with the flaps deflected. However, the model with the high tail had more nearly linear pitching-moment characteristics than the model with the tail in the extended wing-chord plane.

Wing Wake and Effective Downwash at the Horizontal Tail

The dynamic pressure at the horizontal tail, the velocity distribution in the wake of the wing-fuselage combination, the effective angles of downwash at the horizontal tail, and the tail efficiency factors are presented in figures 27 through 36.

Location of the wing wake.- The location of the point of maximum total-pressure loss and the wake boundaries have been determined from measurements of the stagnation pressure behind the wing-fuselage combination at a position corresponding longitudinally to the midchord of the horizontal tail (3.508 wing mean aerodynamic chords behind the quarter point of the wing mean aerodynamic chord) and laterally to the mean aerodynamic chord of the horizontal tail semispan (0.428 wing mean aerodynamic chord from the plane of symmetry). The results of these measurements are presented in figures 27 and 28 where the location of the wake is presented as a function of angle of attack for various Mach numbers and Reynolds numbers. The location of the wake is given with respect to the wing-chord plane at 0° angle of attack. The two alternate positions of the horizontal tail are also identified in these figures so that the location of the tail with respect to the wing-fuselage wake can be readily determined.

The tail mounted in the extended wing-chord plane was in the wake of the wing at all test angles of attack and at all test Mach numbers. The high tail did not enter the wake until the angle of attack exceeded about 7° at Mach numbers below 0.70. As the Mach number was increased above 0.70, the high tail entered the wake at progressively lower angles of attack. With the wing flaps deflected the high tail was above the wake at all angles of attack. (See fig. 28.)

At moderate to large angles of attack and at Mach numbers above 0.85, the wing-fuselage wake was characterized by two distinct regions of large total-pressure loss. These are shown in figure 29 which presents the variation of total-pressure loss across the wake at an angle of attack of 6° and a Mach number of 0.85. The secondary peak of total-pressure loss is believed to be associated with separation at the wing leading edge and usually occurred near the angle of attack at which the aerodynamic center of the wing moved forward. Figure 29 also indicates that the presence of the fuselage influenced the magnitude and the location of the total-pressure losses and the location of the wake boundaries.

Dynamic-pressure ratio and Mach number at the tail.- To determine the ratio of the dynamic pressure at the tail to the free-stream dynamic pressure, measurements were made of the stagnation and static pressures in the region of the horizontal tail. The results of these measurements are presented in figure 30 for various free-stream Mach numbers as a function of angle of attack. The dynamic-pressure ratio at the centroid position of the horizontal tail in the extended wing-chord plane for 0° angle of attack varied from 0.945 at a free-stream Mach number of 0.20 to 0.865 at a free-stream Mach number of 0.95. Due to the symmetry of the model about the wing-chord plane, the dynamic-pressure ratio at the tail mounted in the extended wing-chord plane increased with increasing or decreasing angle of attack, attaining a value of approximately 0.98 at all Mach numbers at angles of attack of ±6°.

At a Mach number of 0.95, the dynamic-pressure ratio at the centroid position of the high horizontal tail was unity at angles of attack less than 2.5° and less than unity at larger angles of attack. (See fig. 30(b).) As free-stream Mach number decreased, the minimum angle of attack for which the dynamic pressure remained at the free-stream value increased to 7° for Mach numbers less than 0.70.

With the wing flaps deflected, the dynamic-pressure ratio at the high tail position was unity, and at the position of the tail in the extended wing-chord plane it varied from approximately 0.99 at 0° angle of attack to approximately 0.84 at 10° angle of attack. The effect of increasing the Reynolds number from 2,000,000 to 10,000,000 was to increase the dynamic-pressure ratio approximately 5.5 percent at an angle of attack of 10° with less effect as the angle of attack was reduced.

The Mach numbers at the tail have been computed from the wake-survey data and are presented as functions of angle of attack for various free-stream Mach numbers in figure 32.

Effective angles of downwash at the tail.- The effective angles of downwash at the horizontal tail have been computed from the moment data and are presented as average values over the stabilizer angle range in figures 33 and 34. The expression used for calculation of the effective angle of downwash is as follows:

$$\epsilon = \alpha + i_t - \frac{(\Delta C_{m_t})_\alpha}{(\partial C_m/\partial i_t)_\alpha}$$

where $(\Delta C_{m_t})_\alpha$ is the increment in pitching-moment coefficient due to the addition of the tail for a constant angle of attack and $(\partial C_m/\partial i_t)_\alpha$ is the stabilizer effectiveness at a constant angle of attack. This expression does not permit the downwash due to the wing to be separated from the downwash due to other components of the model, and thus the stream angle at the horizontal tail due to convergence of the rear end

of the fuselage is included in the value of the downwash computed from the data.

Efficiency of the horizontal tail.- The tail efficiency factor $\eta(q_t/q)$ computed from the force and moment data is presented in figures 35 and 36. The tail efficiency factor, defined as the ratio of the lift produced by the tail in the presence of the fuselage to the lift produced by the isolated tail operating at the same Mach number, was computed by means of the following expression:

$$\eta \frac{q_t}{q} = \left(\frac{\partial C_m}{\partial i_t}\right)_\alpha \frac{1}{(dC_L/d\alpha)_t \left(S_t l_t / S c'\right)}$$

where $(dC_L/d\alpha)_t$ is the lift-curve slope of the isolated horizontal tail operating at the free-stream Mach number of the horizontal tail (figs. 5 and 32). No attempt was made to separate the effects of dynamic-pressure ratio at the tail from the tail efficiency due to the possible large variation of q_t/q along the tail span. The tail efficiency factor is presented as a function of Mach number in figure 35. For either position of the tail with the flaps neutral, the tail efficiency factor was less than 80 percent and varied approximately 10 percent over the test range of Mach numbers and angles of attack.

The Effects of Compressibility

The effects of compressibility on the lift, drag, pitching moment, and downwash of the complete model are summarized in figures 37 through 46.

Lift and drag.- The variation with Mach number of the angle of attack for a constant lift coefficient was small (fig. 37), increasing Mach number usually being accompanied by a decrease in the angle of attack for a given lift coefficient.

The variation with Mach number of the drag coefficient for several constant lift coefficients is shown in figure 38. At a lift coefficient of zero, the drag coefficient of the model with the tail in the extended wing-chord plane started to increase at a Mach number of about 0.80. For the model with the high tail, the drag increase started at a Mach number of about 0.75. The Mach number for drag divergence, defined as the Mach number at which $(\partial C_D/\partial M)_{C_L=0} = 0.10$, was approximately 0.92 for the model with either tail position.

Static longitudinal stability and control.- The variation with Mach number of the pitching-moment coefficient for several constant lift coefficients is shown in figure 39. In general, the pitching-moment coefficient increased with increasing Mach number. The static longitudinal

instability at Mach numbers above about 0.85 of the model with the tail in the extended wing-chord plane, as mentioned previously, is evident from the data of figure 39(a).

The variation with Mach number of the effective angle of downwash at several constant values of the lift coefficient is shown in figure 40, and the variation of $\partial\epsilon/\partial\alpha$ with Mach number is shown in figure 41. For either location of the horizontal tail, $\partial\epsilon/\partial\alpha$ increased with increasing Mach number but the value of $\partial\epsilon/\partial\alpha$ and the rate of increase with Mach number was much larger for the model with the tail in the extended wing-chord plane. The static longitudinal instability at high subsonic Mach numbers with the tail in the extended wing-chord plane was principally a result of this large value of $\partial\epsilon/\partial\alpha$.

The variation with Mach number of the lift coefficient for balance about the quarter point of the wing mean aerodynamic chord is presented in figure 42 for various angles of stabilizer setting. The model with the tail in the extended wing-chord plane was neutrally stable at a Mach number of 0.86 and unstable at higher Mach numbers when the stabilizer setting was 0°. With a stabilizer setting of -1° or -2° the model was longitudinally stable, but the lift coefficient for balance varied erratically with Mach number at Mach numbers above about 0.70.

With the tail mounted above the extended wing-chord plane, the model possessed static longitudinal stability at all stabilizer settings and all Mach numbers. For positive values of lift coefficient, the balanced lift coefficient for a given stabilizer angle increased as the Mach number was increased to about 0.90 and decreased with further increase in the Mach number.

For the model with either position of the horizontal tail, the all-movable stabilizer required only 4° to 6° of deflection to balance the model at the stall with the flaps up.

The experimental results of this investigation have been used to predict the static longitudinal-stability and-control characteristics of a hypothetical airplane with a wing loading of 100 pounds per square foot in flight at an altitude of 10,000 feet. The airplane center of gravity has been assumed to be on an axis perpendicular to the plane of symmetry passing through the quarter point of the wing mean aerodynamic chord. The variation of airplane lift coefficient with Mach number for several values of normal-acceleration factor is presented in figure 43. The calculated effects of flight-path curvature on the flow at the tail were negligible for the assumed flight condition.

The variation with Mach number of the stabilizer angle required to balance the airplane is shown in figure 44 for several values of normal-acceleration factor. With the horizontal tail in the extended wing-chord plane, the airplane would be longitudinally unstable with a normal-

acceleration factor of unity at Mach numbers above about 0.87. Below this Mach number, the variation of stabilizer angle with speed was stable and a total change of stabilizer angle of 1.7° would be necessary to balance the airplane in level flight between Mach numbers of 0.50 and 0.87.

With the tail mounted above the extended wing-chord plane, the airplane would possess static longitudinal stability at all Mach numbers but the variation of stabilizer angle with velocity would be unstable at Mach numbers above about 0.90. A change of 2.4° in the stabilizer angle would be required to balance the airplane in level flight between Mach numbers of 0.50 and 0.95.

To compare the longitudinal control afforded by the all-movable stabilizer with that which could be accomplished with a fixed stabilizer and an elevator, elevator-effectiveness data from reference 6 were applied to the hypothetical airplane. The tail model of reference 6 was equipped with a 20-percent area, constant-chord elevator and the plan form and profile were identical with those of the horizontal tail investigated herein. The elevator-effectiveness data of reference 6 are reproduced herein in figure 45 and in application of the data it was assumed that there was no effect of scale between Reynolds numbers of 2,000,000 and 1,000,000 and that the elevator efficiency factor was 100 percent.

The variation with Mach number of the elevator deflection required to balance the airplane at the previously assumed flight conditions is presented in figure 46.

The calculated static longitudinal stability and control of the airplane with a fixed stabilizer and an elevator are similar to those previously discussed for the airplane with the all-movable stabilizer. About 50-percent greater deflection would be required of the elevator to produce the same balance lift coefficient as the all-movable stabilizer.

Longitudinal Characteristics with the Flaps Deflected

The variation with lift coefficient of the stabilizer angle required to balance the model with the flaps deflected is presented in figure 47 for the model with the horizontal tail in the extended wing-chord plane. The corresponding drag coefficient is shown in the same figure and the lift-drag ratio as a function of lift coefficient for balance is shown in figure 48.

These experimental results have been used to predict the power-off gliding speed and sinking speed at sea level of a hypothetical airplane with a wing loading of 100 pounds per square foot. The effects of the proximity of the ground and the increased drag due to landing gear have

been neglected. The results of these calculations are presented in figure 49. The minimum power-off sinking speed was 46 feet per second and occurred at a forward speed of 175 miles per hour.

SUMMARY OF RESULTS

The results of wind-tunnel tests at Mach numbers up to 0.95 of a semispan model of a hypothetical supersonic airplane with the horizontal tail mounted alternately in the extended wing-chord plane and 0.696 of the wing mean aerodynamic chord above the extended wing-chord plane have been presented. A summary of these results follows:

1. At a lift coefficient of zero, the Mach number for drag divergence was about 0.92. There was a smooth increase of lift-curve slope with increasing Mach number up to a Mach number of 0.95.

2. The contribution of the horizontal tail to the static longitudinal stability decreased with increasing Mach number. This decrease was due primarily to the increase with increasing Mach number in the rate of change with angle of attack of the effective angle of downwash at the tail. With the horizontal tail in the extended wing-chord plane, a further destabilizing effect was the decrease in dynamic-pressure ratio at the tail with increasing Mach number.

3. With the horizontal tail in the extended wing-chord plane, the model was longitudinally unstable at Mach numbers above 0.87 at lift coefficients less than 0.3. With the horizontal tail 0.696 of the wing mean aerodynamic chord above the extended wing-chord plane, the model was longitudinally stable at all lift coefficients for all Mach numbers for which data were obtained.

4. Either an all-movable stabilizer or a fixed stabilizer with a constant-chord elevator provided sufficient longitudinal control to balance the model throughout the test range of Mach numbers.

Ames Aeronautical Laboratory,
National Advisory Committee for Aeronautics,
Moffett Field, Calif.

APPENDIX

The following tables have been included to provide a convenient index to the figures presenting the results of this investigation:

FORCE AND MOMENT CHARACTERISTICS

Wing Alone

Results presented	Flap deflection	Mach number	Reynolds number	Figure number
α, C_D, & C_m vs C_L	0°	0.20 to 0.94	2×10^6	3
α, C_D, & C_m vs C_L	$\delta_n=30^\circ,\delta_f=50^\circ$	0.20	3×10^6 to 10×10^6	4

Wing Alone With All Gaps Sealed

Results presented	Flap deflection	Mach number	Reynolds number	Figure number
C_L vs α	- - -	0.20 to 0.94	1×10^6	5

Wing-Fuselage Combination

Results presented	Flap deflection	Mach number	Reynolds number	Figure number
C_L vs α	0°	0.20 to 0.95	2×10^6	6
C_L vs C_D	↓	↓	↓	7
C_L vs C_m	↓	↓	↓	8
α, C_D & C_m vs C_L	$\delta_n=30^\circ,\delta_f=50^\circ$	0.20	2×10^6 to 10×10^6	9

Wing, Fuselage, and Horizontal Tail in Extended Wing-Chord Plane

Results presented	Flap deflection	Stabilizer angle	Mach number	Reynolds number	Figure number
C_L vs α	0°	4° to -10°	0.20 to 0.95	2×10^6	10(a) to 10(h)
C_L vs C_D	↓	↓	↓	↓	11(a) to 11(h)
C_L vs C_m	↓	↓	↓	↓	12(a) to 12(h)
C_L vs α	$\delta_n=30^\circ,\delta_f=50^\circ$	4° to -10°	0.20	2×10^6 to 10×10^6	13(a) to 13(c)
C_L vs C_D	↓	↓	↓	↓	14(a) to 14(c)
C_L vs C_m	↓	↓	↓	↓	15(a) to 15(c)

Wing–Fuselage Combination with Bracket for Mounting Tail Above Fuselage

Results presented	Flap deflection	Mach number	Reynolds number	Figure number
C_L vs α	0°	0.20 to 0.95	2×10^6	16
C_L vs C_D	↓	↓	↓	17
C_L vs C_m	↓	↓	↓	18
α, C_D & C_m vs C_L	$\delta_n=30^\circ,\delta_f=50^\circ$	0.20	2×10^6 to 10×10^6	19

Wing, Fuselage, and Horizontal Tail Above Extended Wing–Chord Plane

Results presented	Flap deflection	Stabilizer angle	Mach number	Reynolds number	Figure number
C_L vs α	0°	4° to -6°	0.20 to 0.95	2×10^6	20(a) to 20(h)
C_L vs C_D	↓	↓	↓	↓	21(a) to 21(h)
C_L vs C_m	↓	↓	↓	↓	22(a) to 22(h)
[1]C_L vs C_m	↓	0°	0.20, 0.90 0.92, 0.93	2×10^6	23
C_L vs α	$\delta_n=30^\circ,\delta_f=50^\circ$	$4^\circ,0^\circ$, & -8°	0.20	2×10^6 to 10×10^6	24
C_L vs C_D	↓	↓	↓	↓	25
C_L vs C_m	↓	↓	↓	↓	26

[1]Shows the effect of modifying the rear of the fuselage.

FLOW CONDITIONS IN THE REGION OF THE HORIZONTAL TAIL

Characteristics of Wing–Fuselage Wake

Results presented	Flap deflection	Mach number	Reynolds number	Figure number
Location of wake vs α	0°	0.20 to 0.95	2×10^6	27(a) to 27(g)
↓	$\delta_n=30^\circ,\delta_f=60^\circ$	0.20	2×10^6 to 10×10^6	28
Pressure loss in wake vs distance from wing–chord plane	0°	0.85	2×10^6	29

Dynamic Pressure Ratio, Mach Number, and Effective Angle of Downwash at the Tail

Results presented	Flap deflection	Mach number	Reynolds number	Figure number
q_t/q vs α	0°	0.20 to 0.95	2×10^6	30(a) & 30(b)
↓	$\delta_n=30^\circ,\delta_f=60^\circ$	0.20	2×10^6 to 10×10^6	31
M_t vs α	0°	0.20 to 0.95	2×10^6	32(a) & 32(b)
ϵ vs α	0°	0.20 to 0.95	2×10^6	33(a) & 33(b)
ϵ vs α	$\delta_n=30^\circ,\delta_f=60^\circ$	0.20	2×10^6 to 10×10^6	34(a) & 34(b)
$\eta(q_t/q)$ vs M	0°	0.20 to 0.95	2×10^6	35(a) & 35(b)
$\eta(q_t/q)$ vs α	$\delta_n=30^\circ,\delta_f=60^\circ$	0.20	2×10^6 to 10×10^6	36(a) & 36(b)

SUMMARY CURVES

The Effects of Compressibility on the Characteristics of the Model
[Flap deflection, 0°; Reynolds number, 2×10^6]

Lift and drag:

Results presented	Lift coefficient	Stabilizer angle	Mach number	Figure number
α vs M	0 to 0.6	0°	0.20 to 0.95	37(a) & 37(b)
C_D vs M	↓	↓	↓	38(a) & 38(b)

Longitudinal stability and control characteristics:

Results presented	Lift coefficient	Stabilizer angle	Mach number	Figure number
C_m vs M	0 to 0.6	0°	0.20 to 0.95	39(a) & 39(b)
ϵ vs M	↓	↓	↓	40(a) & 40(b)
$\partial\epsilon/\partial\alpha$ vs M				41
C_L for $C_m=0$ vs M		0° to -4°		42(a) & 42(b)
[2]C_L vs M	- - -	- - -	0.50 to 0.95	43
i_t for $C_m=0$ vs M	- - -	- - -	0.20 to 0.95	44
C_{L_t} vs δ_e	- - -	- - -	0.20 to 0.94	45
δ_e for $C_m=0$ vs M	- - -	- - -	0.20 to 0.95	46

Longitudinal Characteristics with the Flaps Deflected

Results presented	Flap deflection	Mach number	Reynolds number	Figure number
i_t for $C_m=0$ & C_D vs C_L	$\delta_n=30^\circ,\delta_f=50^\circ$	0.20	10×10^6	47
L/D vs C_L for $C_m=0$	↓	↓	↓	48
[3]Sinking speed vs Gliding speed	↓	↓	↓	49

[2]Lift requirements of hypothetical airplane with a wing loading of 100 pounds per square foot in flight at an altitude of 10,000 feet.

[3]Sinking speed for hypothetical airplane with a wing loading of 100 pounds per square foot in flight at sea level. Power off.

REFERENCES

1. Johnson, Ben H., Jr.: Investigation of a Thin Wing of Aspect Ratio 4 in the Ames 12-Foot Pressure Wind Tunnel. I - Characteristics of a Plain Wing. NACA RM A8D07, 1948.

2. Johnson, Ben H., Jr., and Bandettini, Angelo: Investigation of a Thin Wing of Aspect Ratio 4 in the Ames 12-Foot Pressure Wind Tunnel. II - The Effect of Constant-Chord Leading- and Trailing-Edge Flaps on the Low-Speed Characteristics of the Wing. NACA RM A8F15, 1948.

3. Johnson, Ben H., Jr., and Demele, Fred A.: Investigation of a Thin Wing of Aspect Ratio 4 in the Ames 12-Foot Pressure Wind Tunnel. III - The Effectiveness of a Constant-Chord Aileron. NACA RM A8I17, 1948.

4. Johnson, Ben H., Jr., and Reed, Verlin D.: Investigation of a Thin Wing of Aspect Ratio 4 in the Ames 12-Foot Pressure Wind Tunnel. IV - The Effect of a Constant-Chord Leading-Edge Flap at High Subsonic Speeds. NACA RM A8K19, 1949.

5. Rathert, George A., Hanson, Carl M., and Rolls, L. Stewart: Investigation of a Thin Straight Wing of Aspect Ratio 4 by the NACA Wing-Flow Method. - Lift and Pitching-Moment Characteristics of the Wing Alone. NACA RM A8L20, 1949.

6. Bandettini, Angelo, and Reed, Verlin D.: The Aerodynamic Characteristics Throughout the Subsonic Speed Range of a Thin, Sharp-Edged Horizontal Tail of Aspect Ratio 4 Equipped with a Constant-Chord Elevator. NACA RM A9E05, 1949.

7. Sivells, James C., and Deters, Owen J.: Jet-Boundary and Plan-Form Corrections for Partial-Span Models with Reflection Plane, End Plate, or No End Plate in a Closed Circular Wind Tunnel. NACA Rep. 843, 1946.

8. Herriot, John G.: Blockage Corrections for Three-Dimensional-Flow Closed-Throat Wind Tunnels, with Consideration of the Effect of Compressibility. NACA RM A7B28, 1947.

All dimensions given in inches unless otherwise specified.

Note: Leading- and trailing-edge radii are 0.005 inch

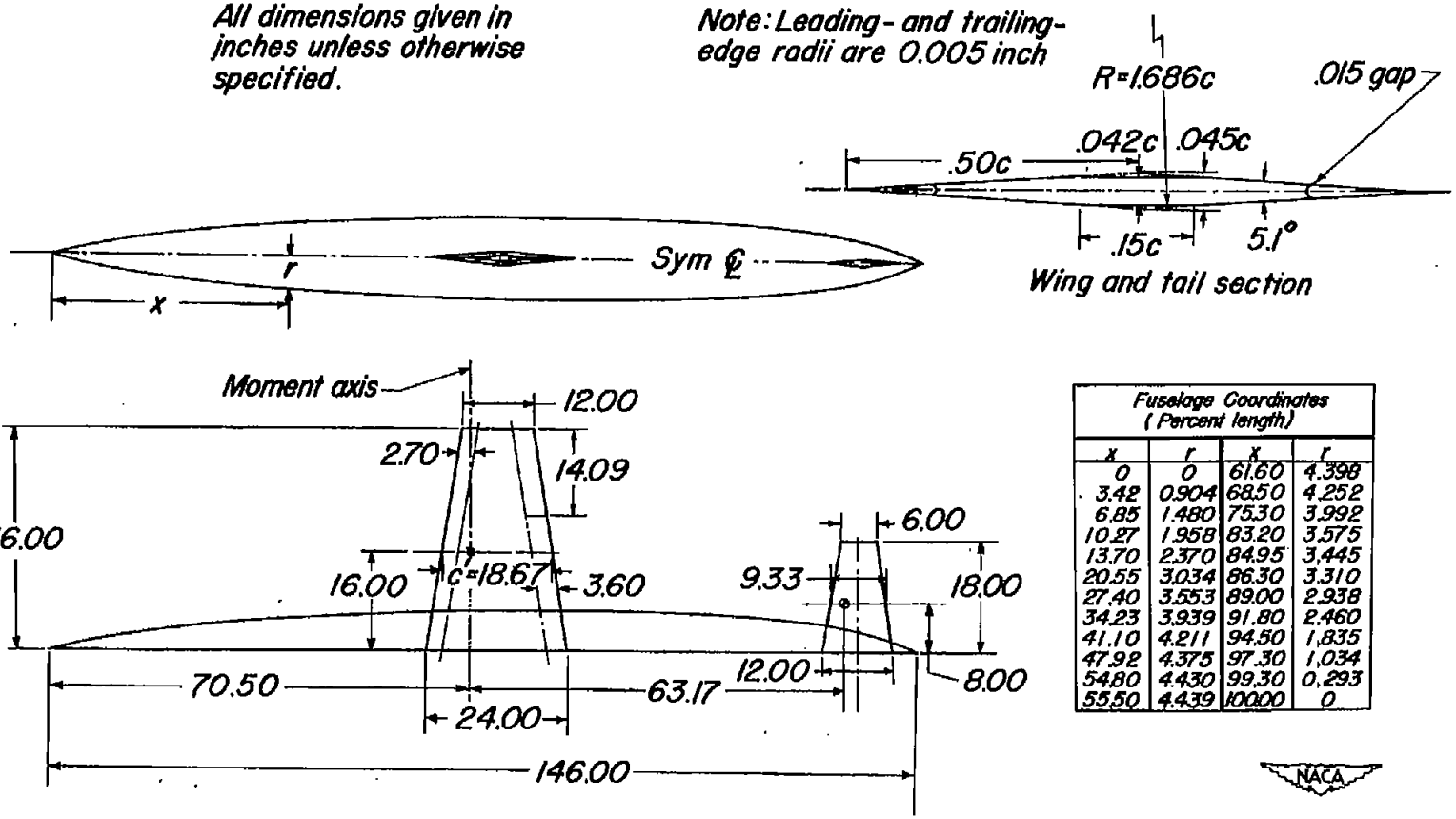

Fuselage Coordinates (Percent length)			
x	r	x	r
0	0	61.60	4.398
3.42	0.904	68.50	4.252
6.85	1.480	75.30	3.992
10.27	1.958	83.20	3.575
13.70	2.370	84.95	3.445
20.55	3.034	86.30	3.310
27.40	3.553	89.00	2.938
34.23	3.939	91.80	2.460
41.10	4.211	94.50	1.835
47.92	4.375	97.30	1.034
54.80	4.430	99.30	0.293
55.50	4.439	100.00	0

(a) Horizontal tail mounted in extended wing-chord plane.

Figure 1.- Semispan model of an airplane with a wing and all- movable horizontal tail of aspect ratio 4.

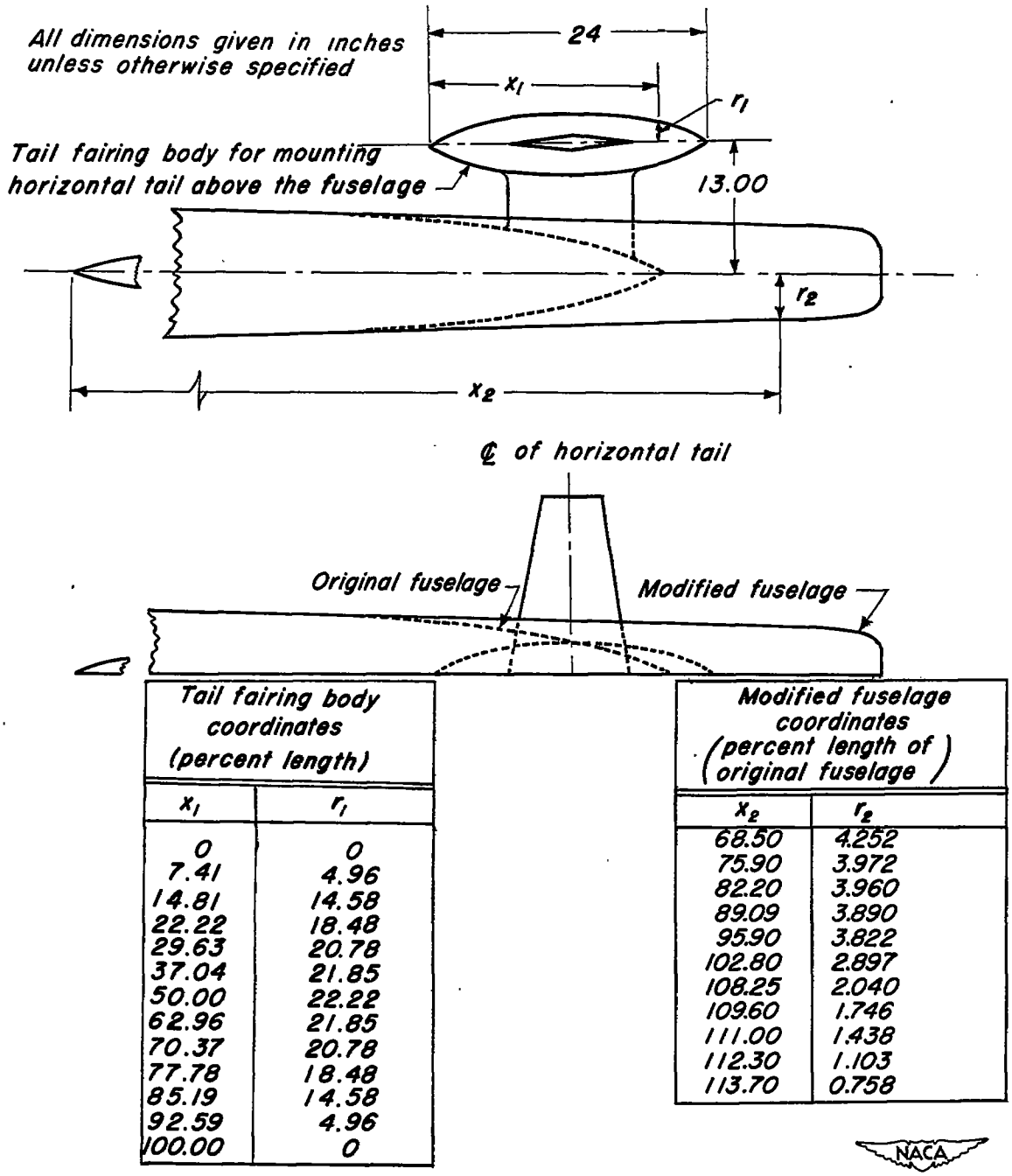

Tail fairing body coordinates (percent length)	
x_1	r_1
0	0
7.41	4.96
14.81	14.58
22.22	18.48
29.63	20.78
37.04	21.85
50.00	22.22
62.96	21.85
70.37	20.78
77.78	18.48
85.19	14.58
92.59	4.96
100.00	0

Modified fuselage coordinates (percent length of original fuselage)	
x_2	r_2
68.50	4.252
75.90	3.972
82.20	3.960
89.09	3.890
95.90	3.822
102.80	2.897
108.25	2.040
109.60	1.746
111.00	1.438
112.30	1.103
113.70	0.758

NACA

(b) Horizontal tail mounted above the original and the modified fuselage.

Figure 1.- Concluded.

(a) Horizontal tail mounted in the extended wing-chord plane.

Figure 2.- Semispan model of the airplane mounted in the Ames 12-foot pressure wind tunnel.

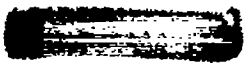

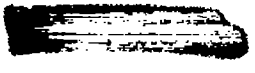

(b) Horizontal tail mounted above the fuselage.

Figure 2.- Continued.

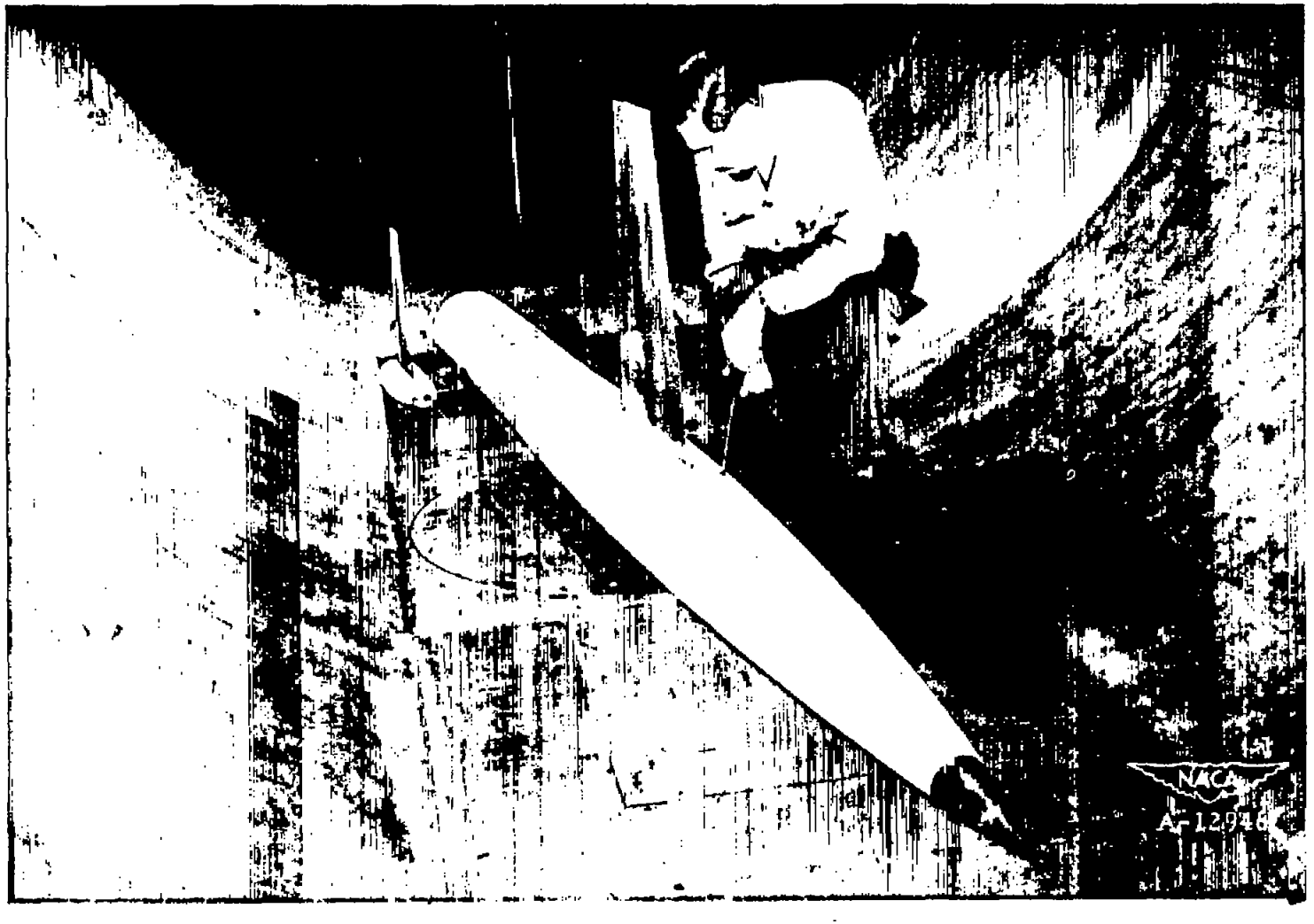

(c) Modified fuselage with the horizontal tail mounted above the fuselage.

Figure 2.- Continued.

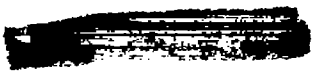

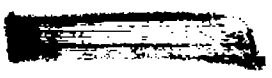

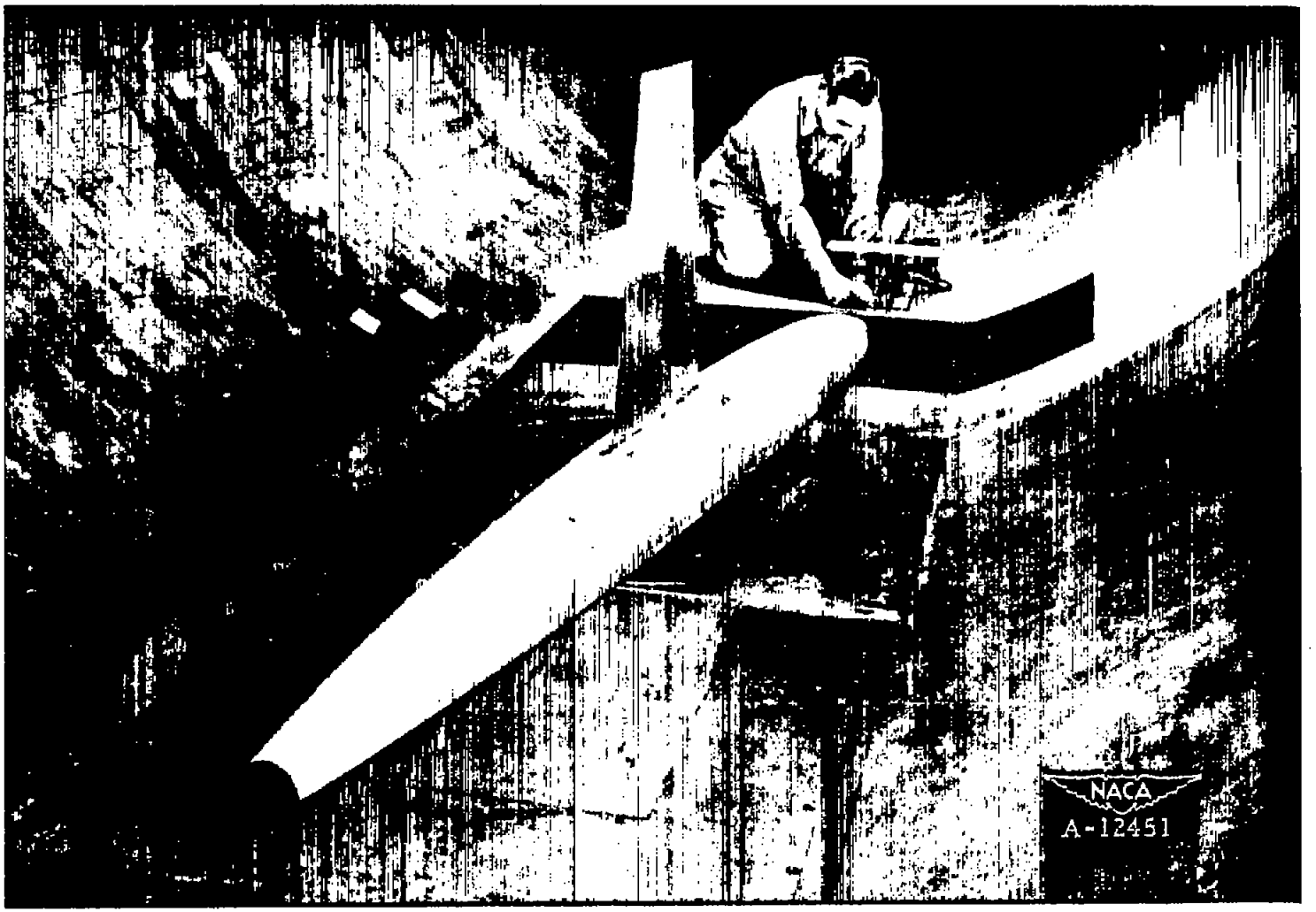

(d) Rake of pressure tubes mounted behind the wing-fuselage combination at the location of the horizontal tail.

Figure 2.- Concluded.

[redacted]

[redacted]

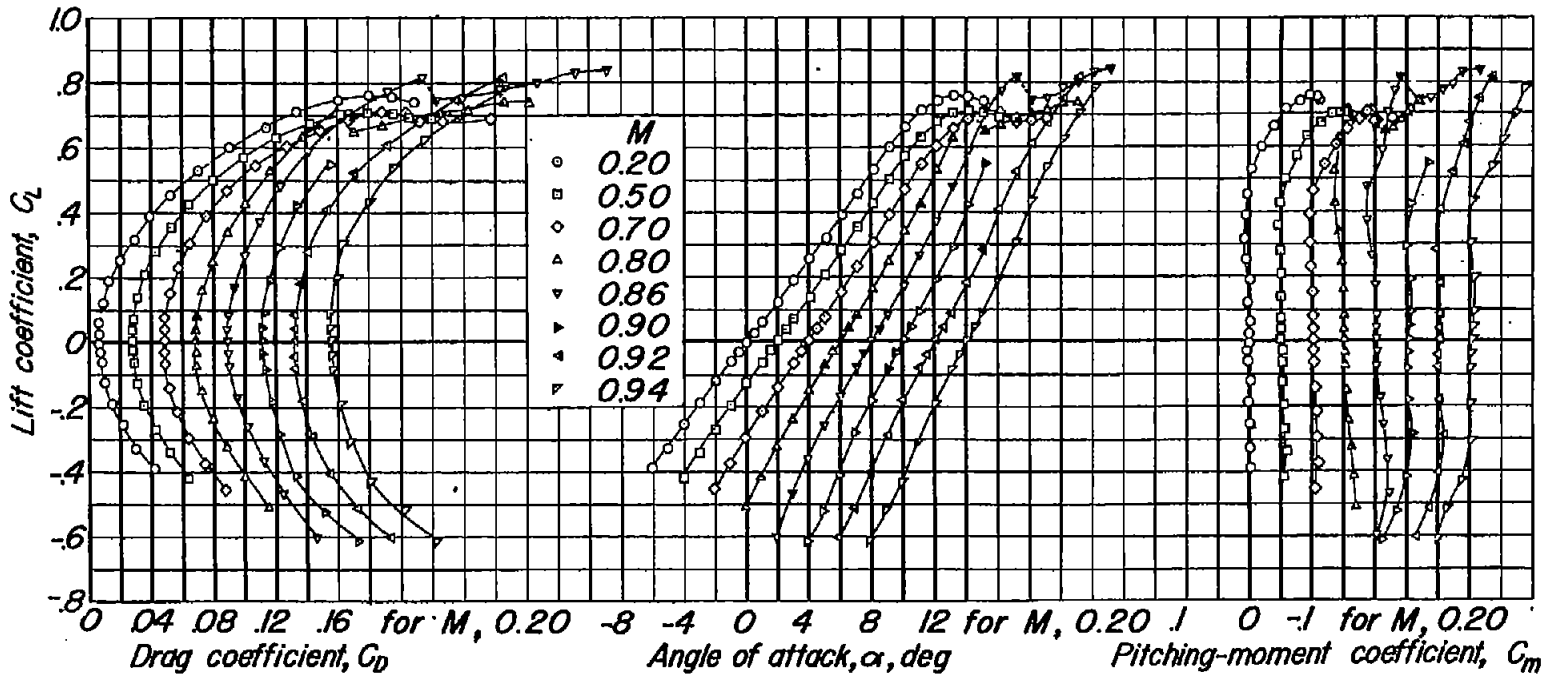

Figure 3.- The lift, drag, and pitching-moment characteristics of the plain wing. R, 2,000,000.

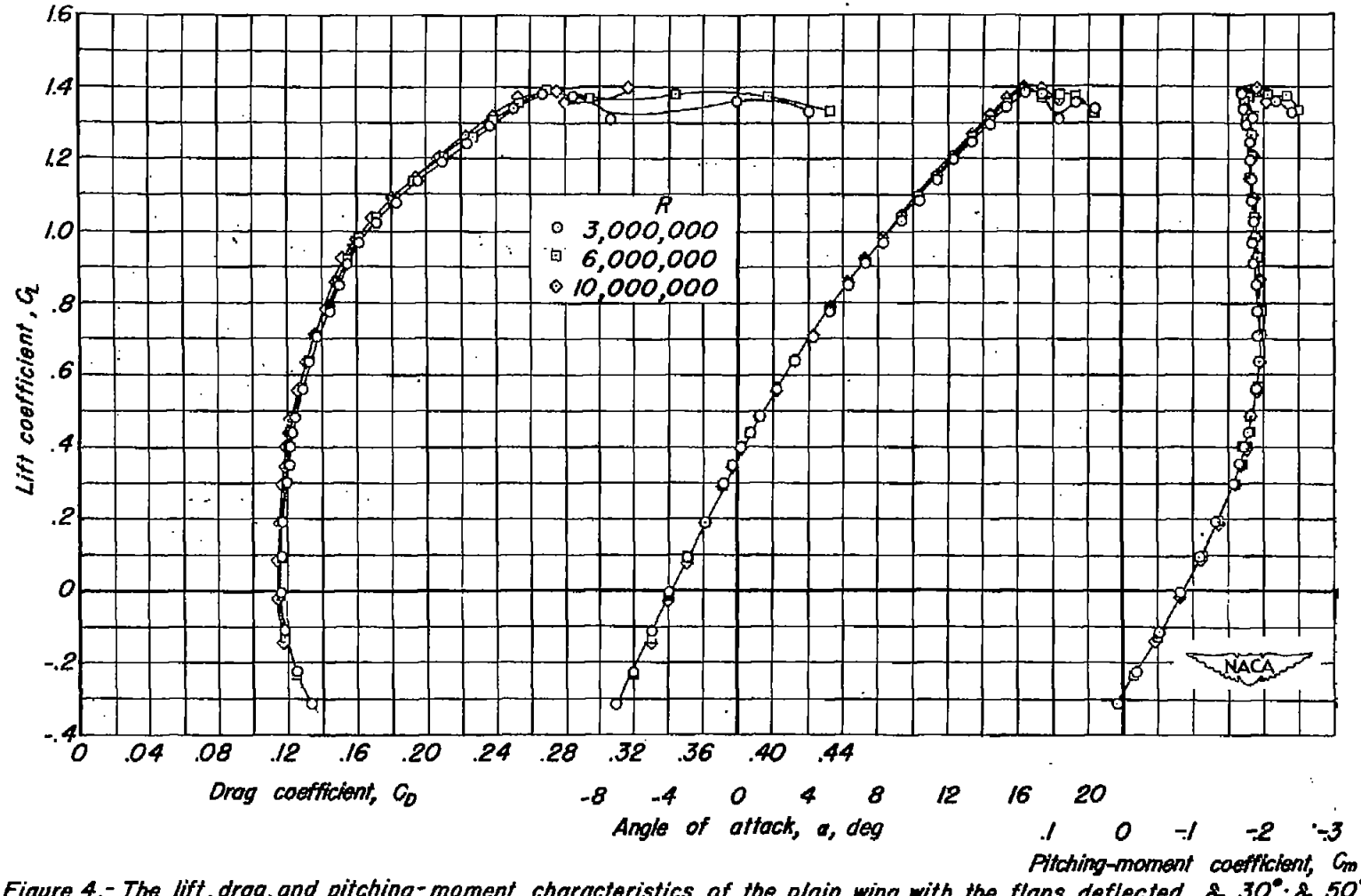

Figure 4.- The lift, drag, and pitching-moment characteristics of the plain wing with the flaps deflected. δ_n, 30°; δ_f, 50°; M, 0.20.

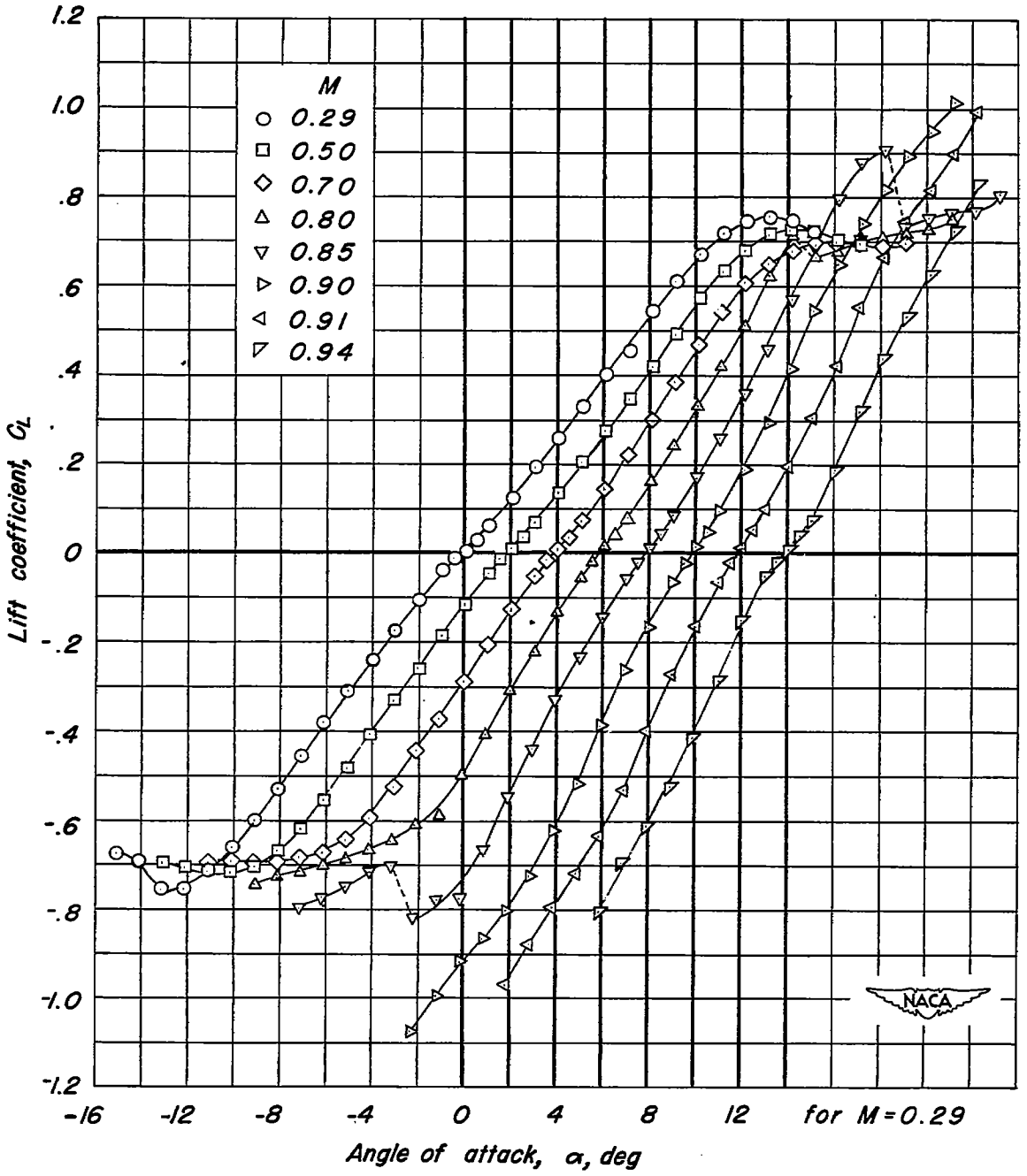

Figure 5.- The lift characteristics of the plain wing, gaps sealed. R, 1,000,000.

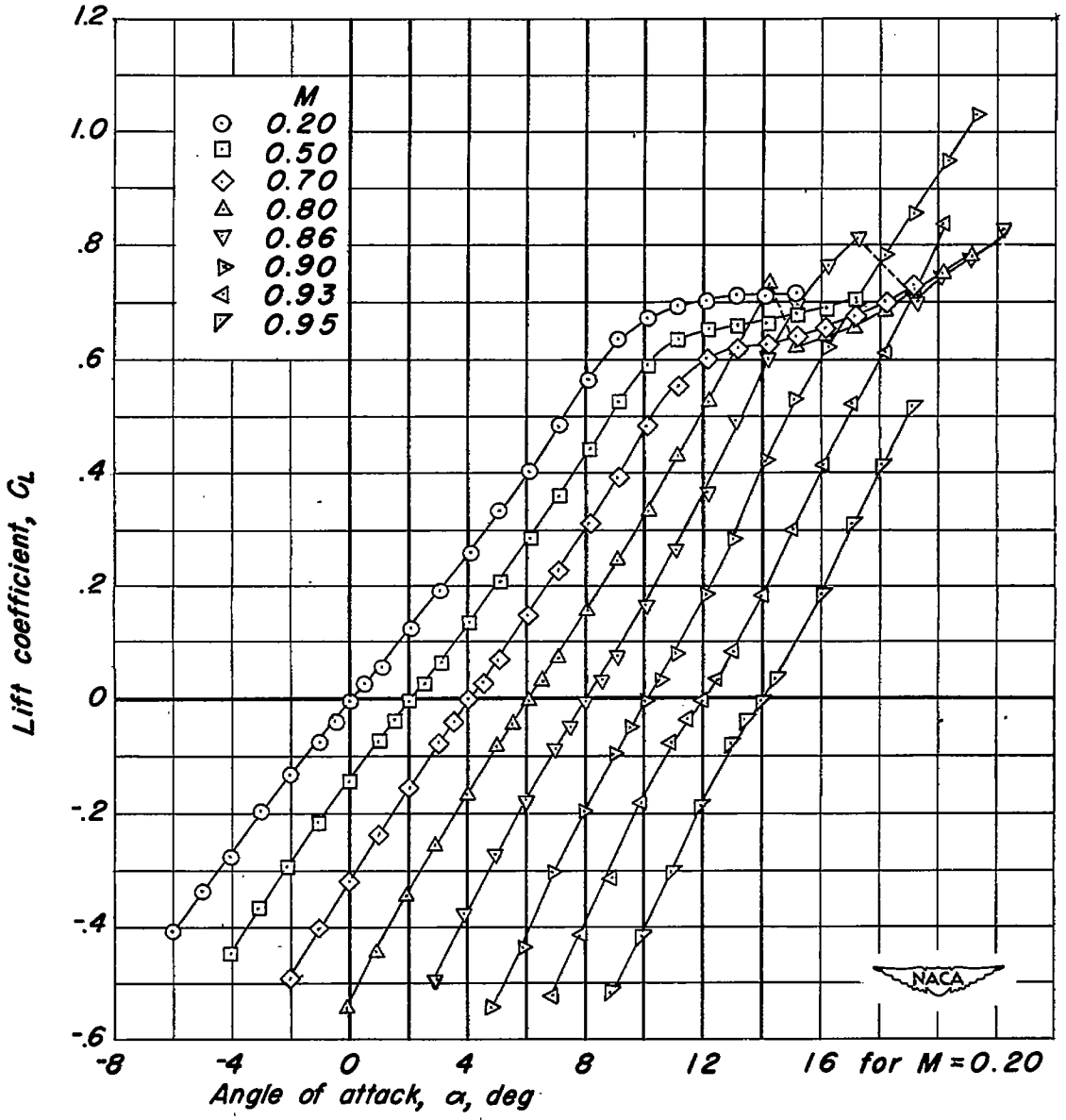

Figure 6.— The lift characteristics of the wing and fuselage. R, 2,000,000.

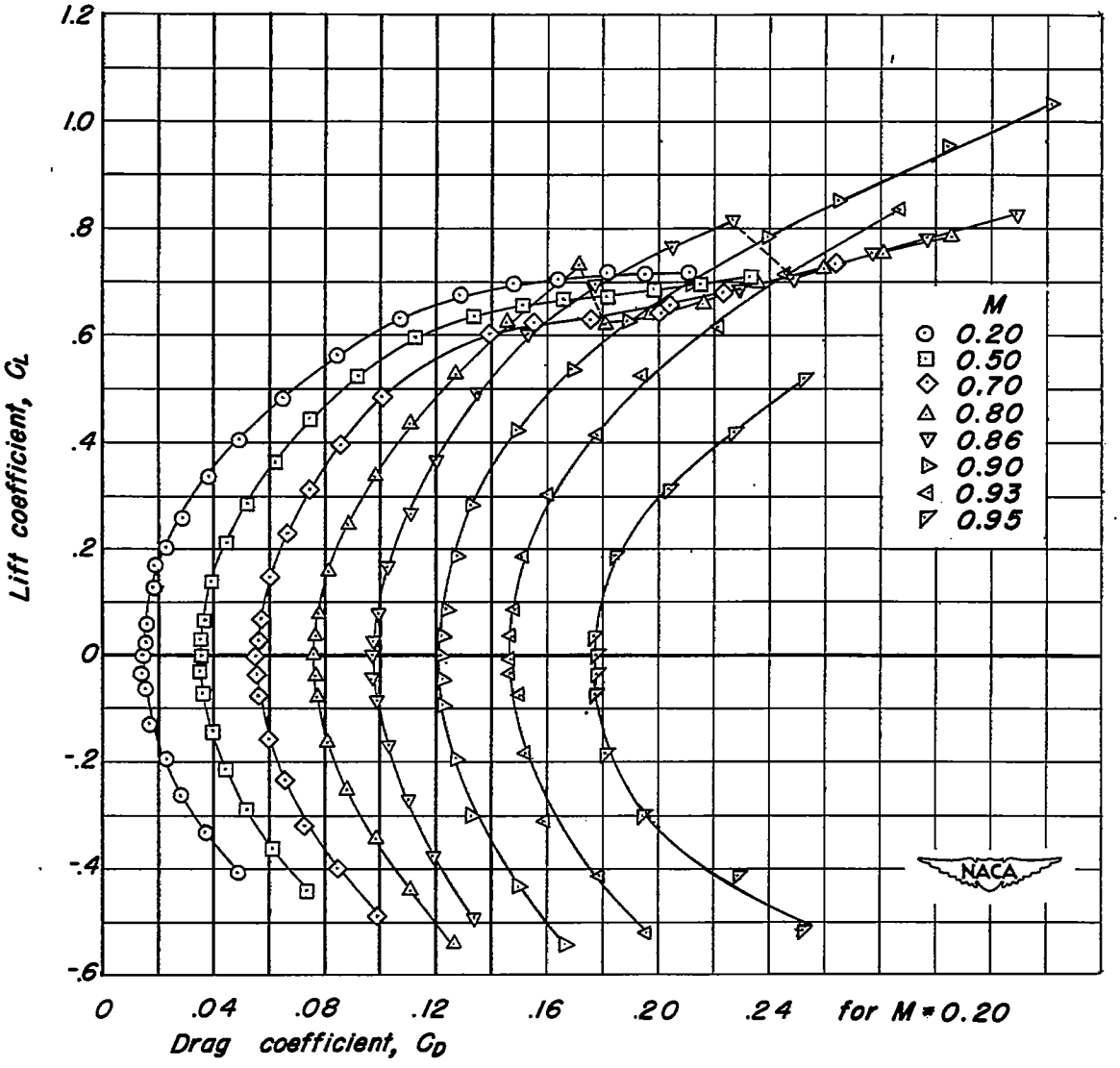

Figure 7.— The drag characteristics of the wing and fuselage. R, 2,000,000.

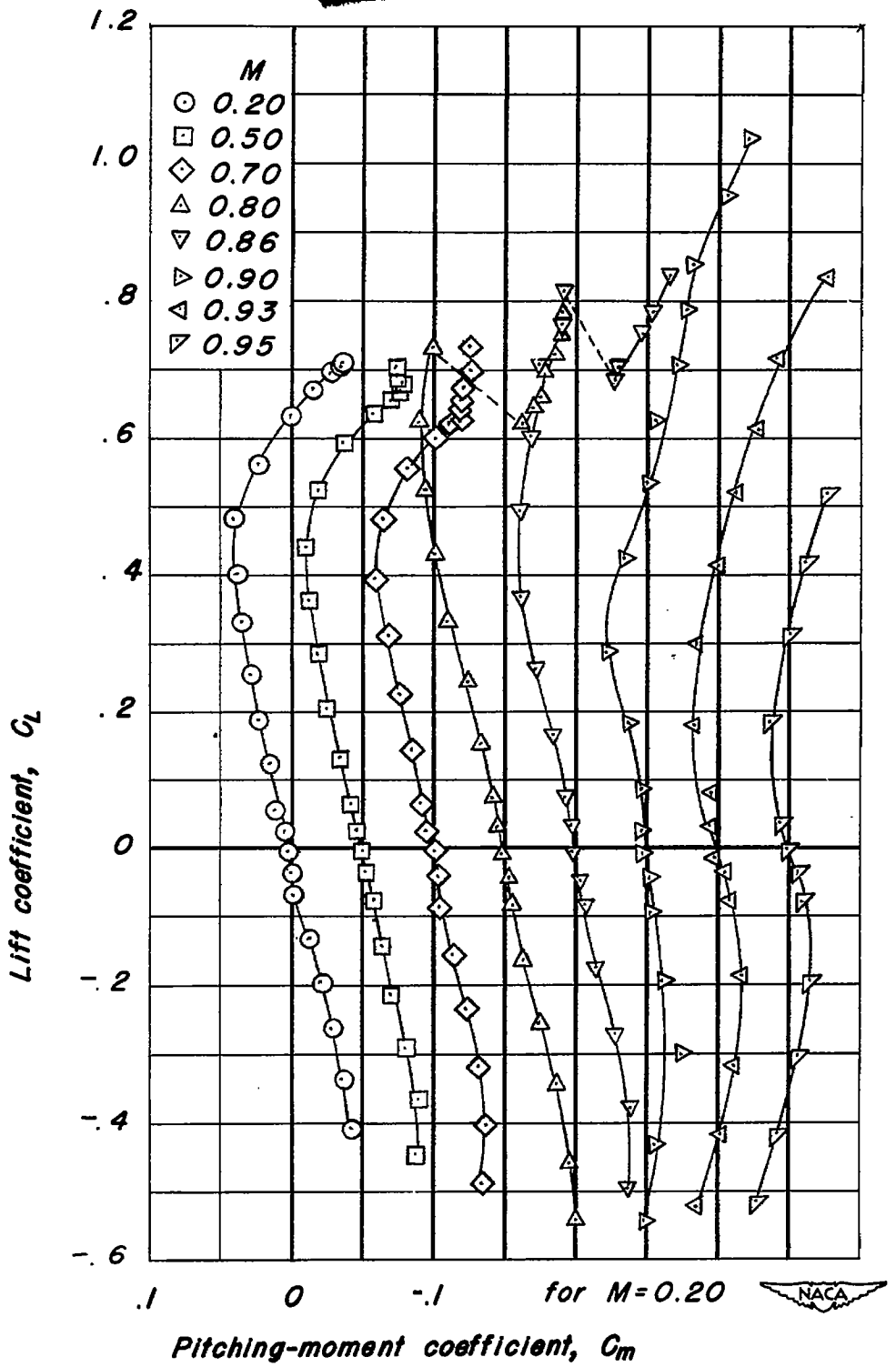

Figure 8.— The pitching-moment characteristics of the wing and fuselage. R, 2,000,000.

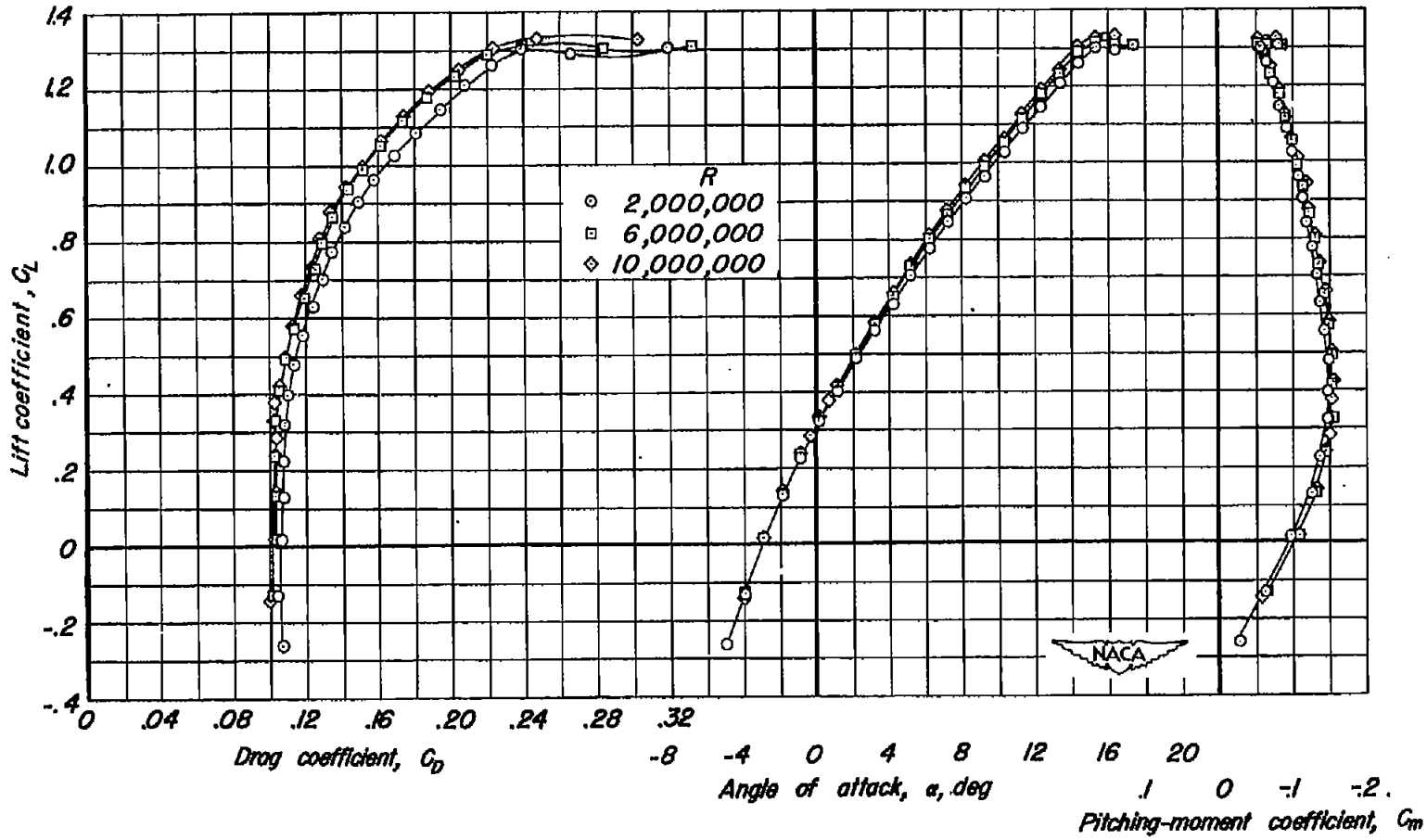

Figure 9.- The lift, drag, and pitching-moment characteristics of the wing and fuselage with the flaps deflected. δ_n, 30°; δ_f, 50°; M, 0.20.

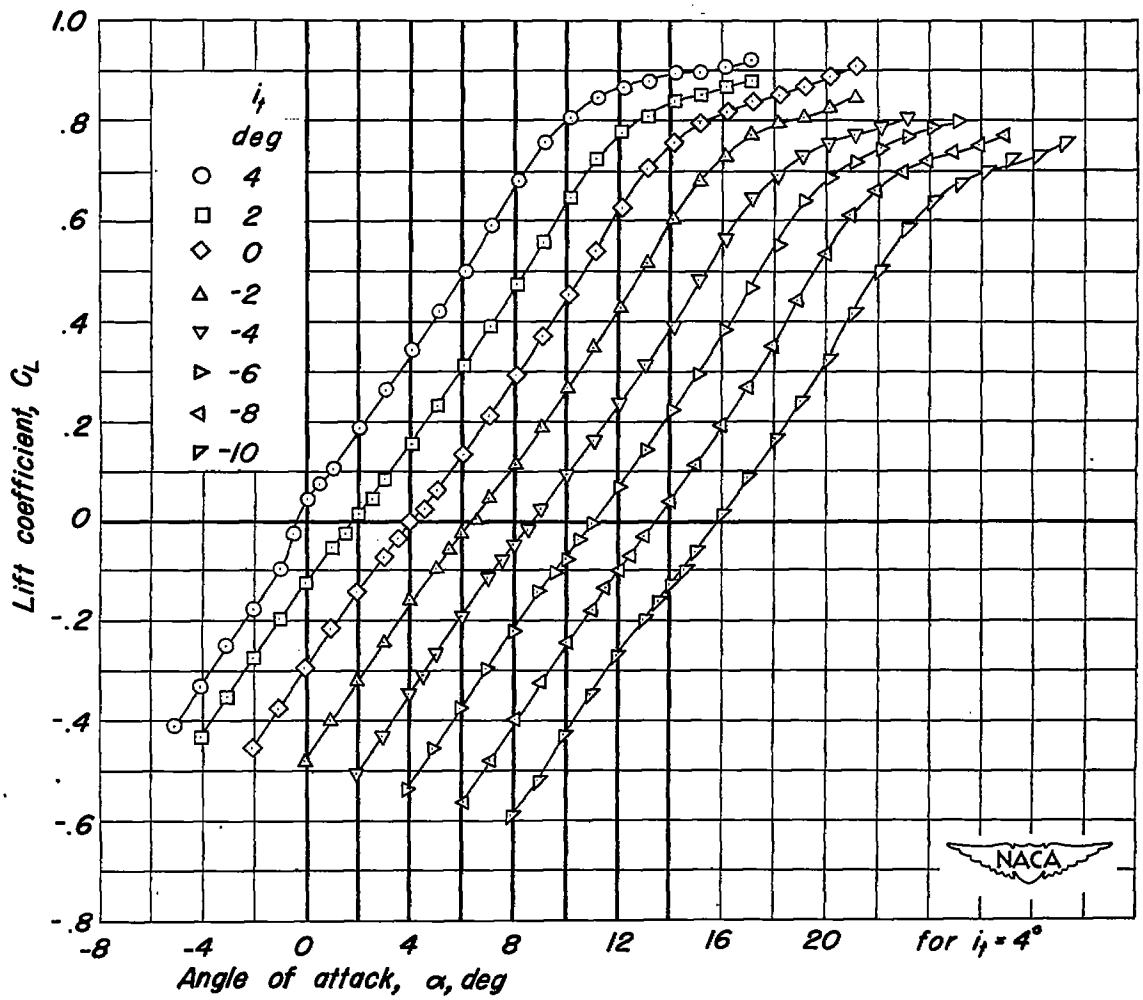

(a) M, 0.20.

Figure 10.— The lift characteristics of the airplane model with the horizontal tail mounted in the extended wing-chord plane. R, 2,000,000.

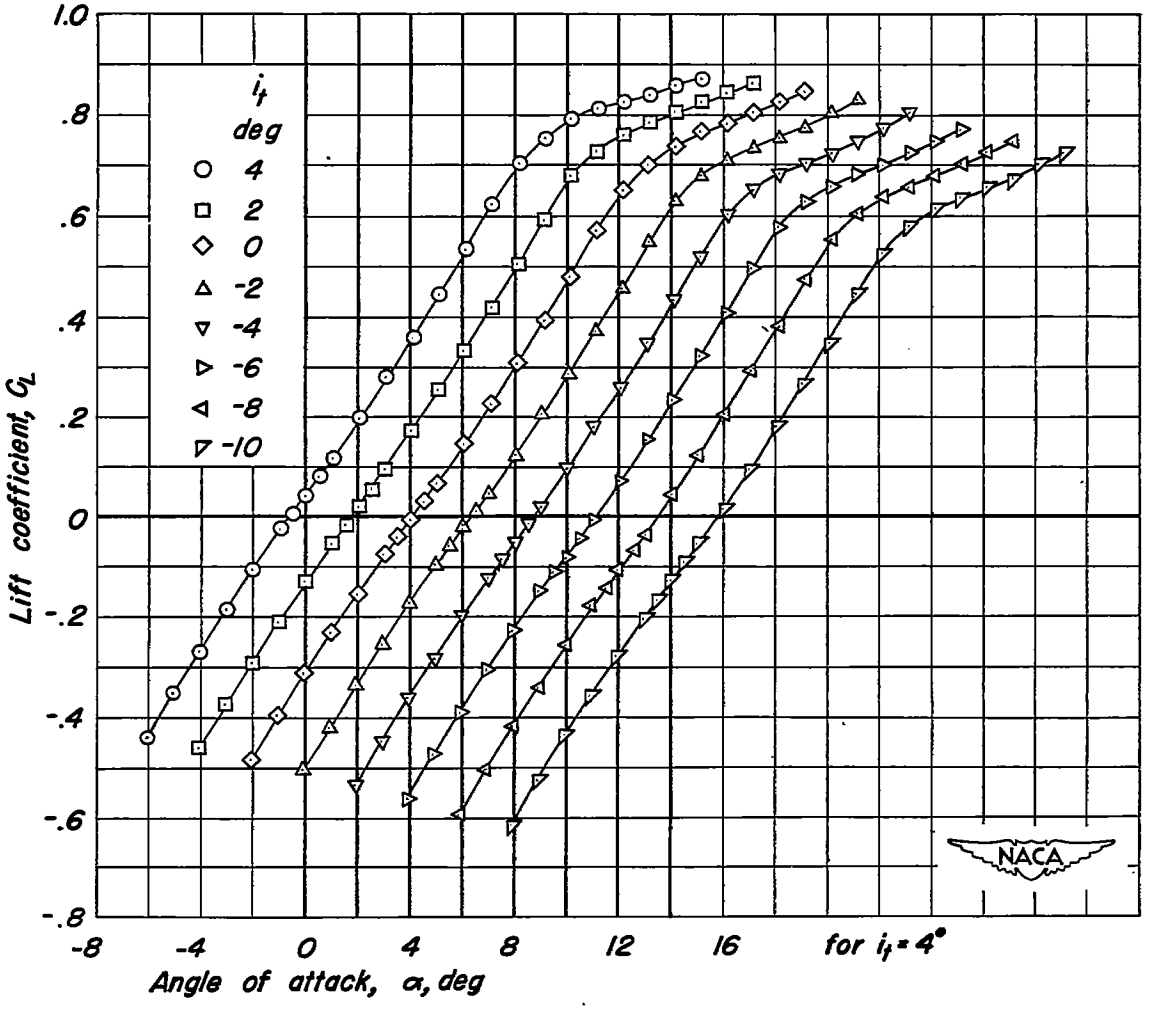

(b) M, 0.50.

Figure 10.— Continued.

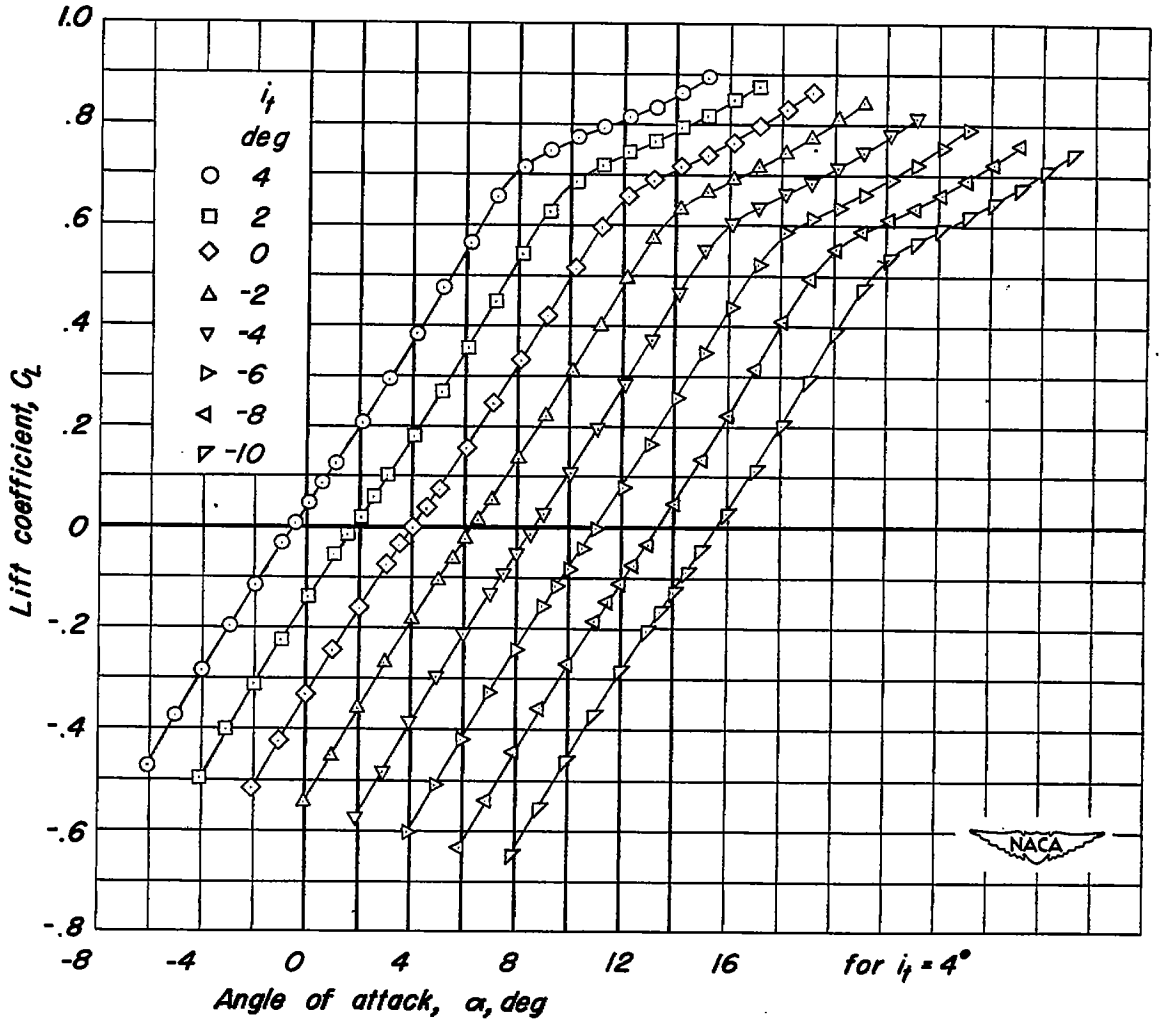

(c) M, 0.70.

Figure 10.— Continued.

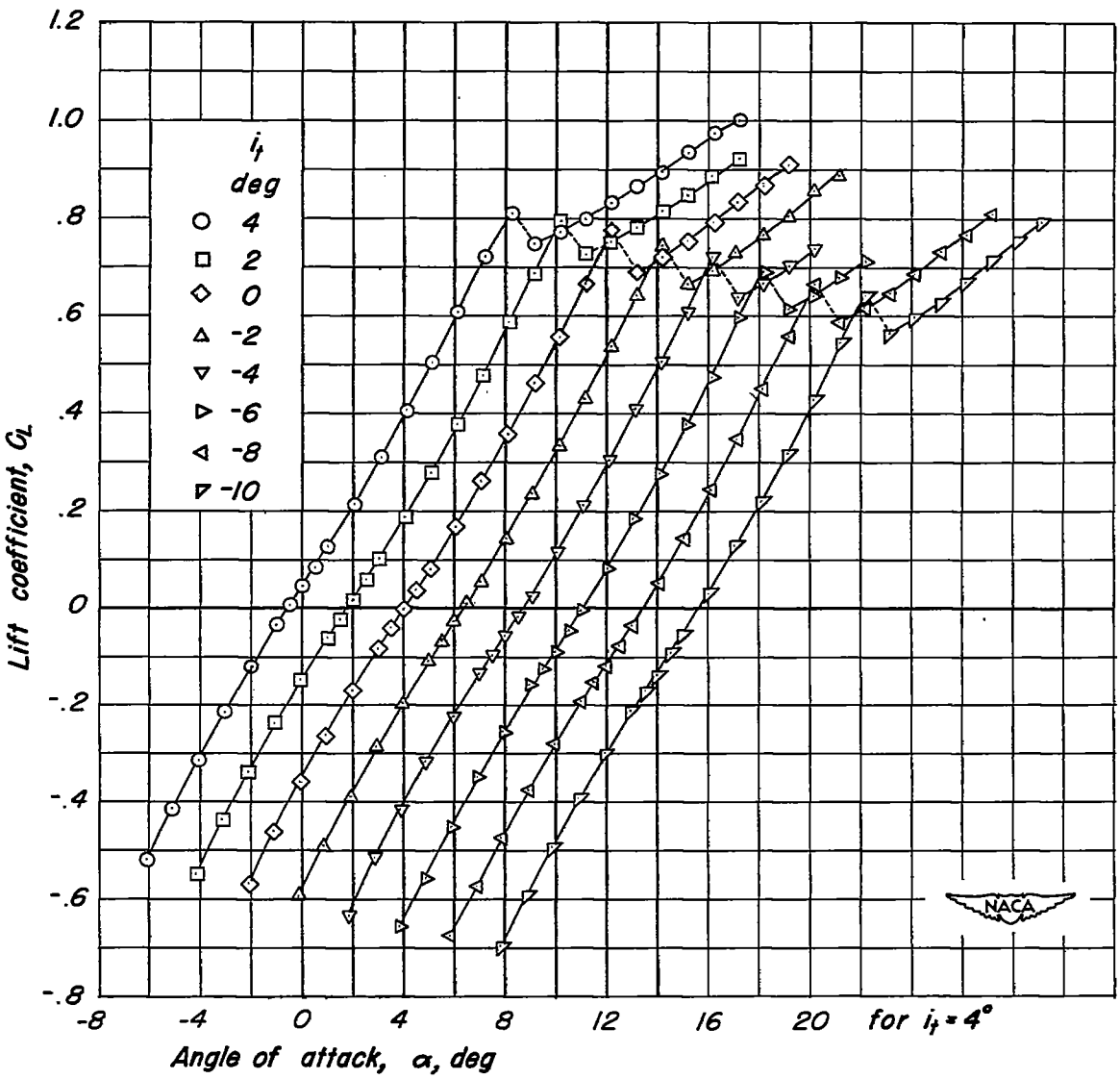

(d) M, 0.80.

Figure 10.— Continued.

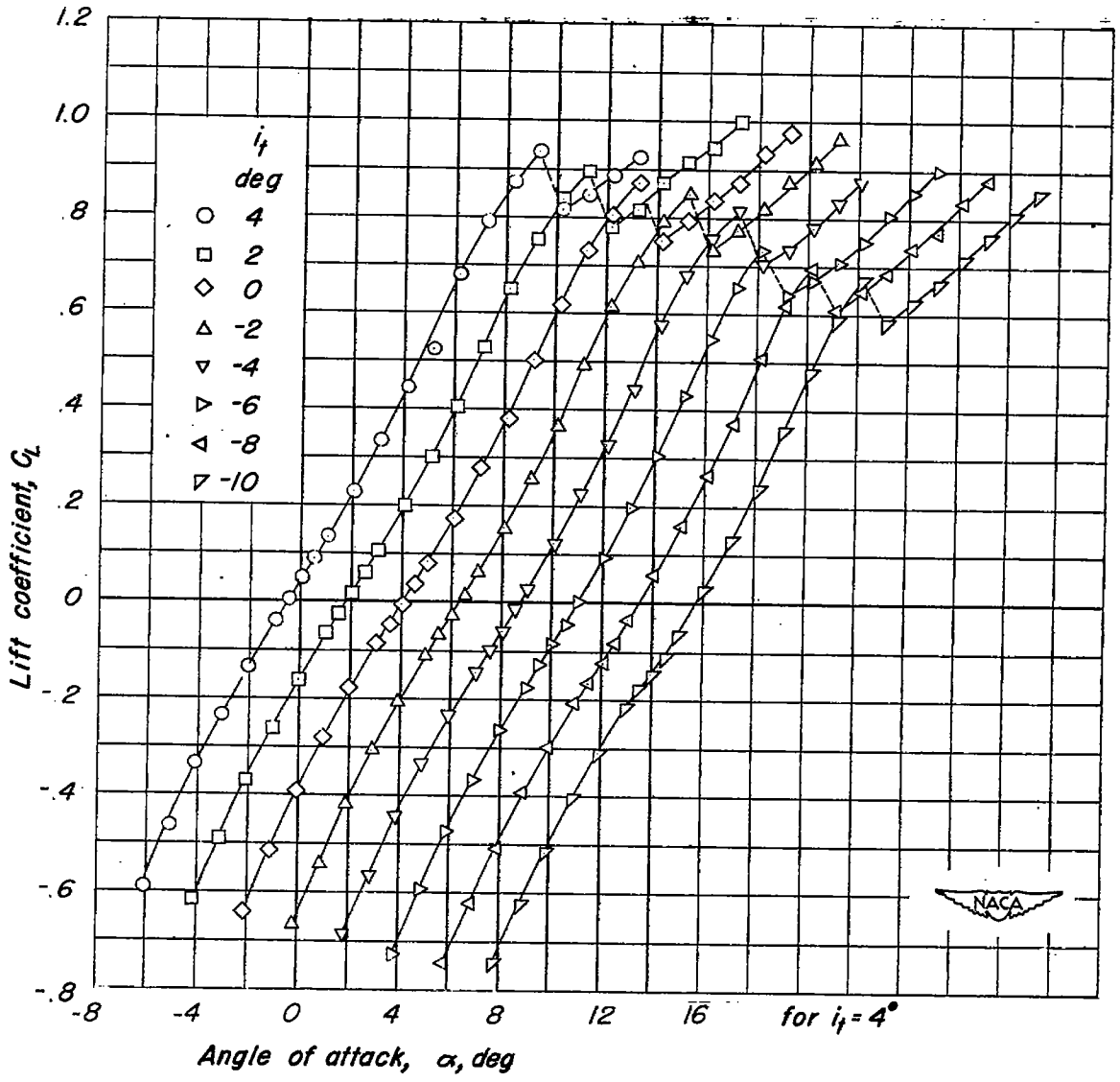

(e) M, 0.85.

Figure 10.— Continued.

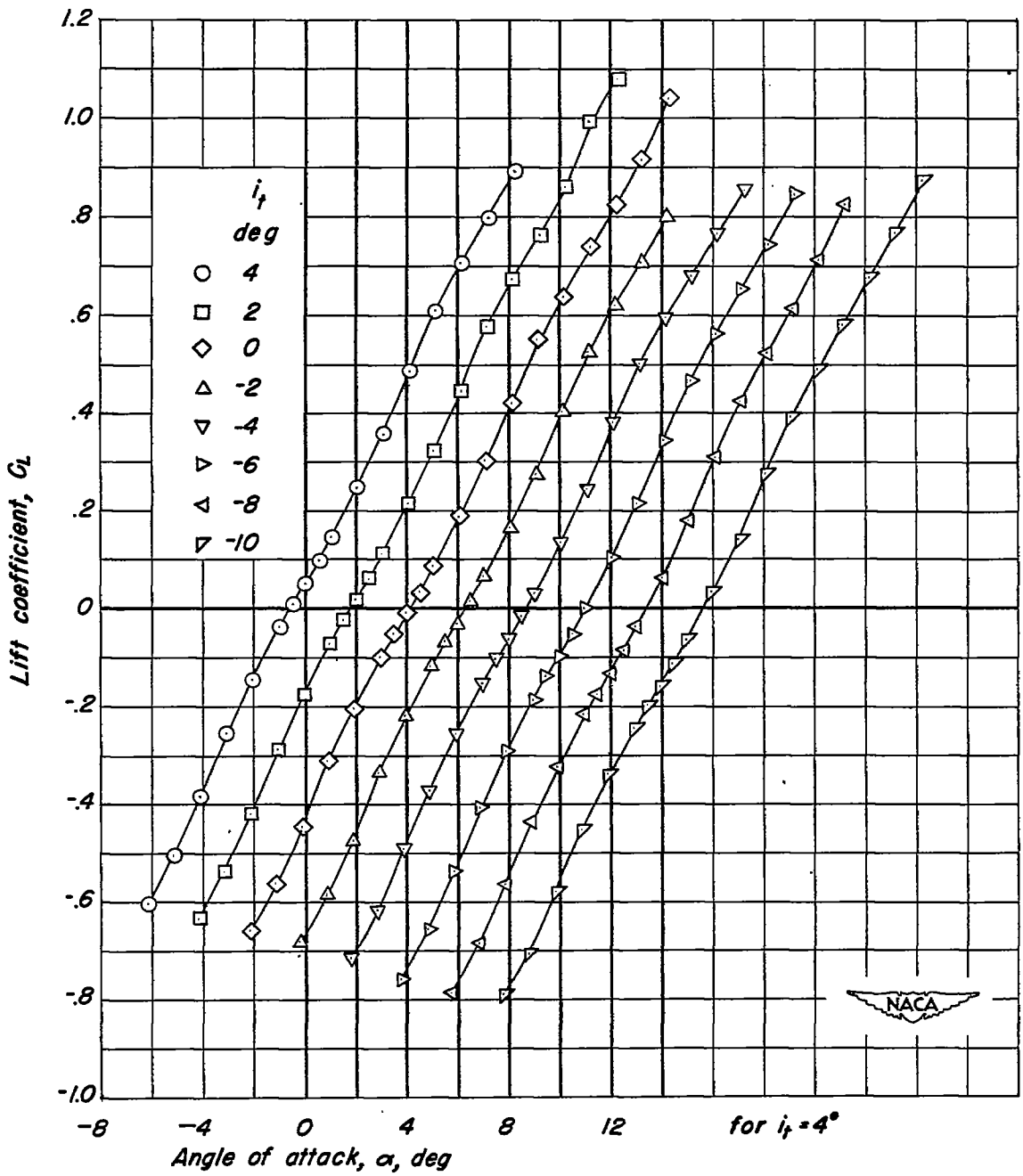

(f) M, 0.90.

Figure 10.- Continued.

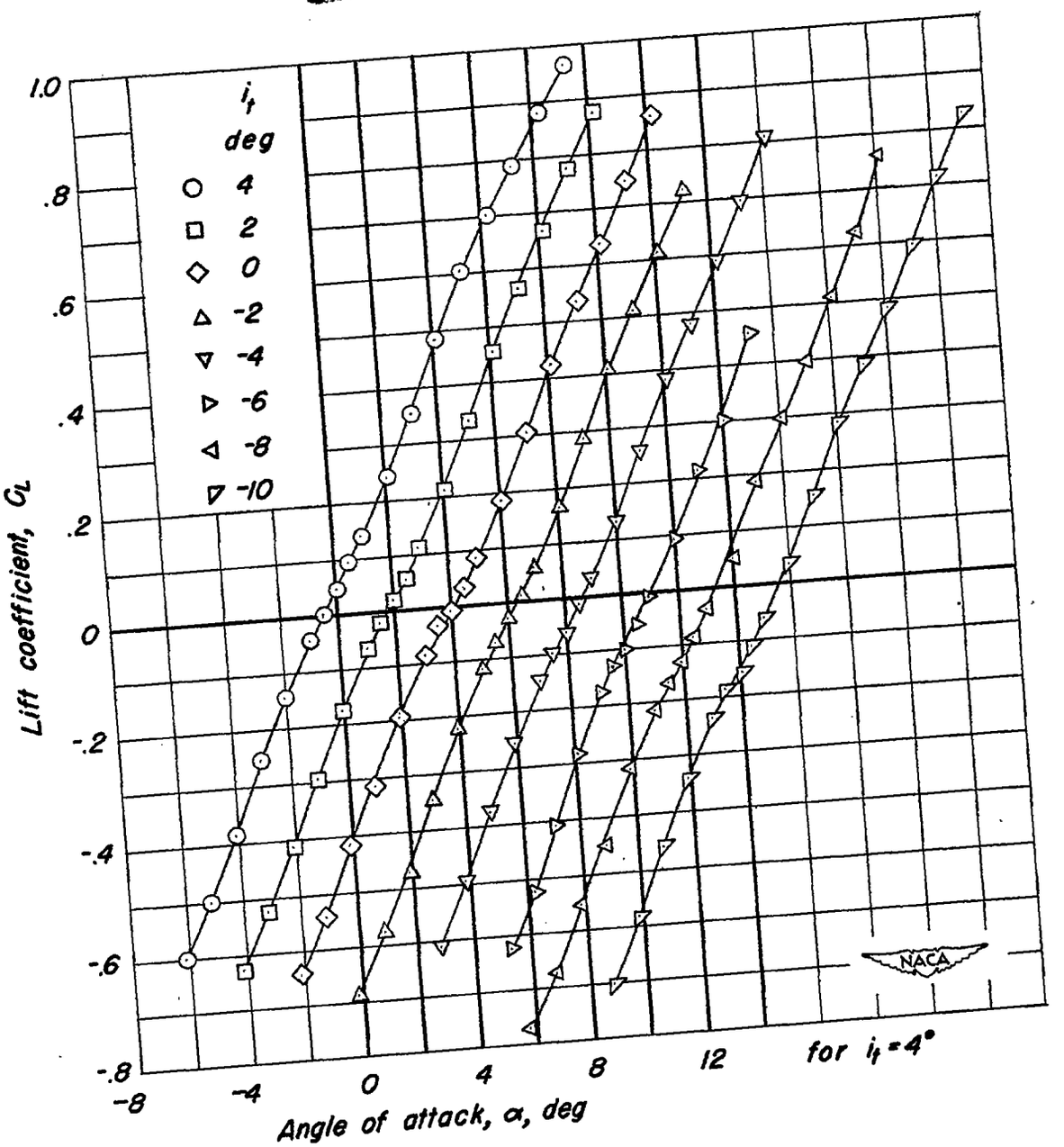

(g) M, 0.92.

Figure 10.- Continued.

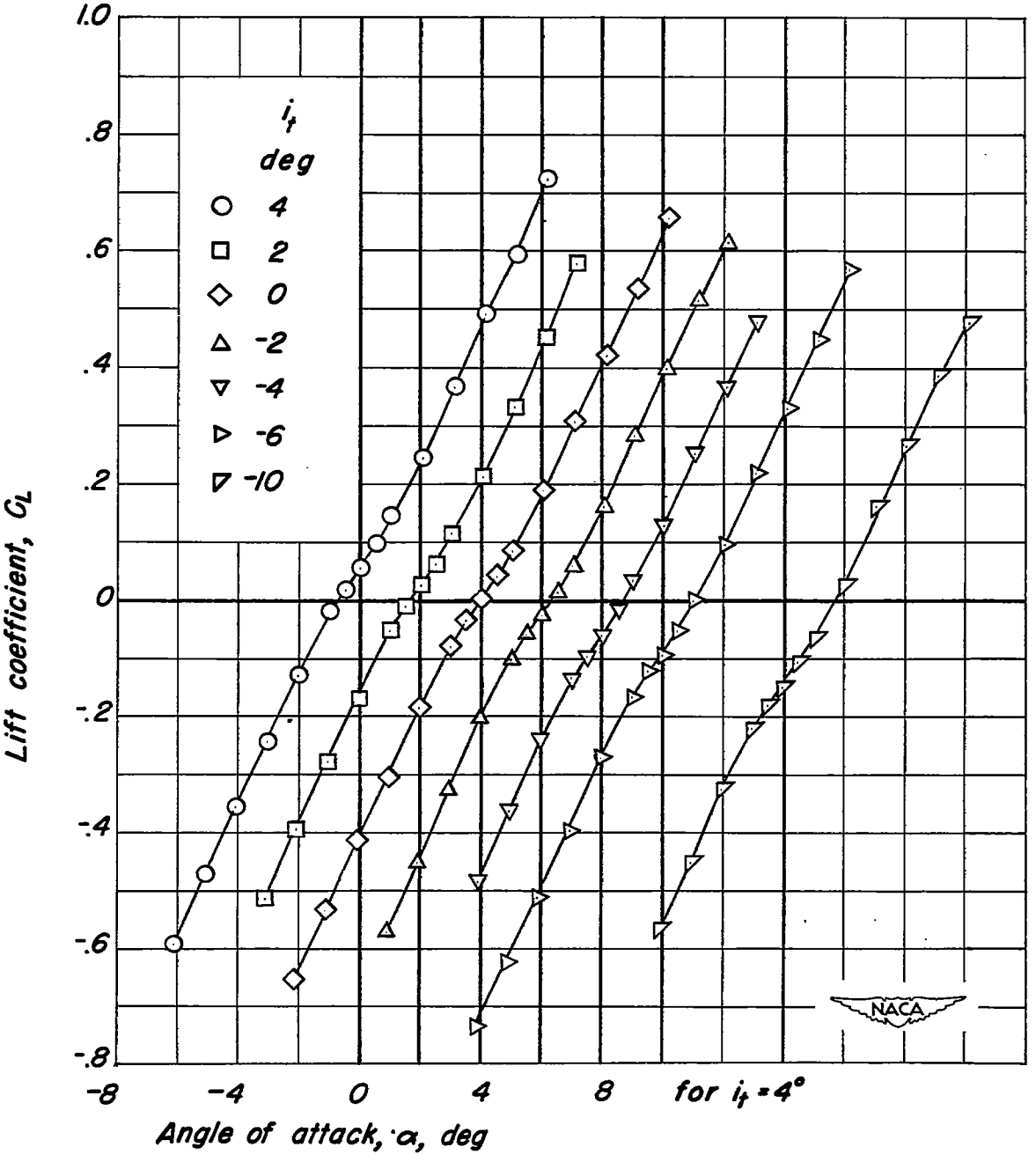

(h) M, 0.95.

Figure 10.— Concluded.

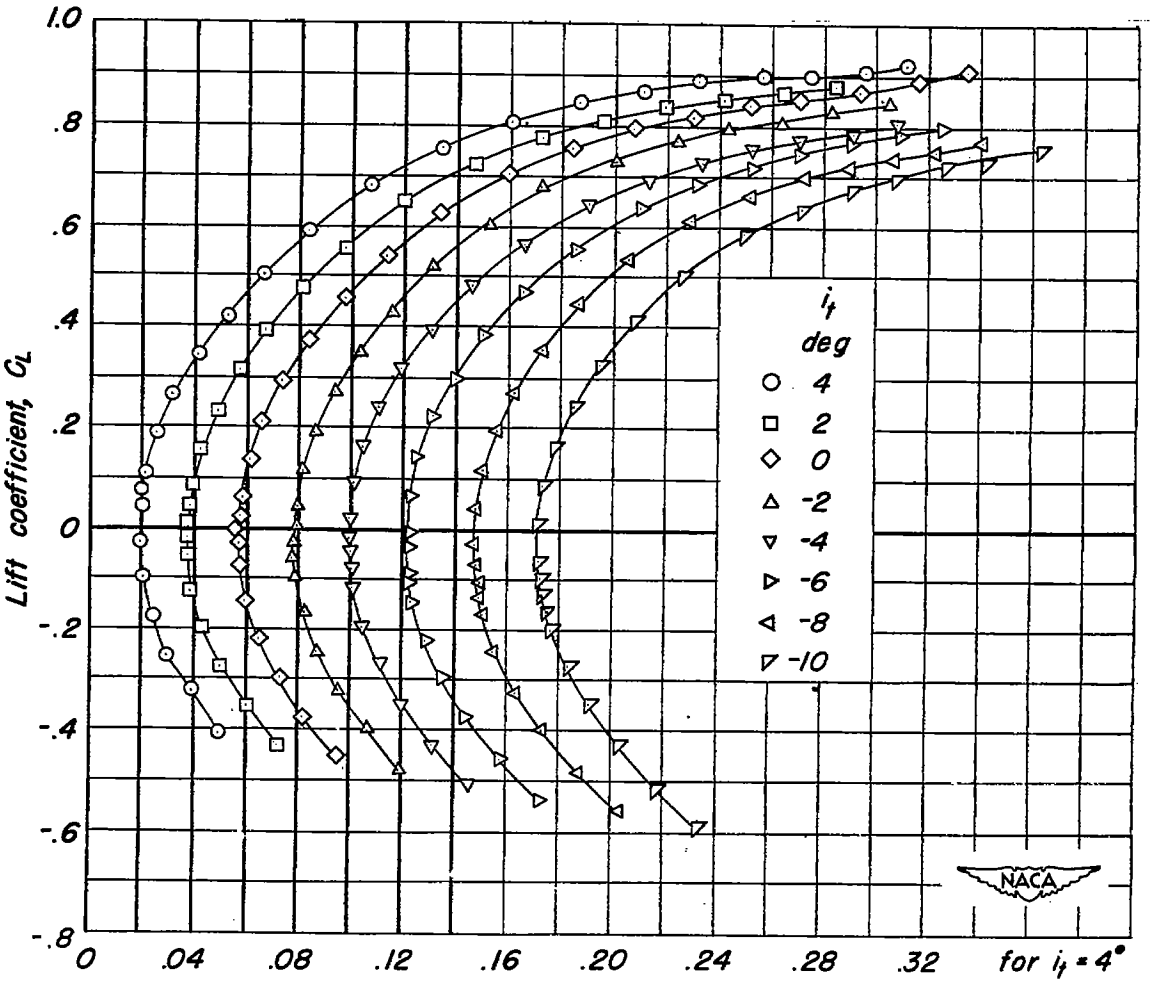

(a) M, 0.20.

Figure 11.— The drag characteristics of the airplane model with the horizontal tail mounted in the extended wing-chord plane. R, 2,000,000.

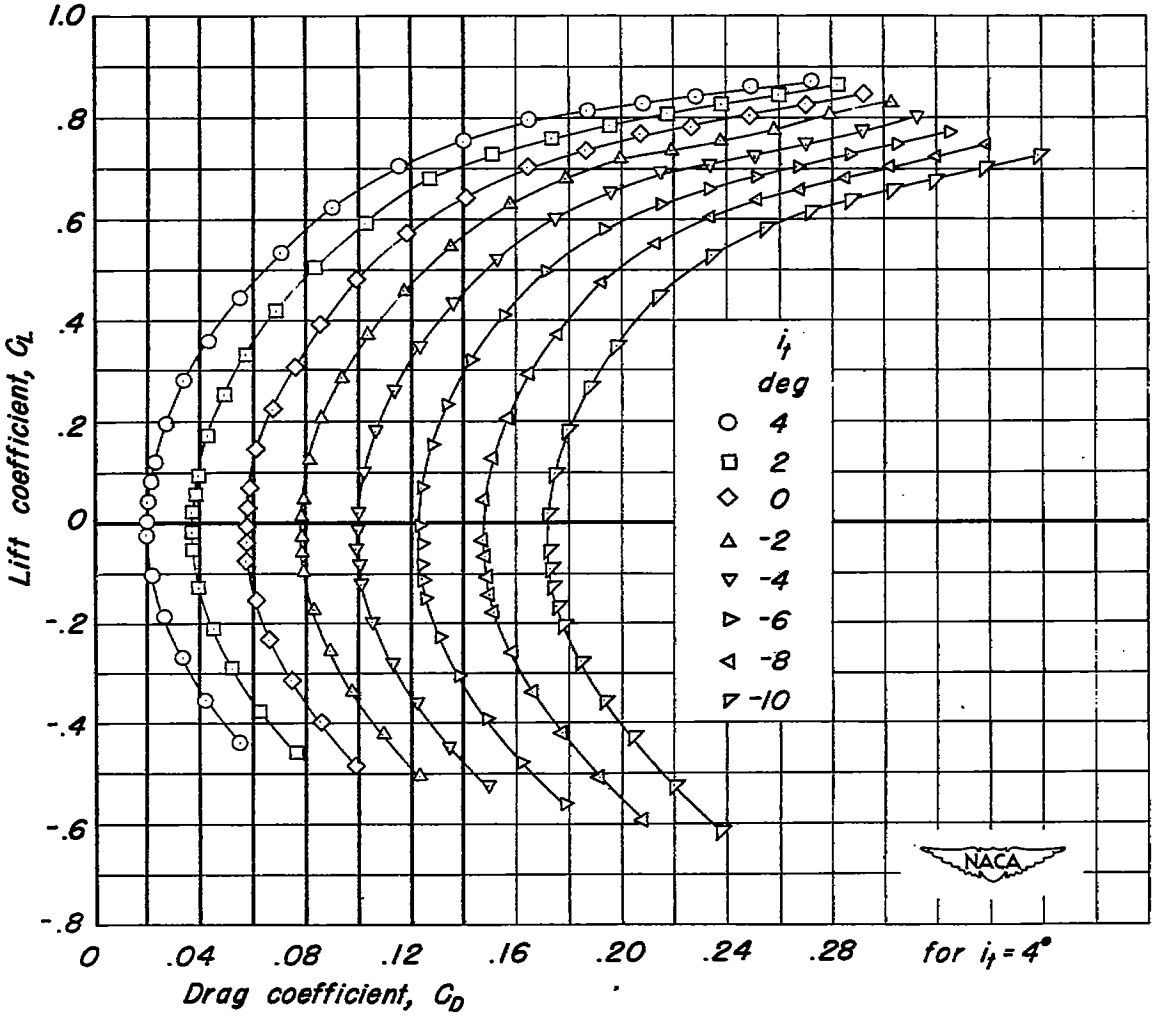

(b) M, 0.50.

Figure 11.— Continued.

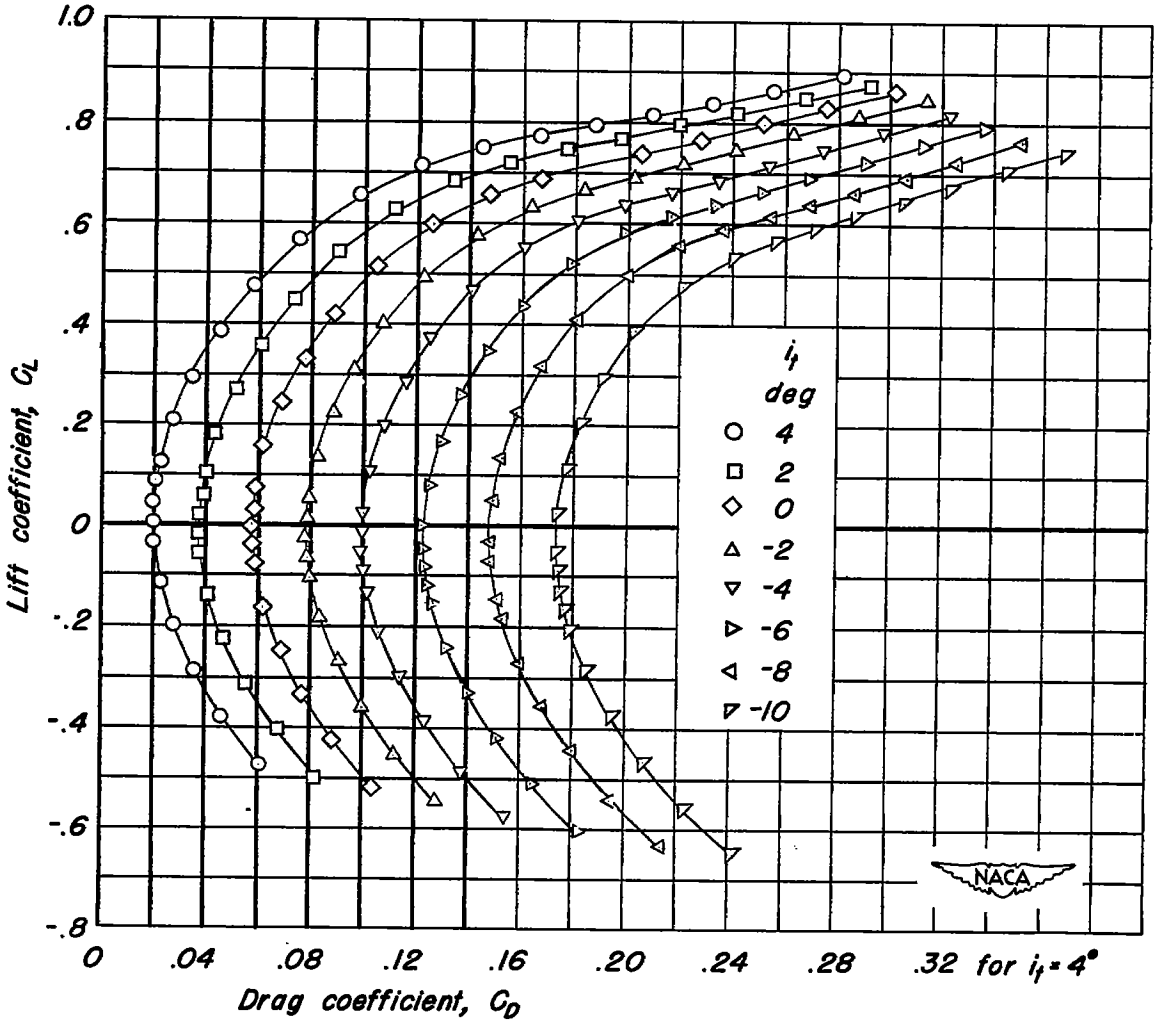

(c) M, 0.70.

Figure 11.— Continued.

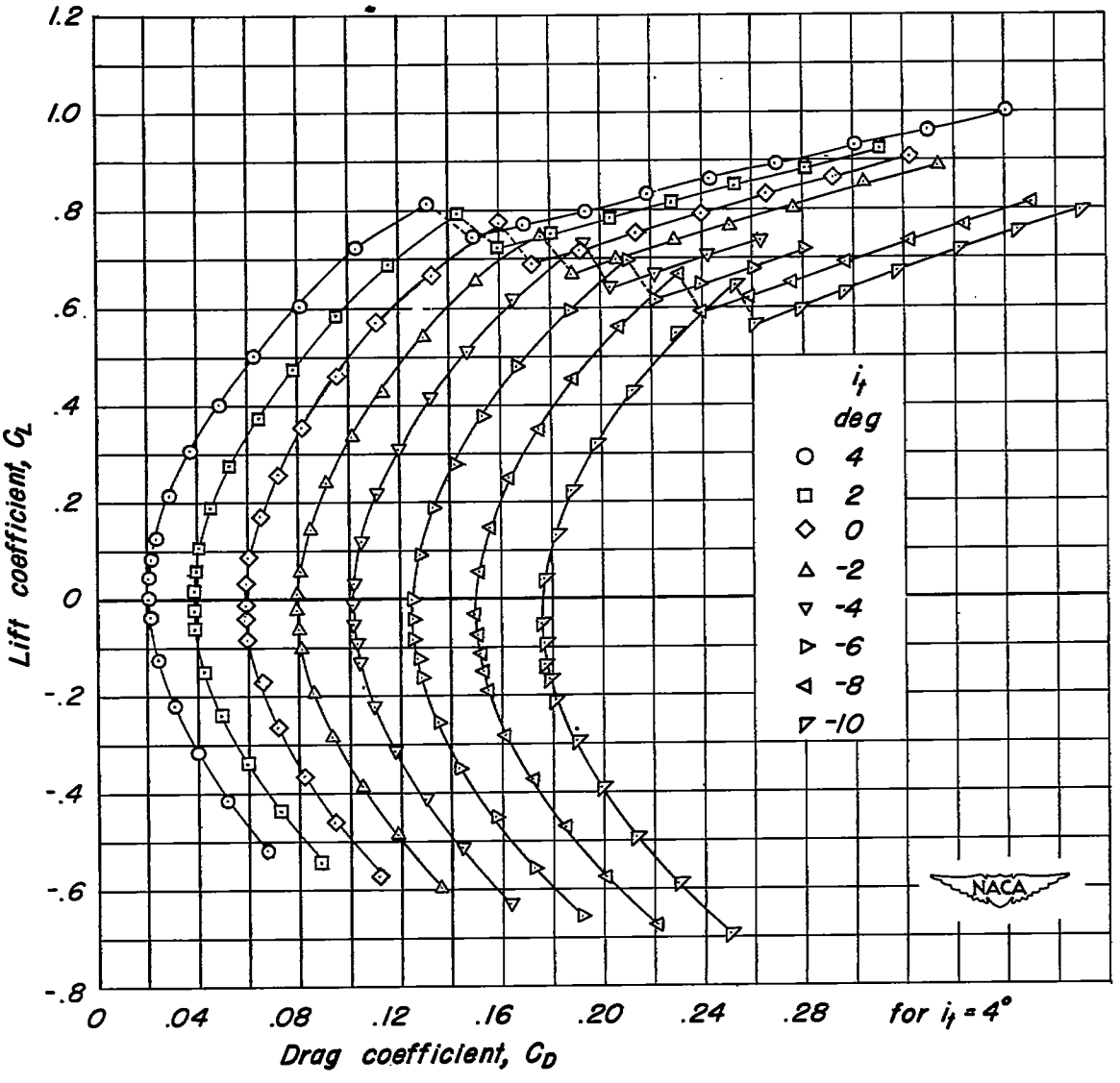

(d) M, 0.80.

Figure 11.— Continued.

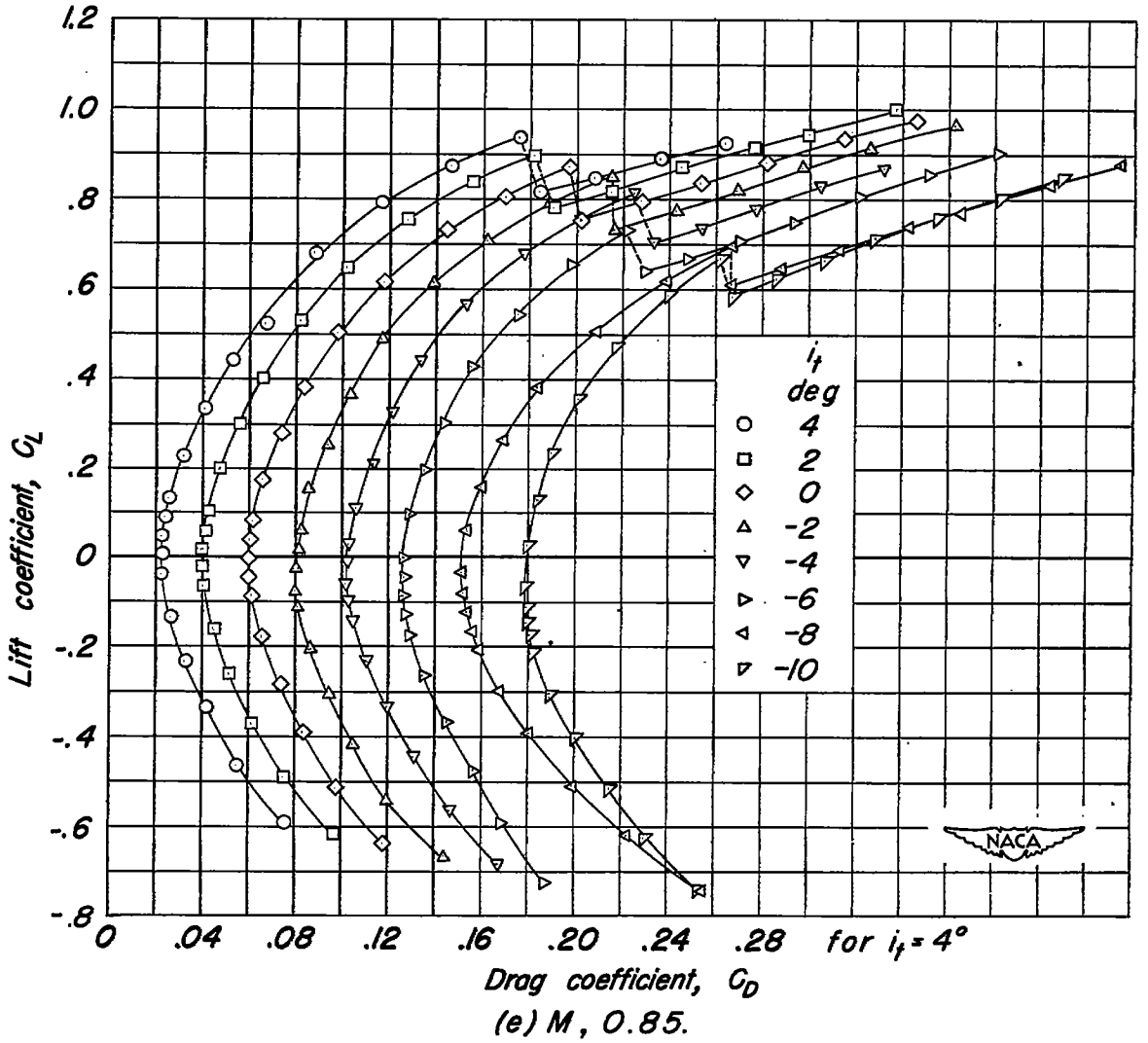

(e) M, 0.85.

Figure 11.— Continued.

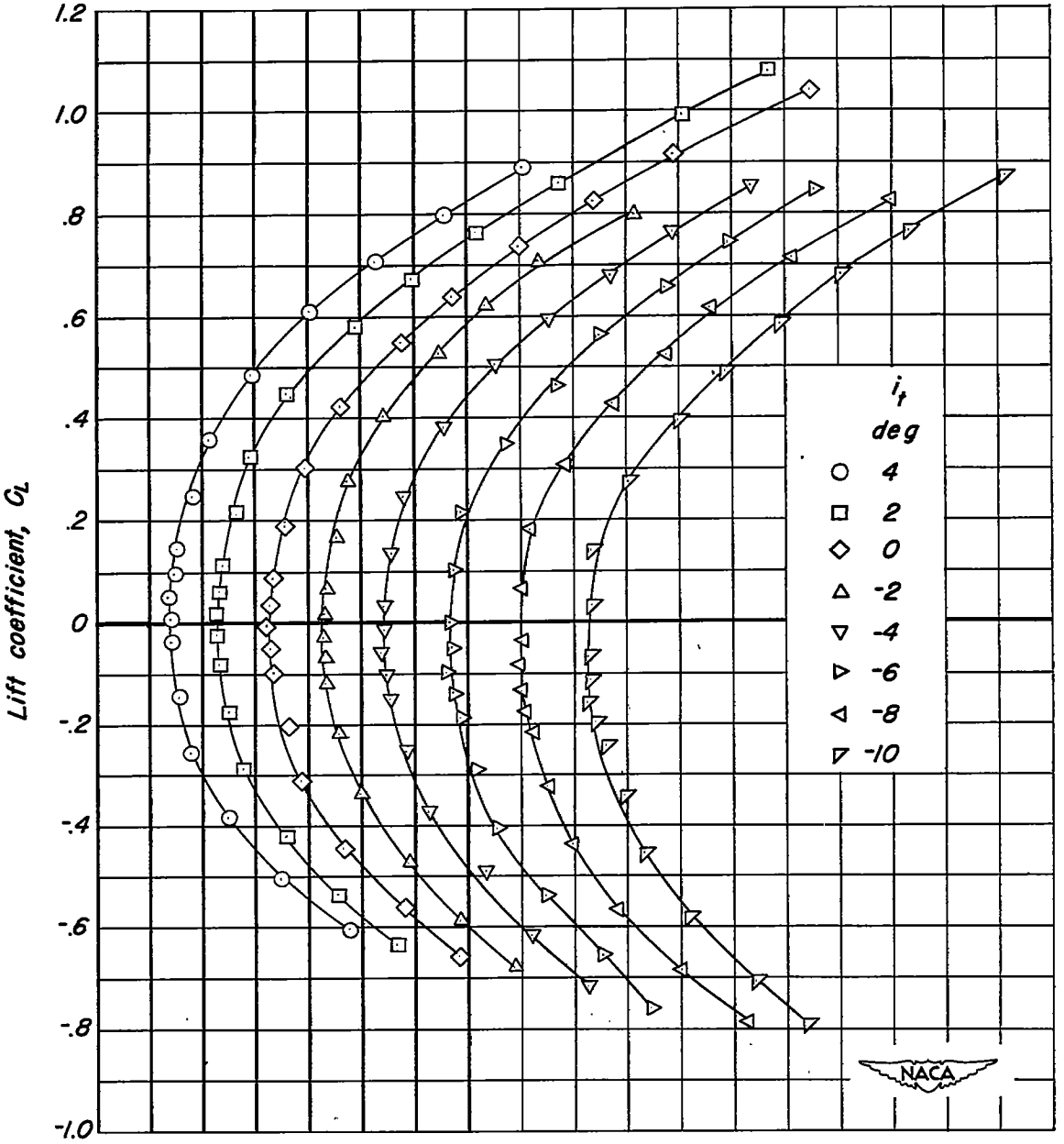

(f) M, 0.90.

Figure 11.— Continued.

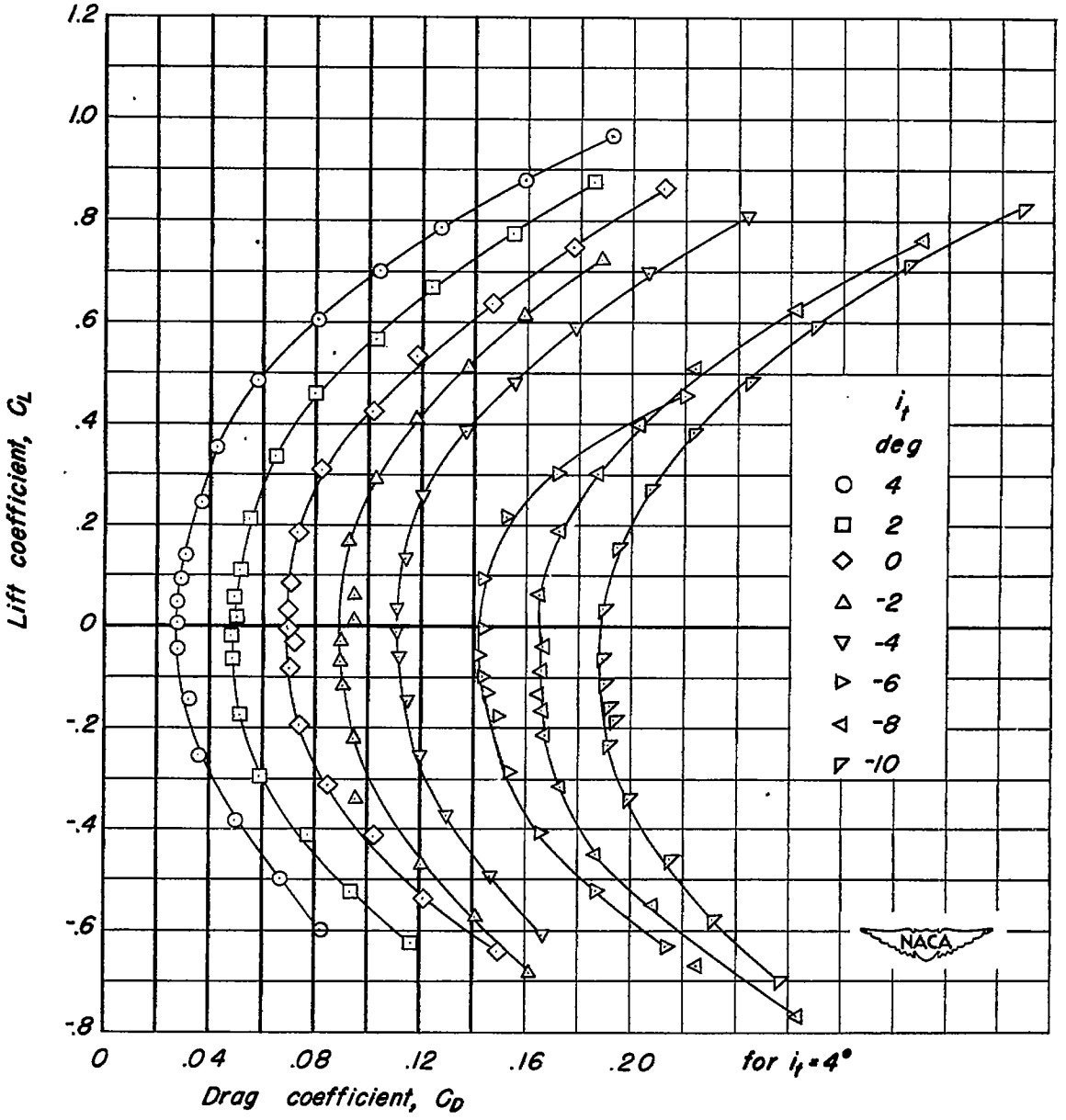

(g) M, 0.92.

Figure 11.- Continued.

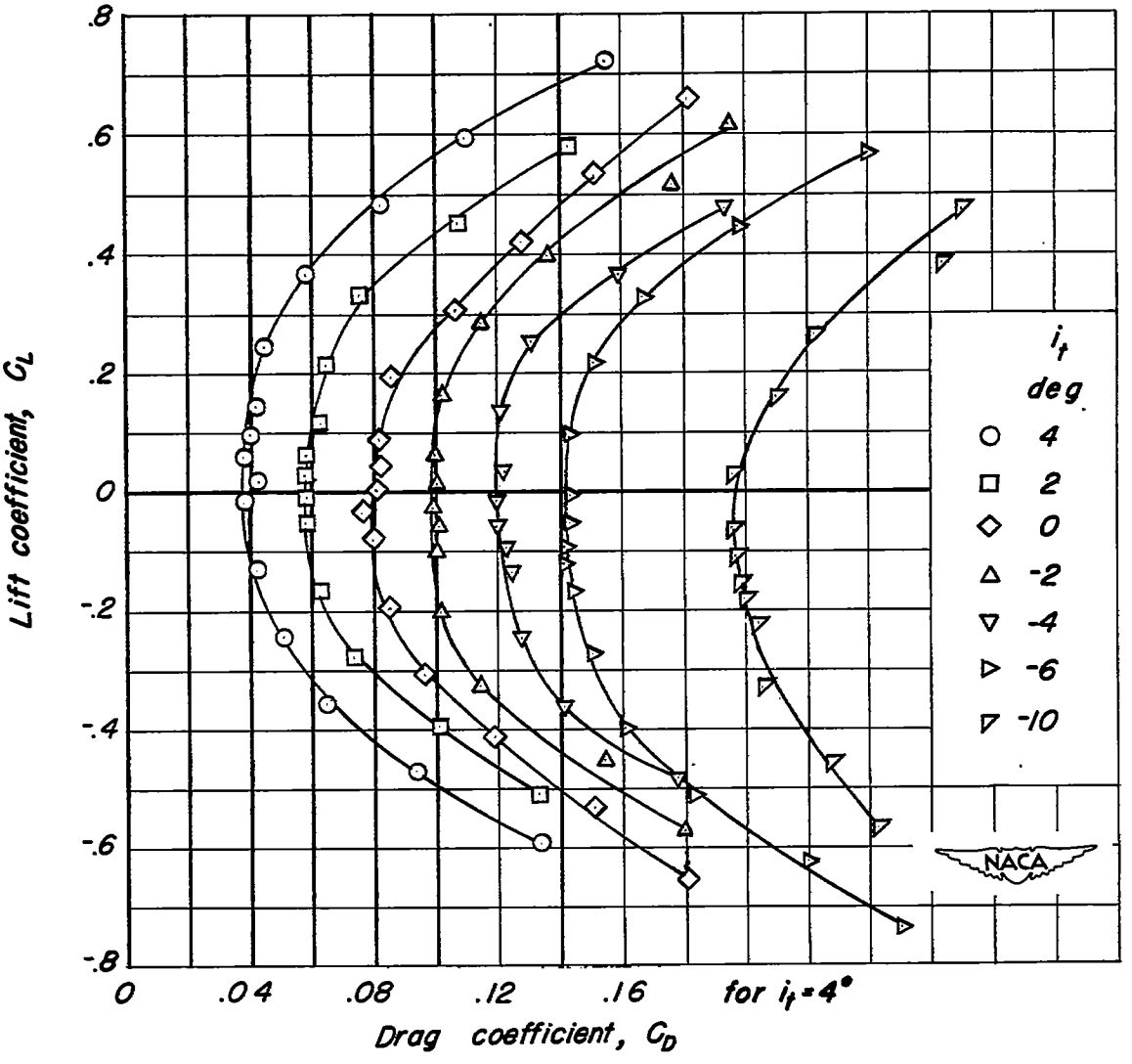

(h) M, 0.95.

Figure 11.— Concluded.

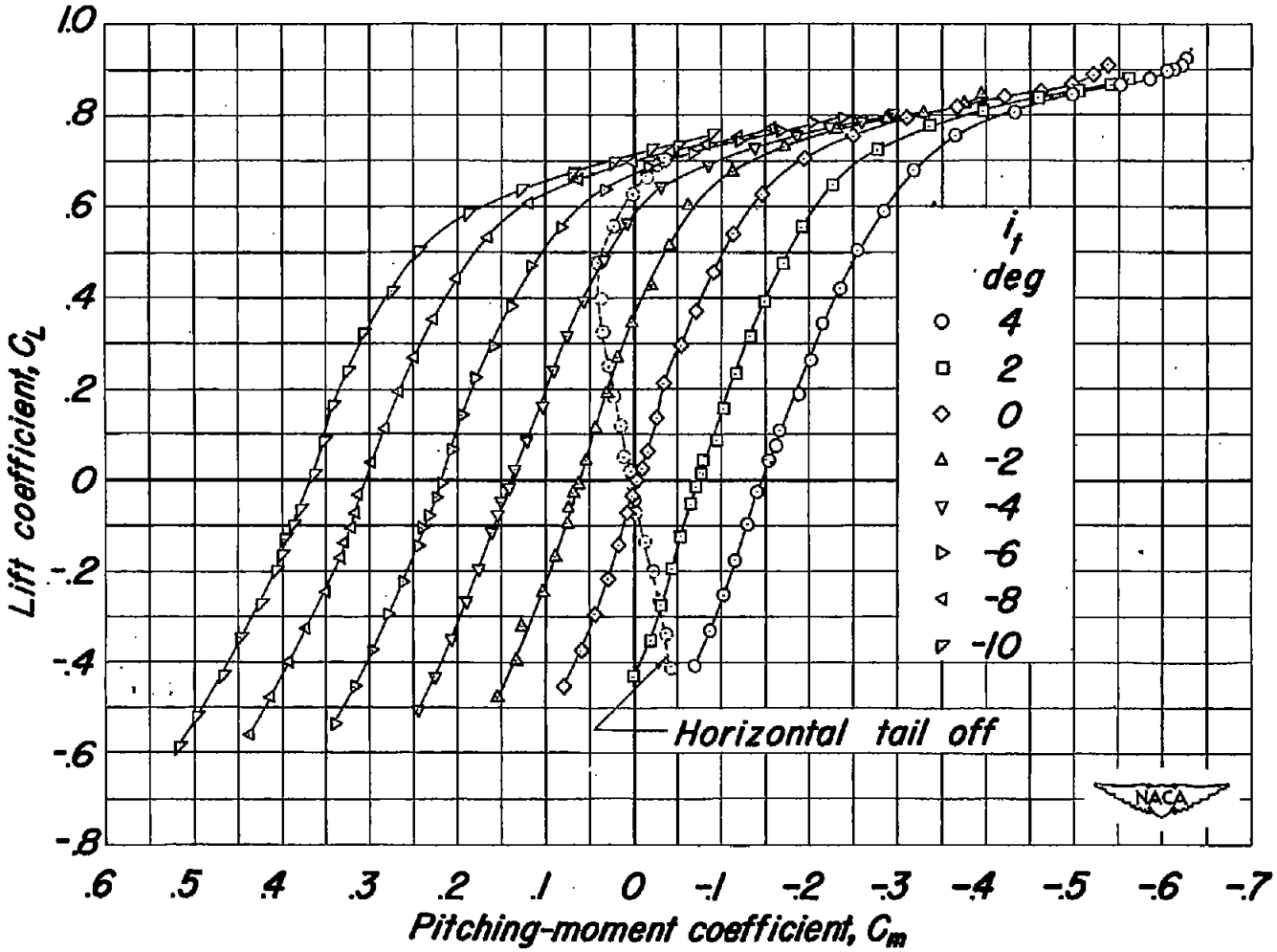

(a) M, 0.20.

Figure 12.- The pitching-moment characteristics of the airplane model with the horizontal tail mounted in the extended wing-chord plane. R, 2,000,000.

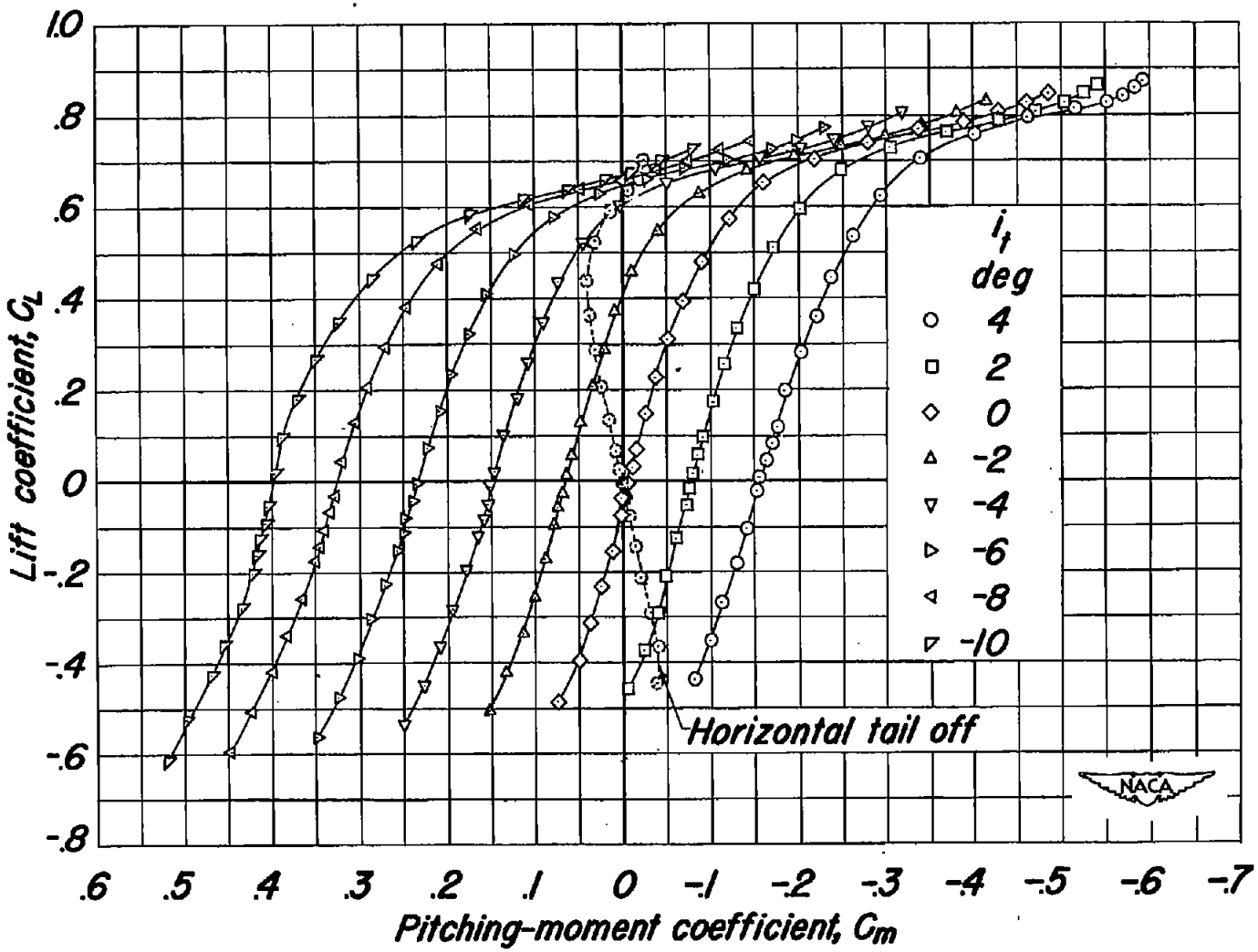

(b) M, 0.50.

Figure 12.- Continued.

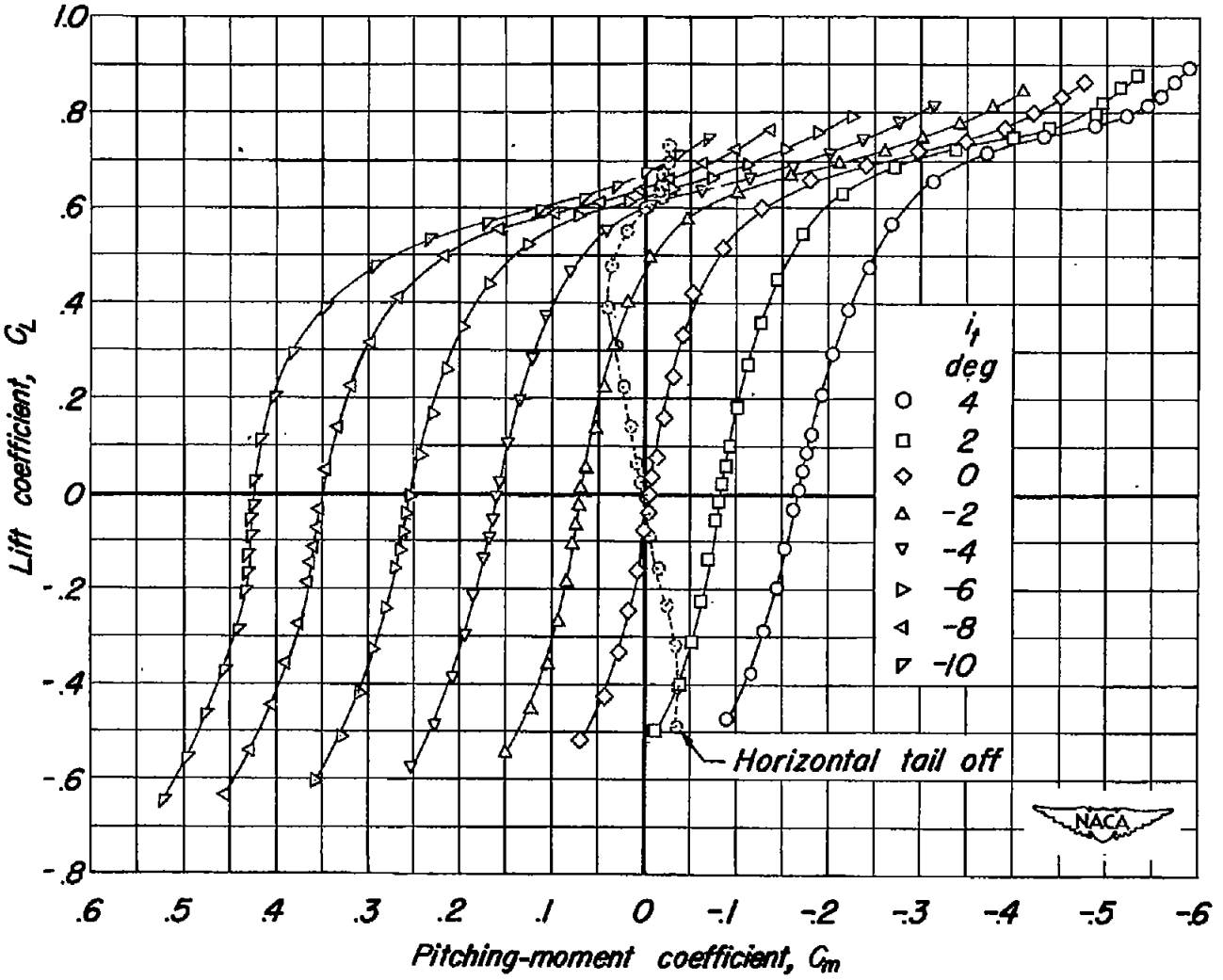

(c) M, 0.70.

Figure 12.- Continued.

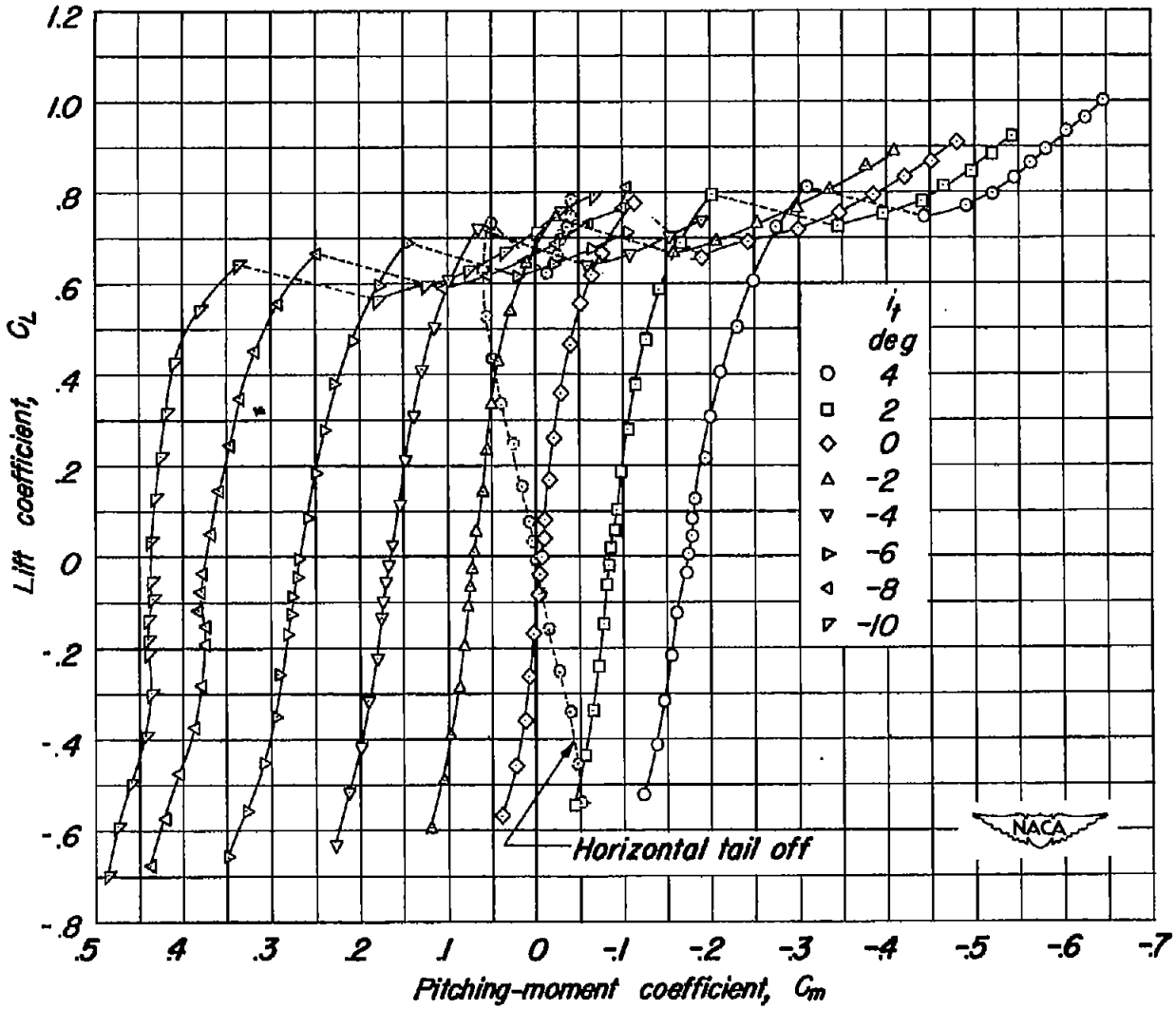

(d) M, 0.80.

Figure 12.- Continued.

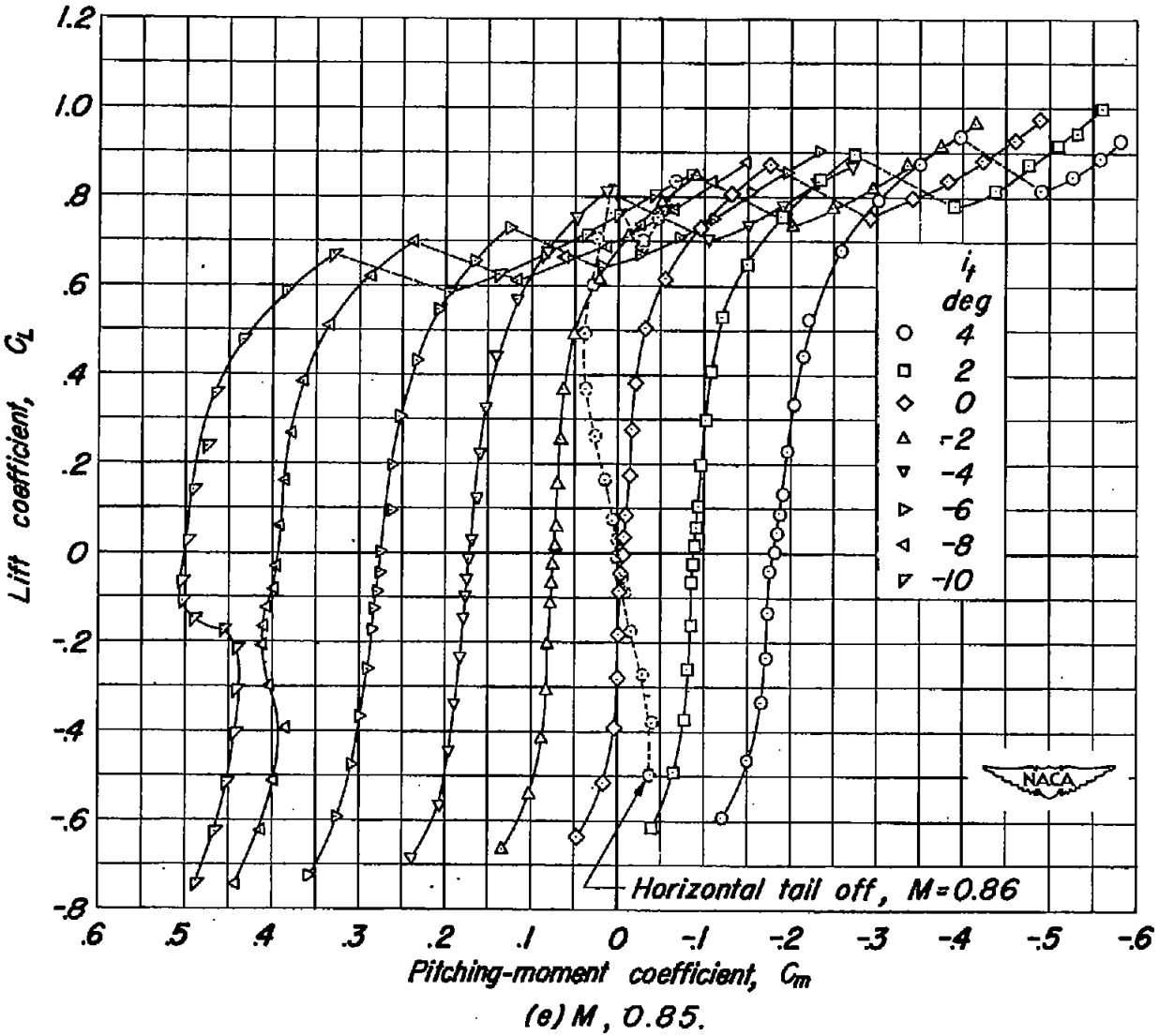

(e) M, 0.85.

Figure 12:- Continued.

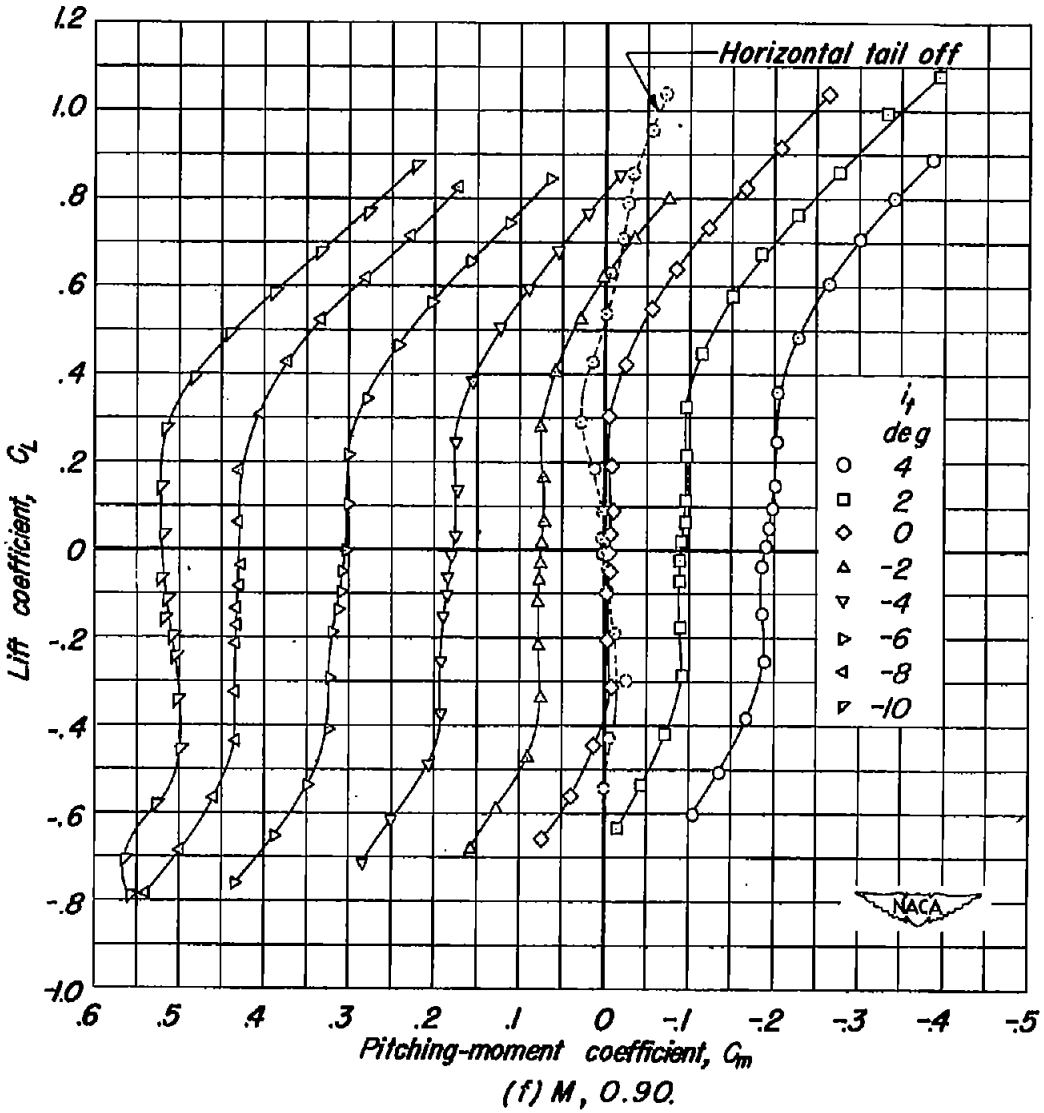

(f) M, 0.90.

Figure 12.— Continued.

CONFIDENTIAL

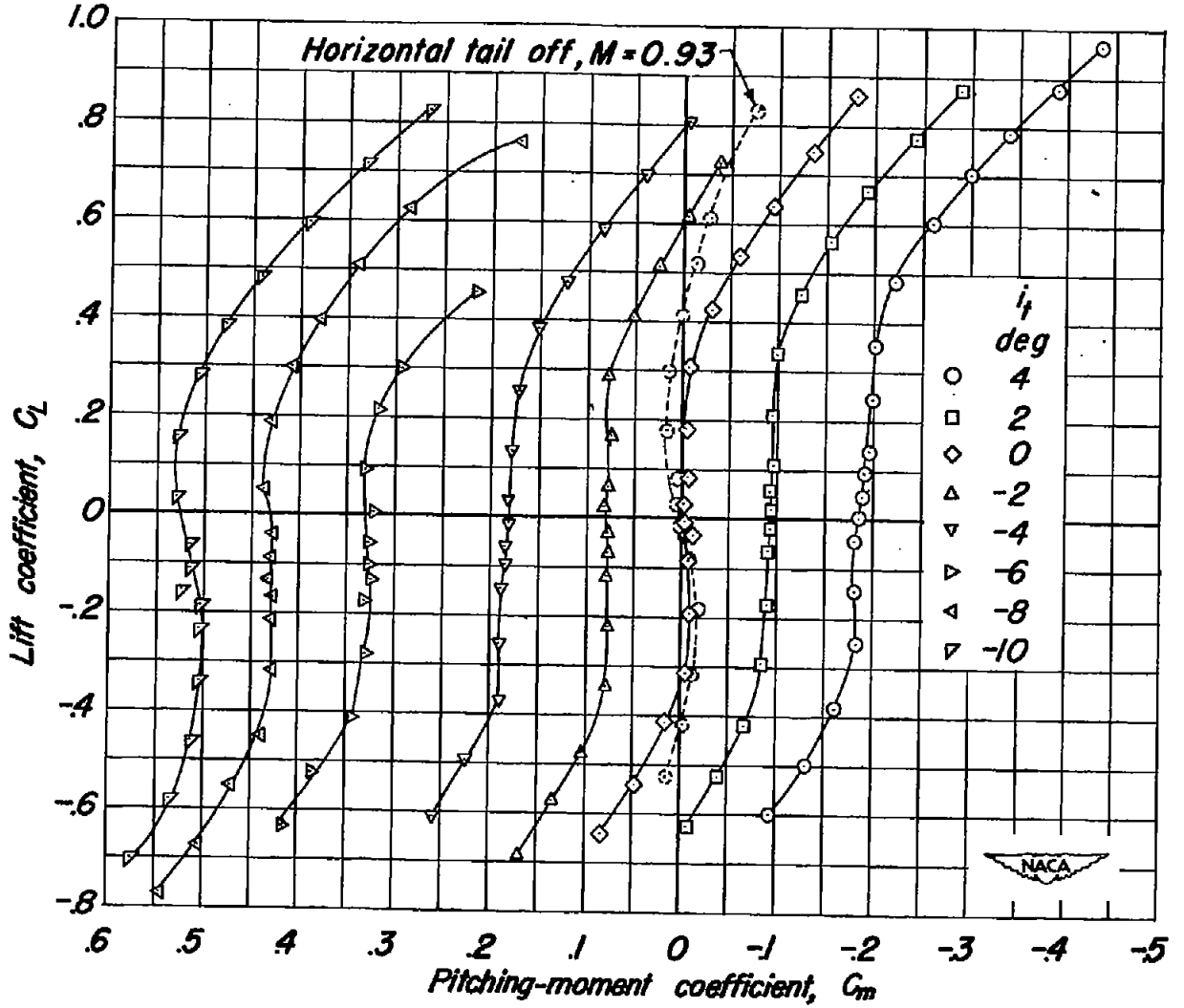

(g) M, 0.92.

Figure 12:— Continued.

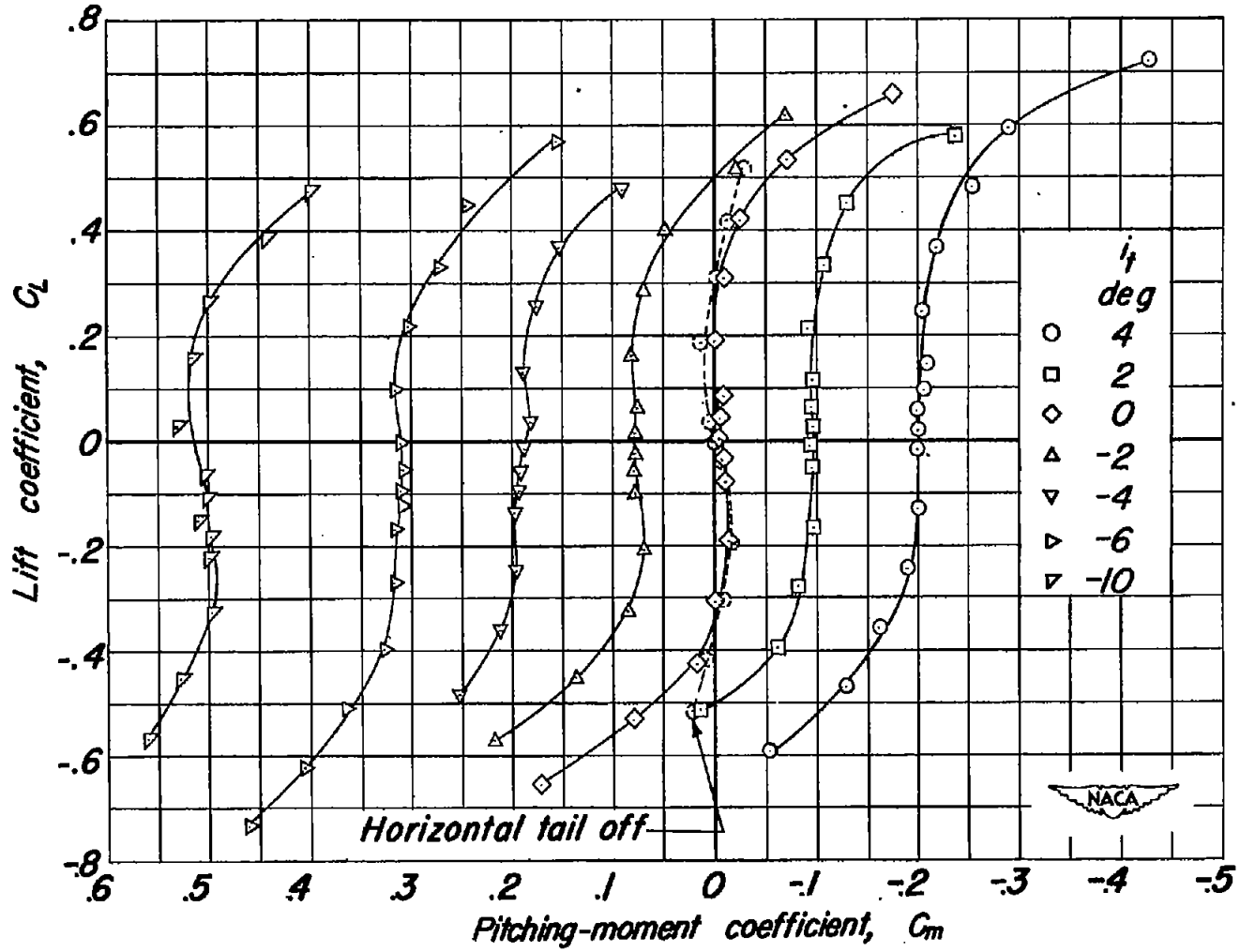

(h) M, 0.95.

Figure 12.— Concluded.

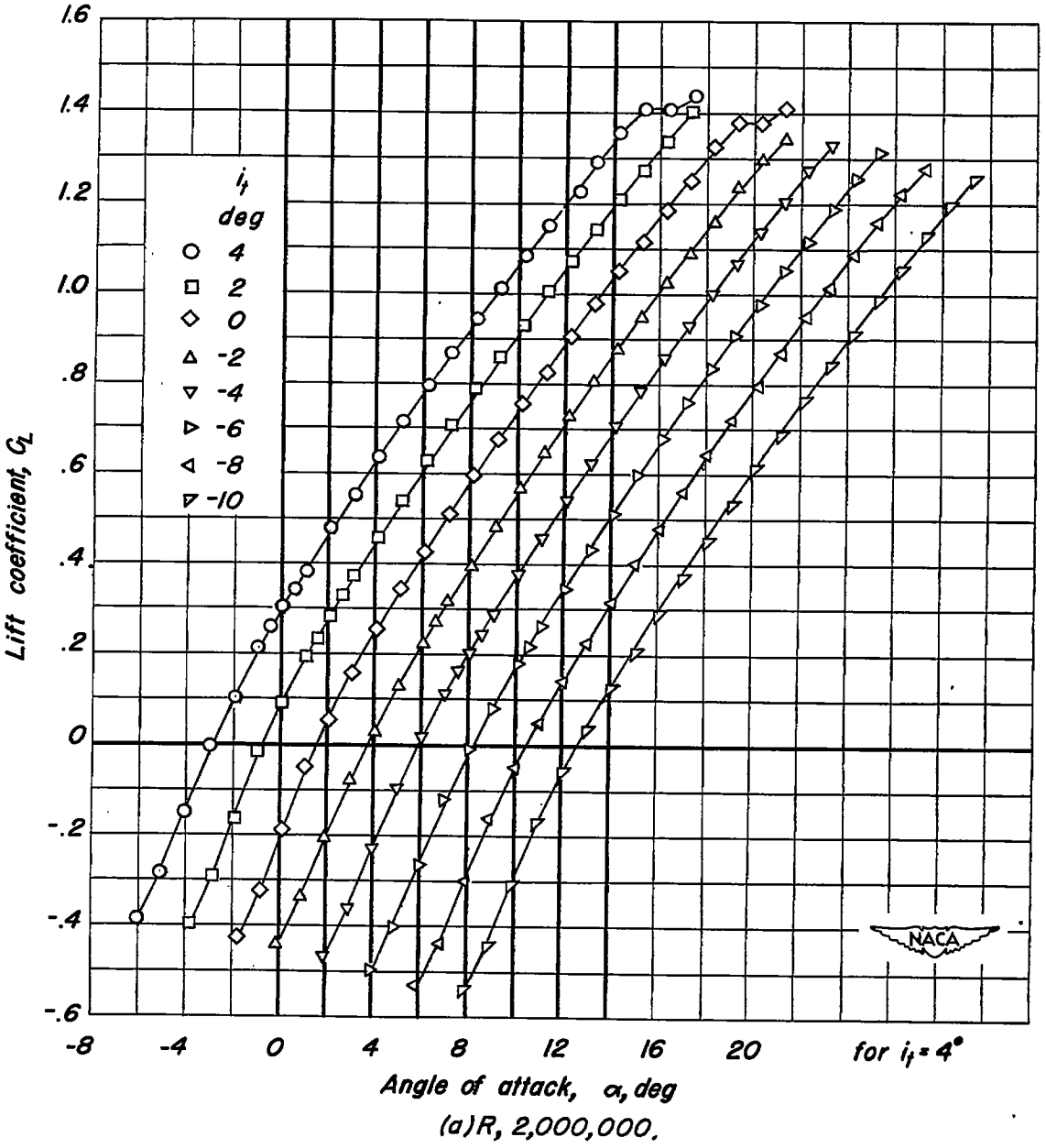

Figure 13.— The lift characteristics of the airplane model with the horizontal tail mounted in the extended wing-chord plane and with the flaps deflected. δ_n, 30°; δ_f, 50°; M, 0.20.

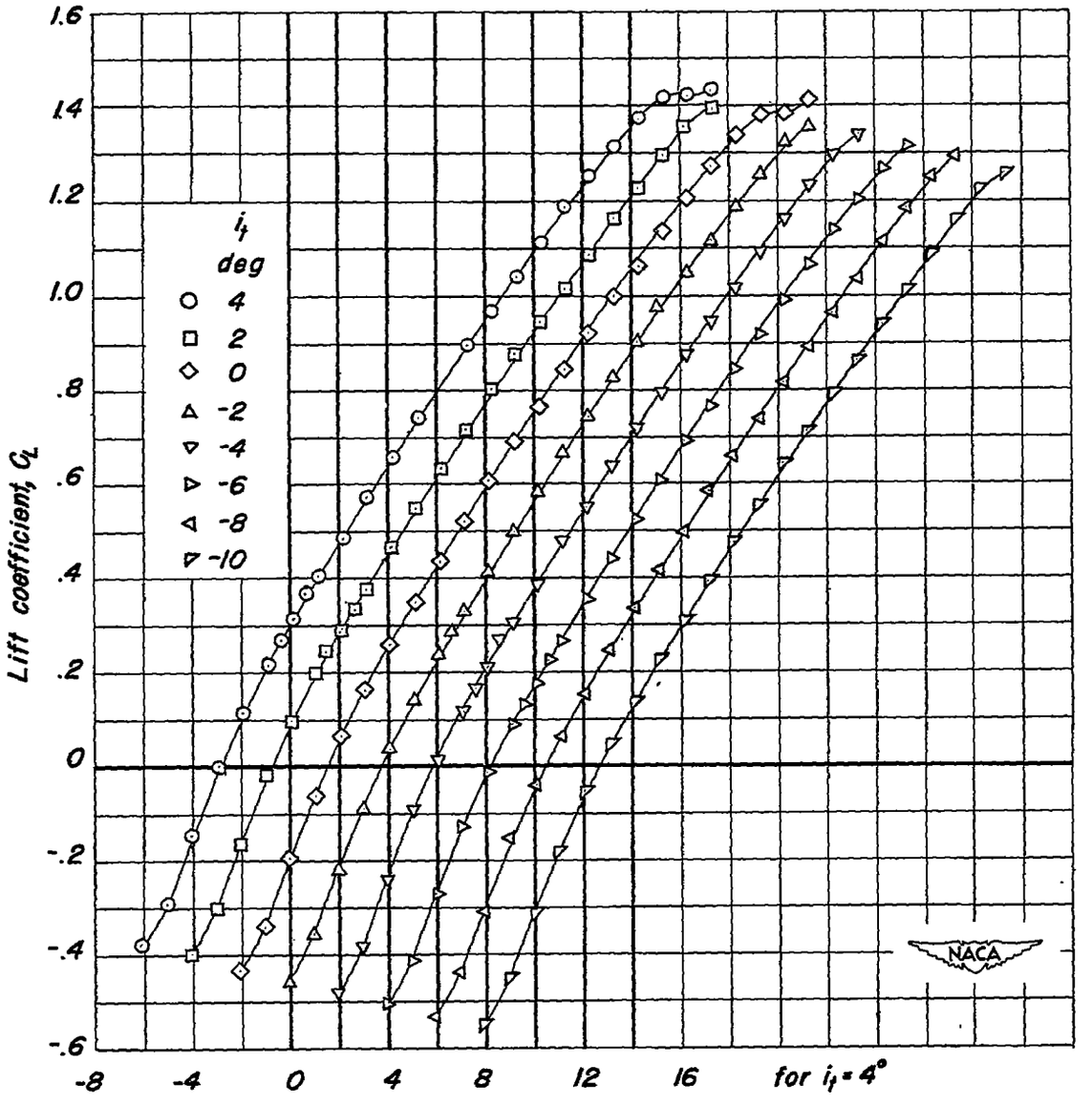

(b) R, 6,000,000.

Figure 13.- Continued.

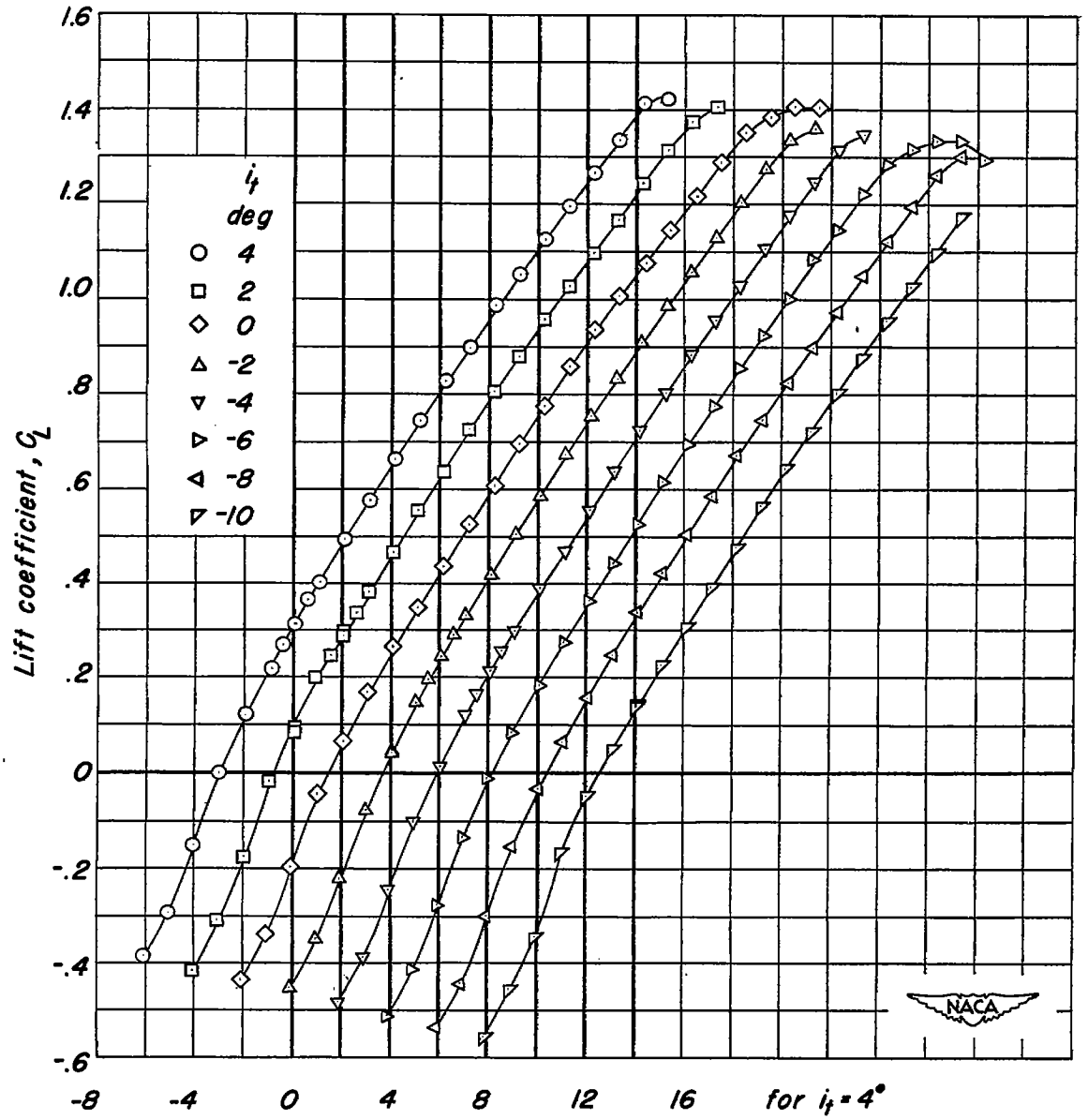

(c) R, 10,000,000.

Figure 13.— Concluded.

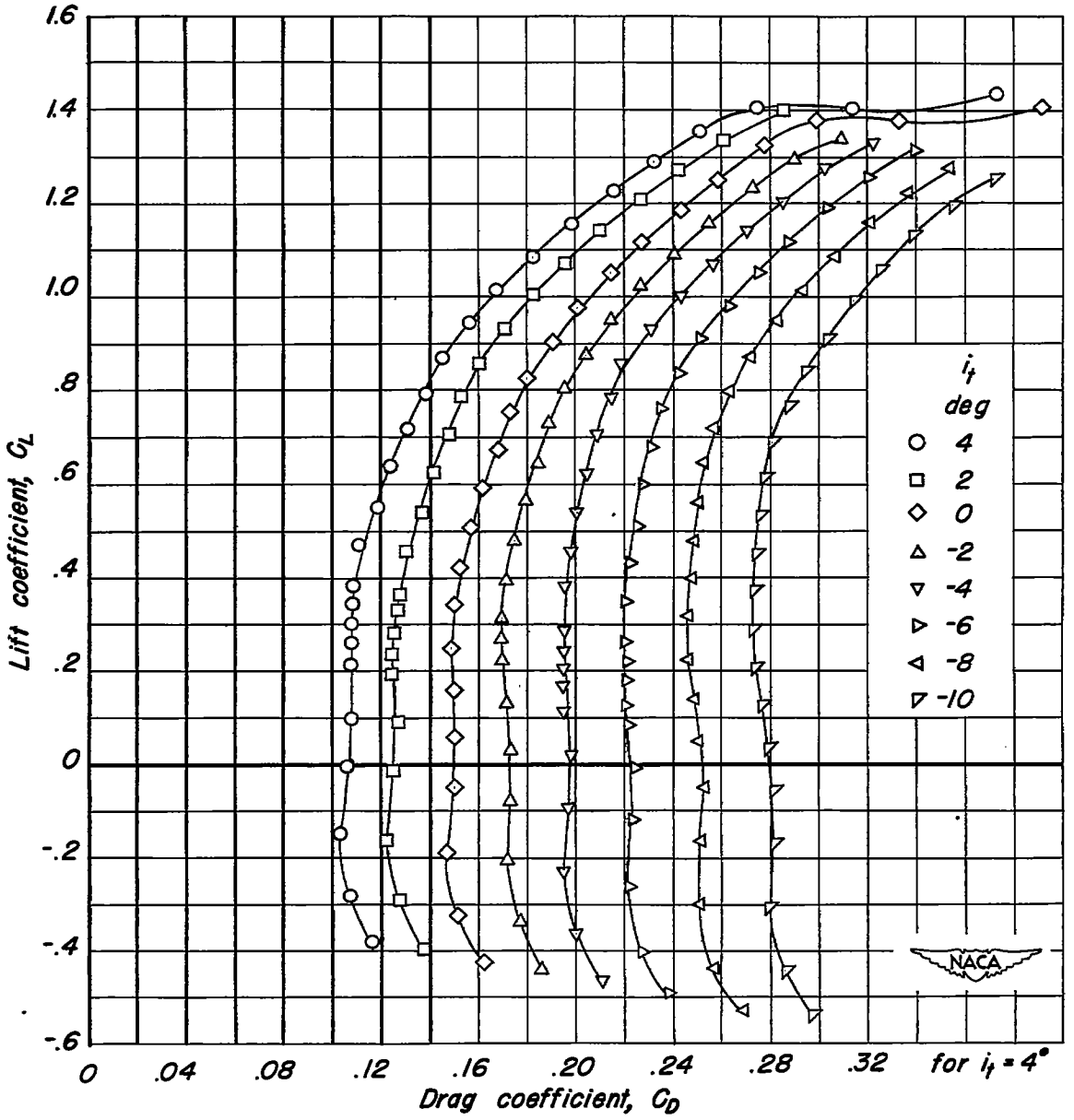

(a) R, 2,000,000.

Figure 14.— The drag characteristics of the airplane model with the horizontal tail mounted in the extended wing-chord plane with the flaps deflected. δ_n, 30°; δ_f, 50°; M, 0.20.

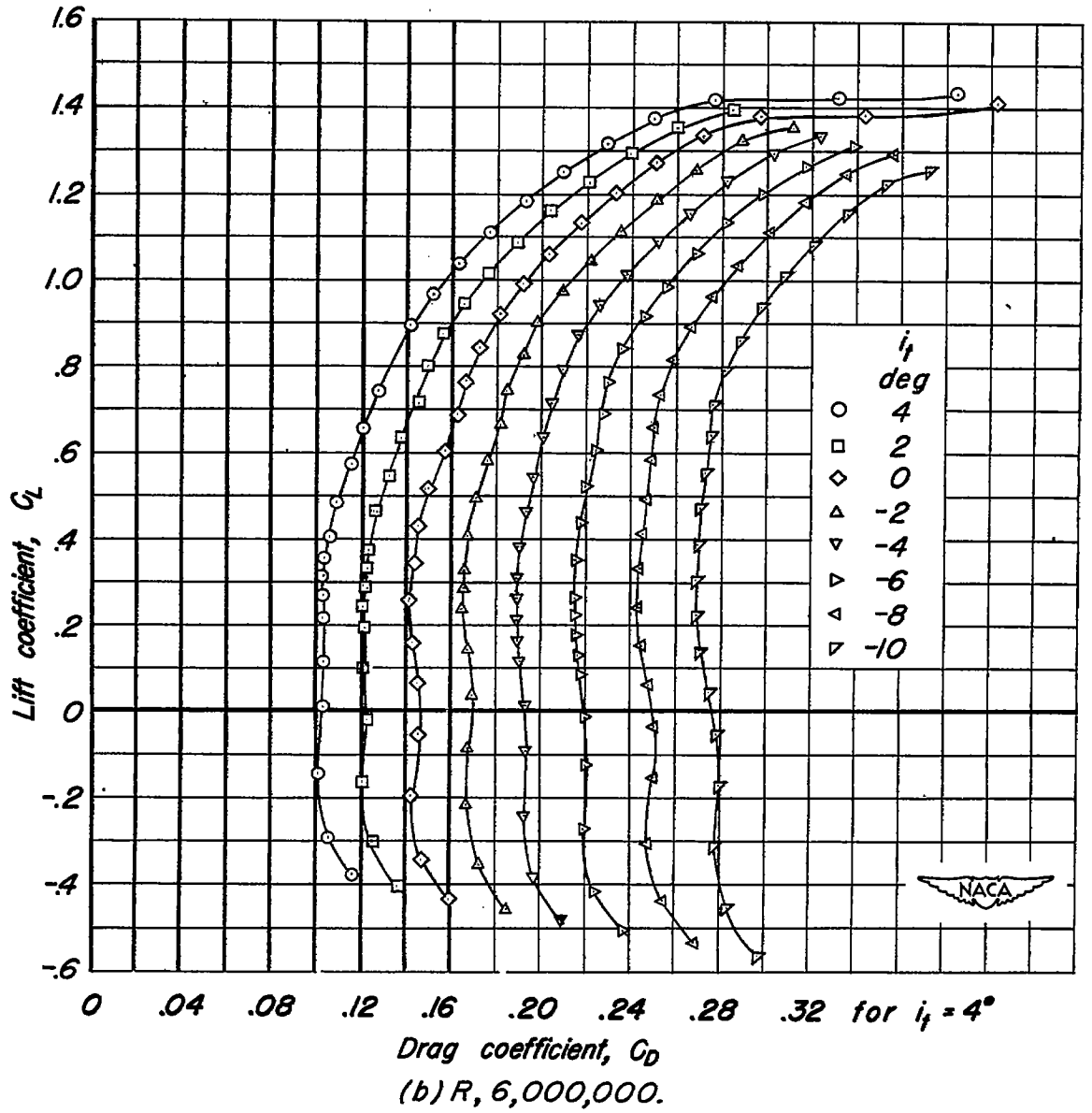

(b) R, 6,000,000.

Figure 14.- Continued.

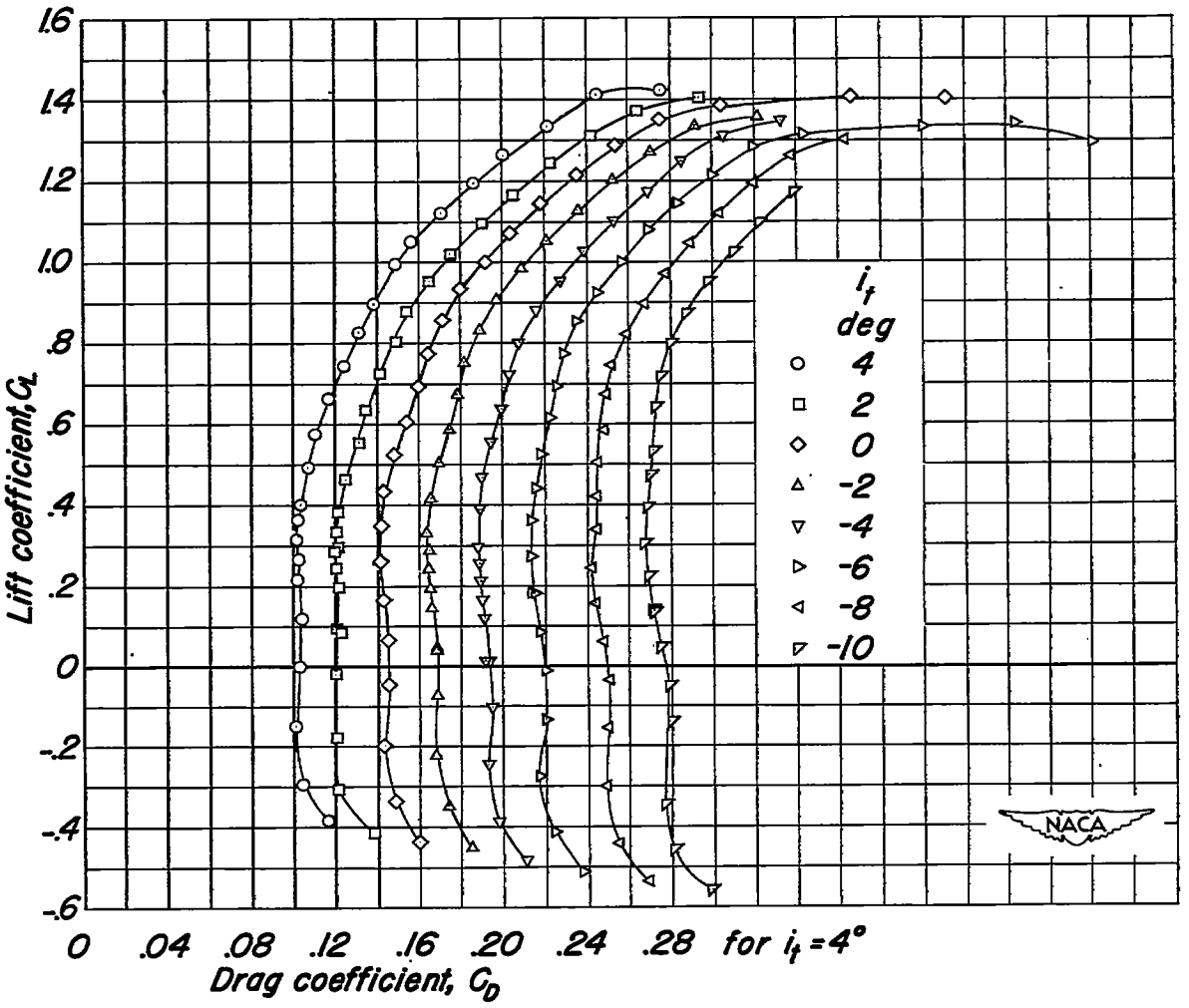

(c) R, 10,000,000.

Figure 14.- Concluded.

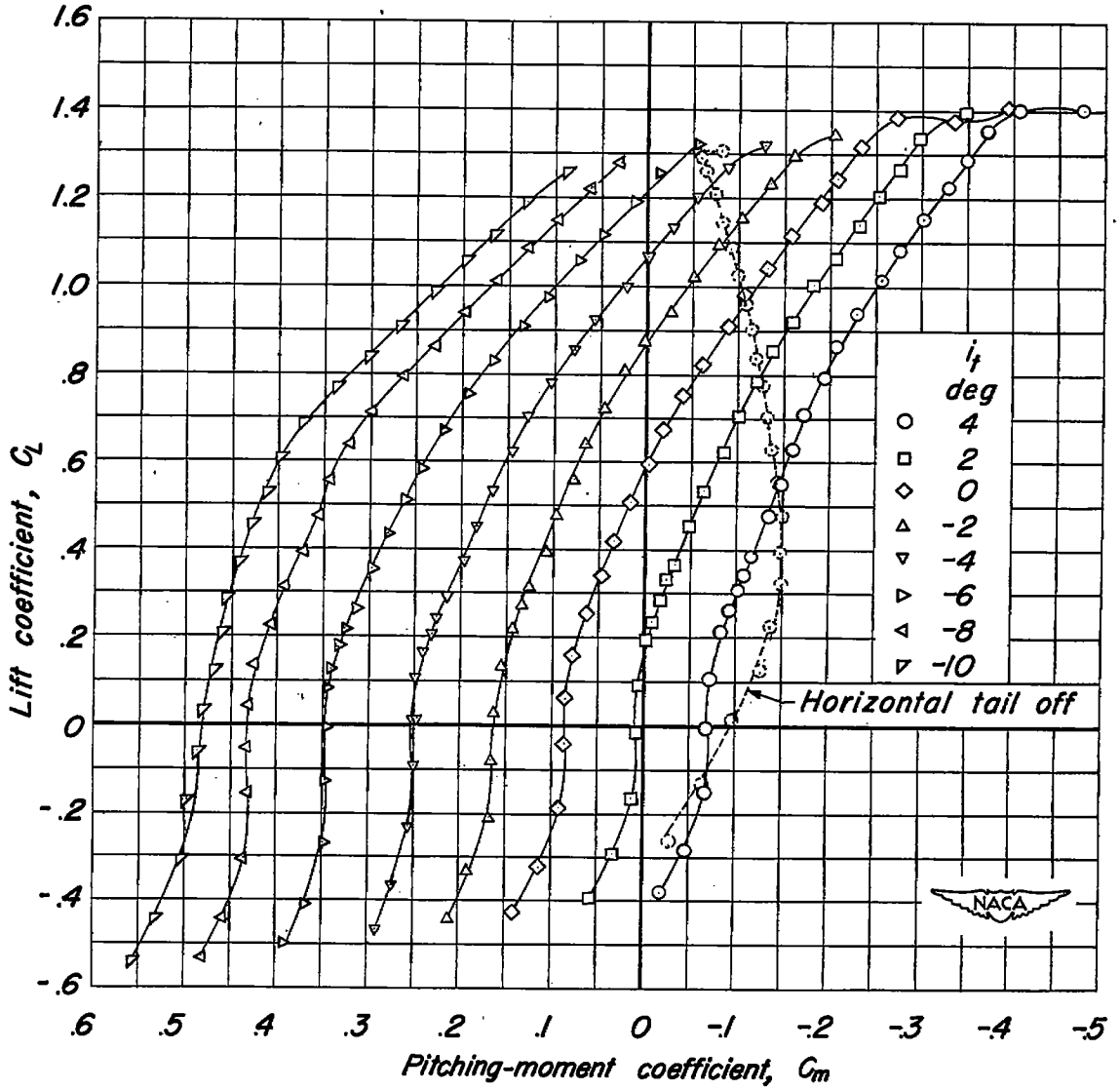

(a) R, 2,000,000.

Figure 15.- The pitching-moment characteristics of the airplane model with the horizontal tail mounted in the extended wing-chord plane and with the flaps deflected. δ_n, 30°; δ_f, 50°; M, 0.20.

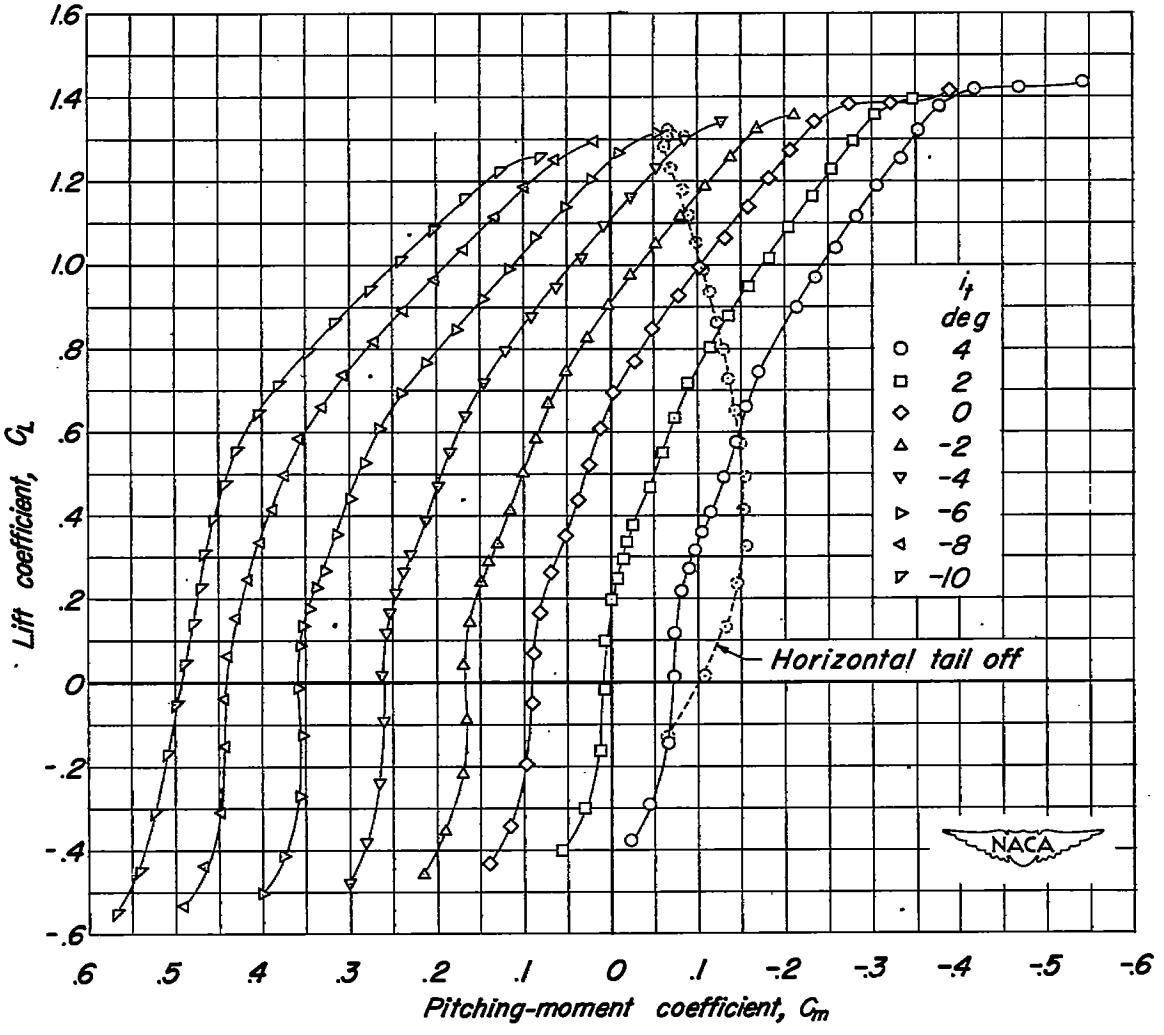

(b) R, 6,000,000.

Figure 15.— Continued.

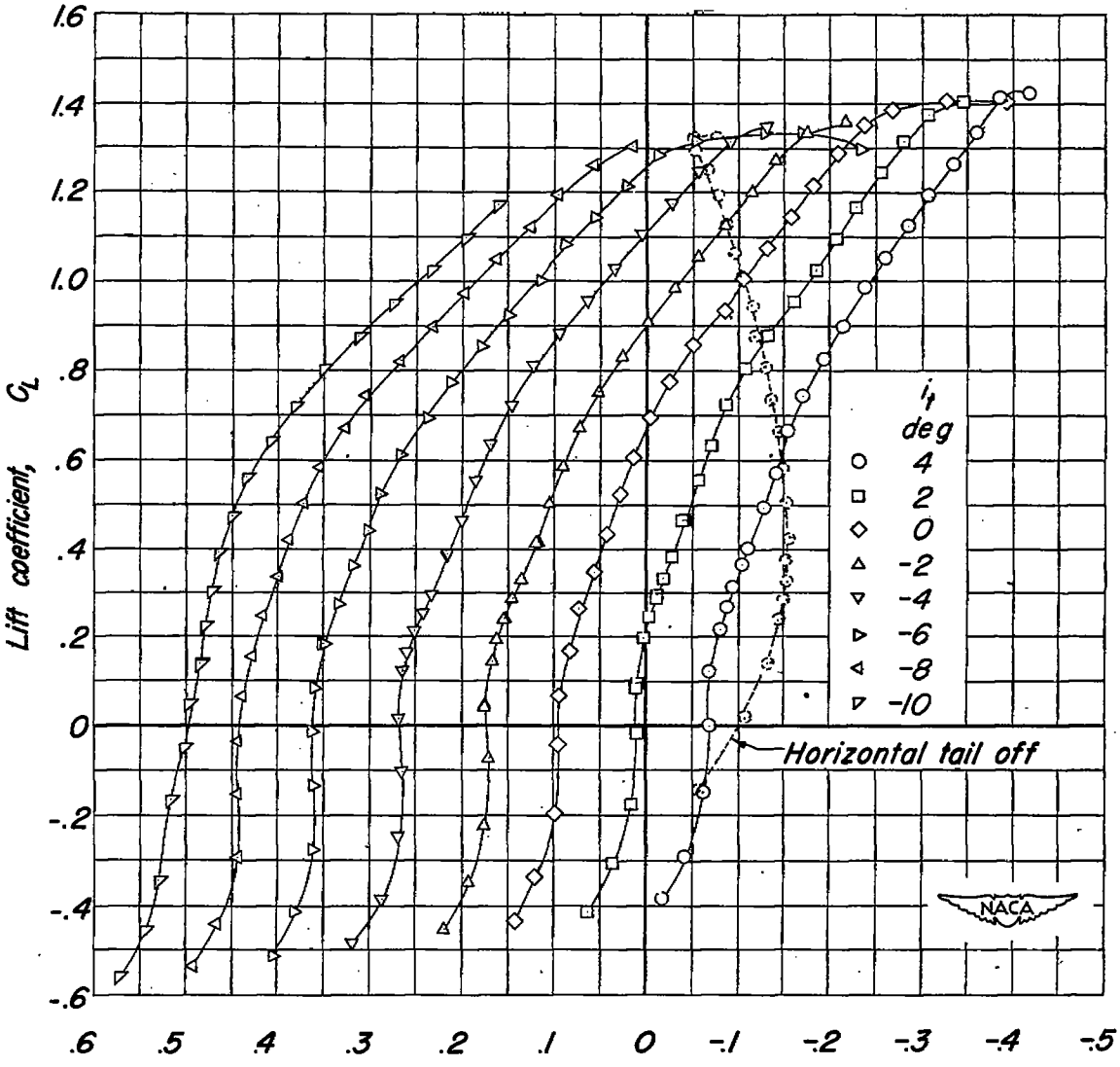

(c) R, 10,000,000.

Figure 15.— Concluded.

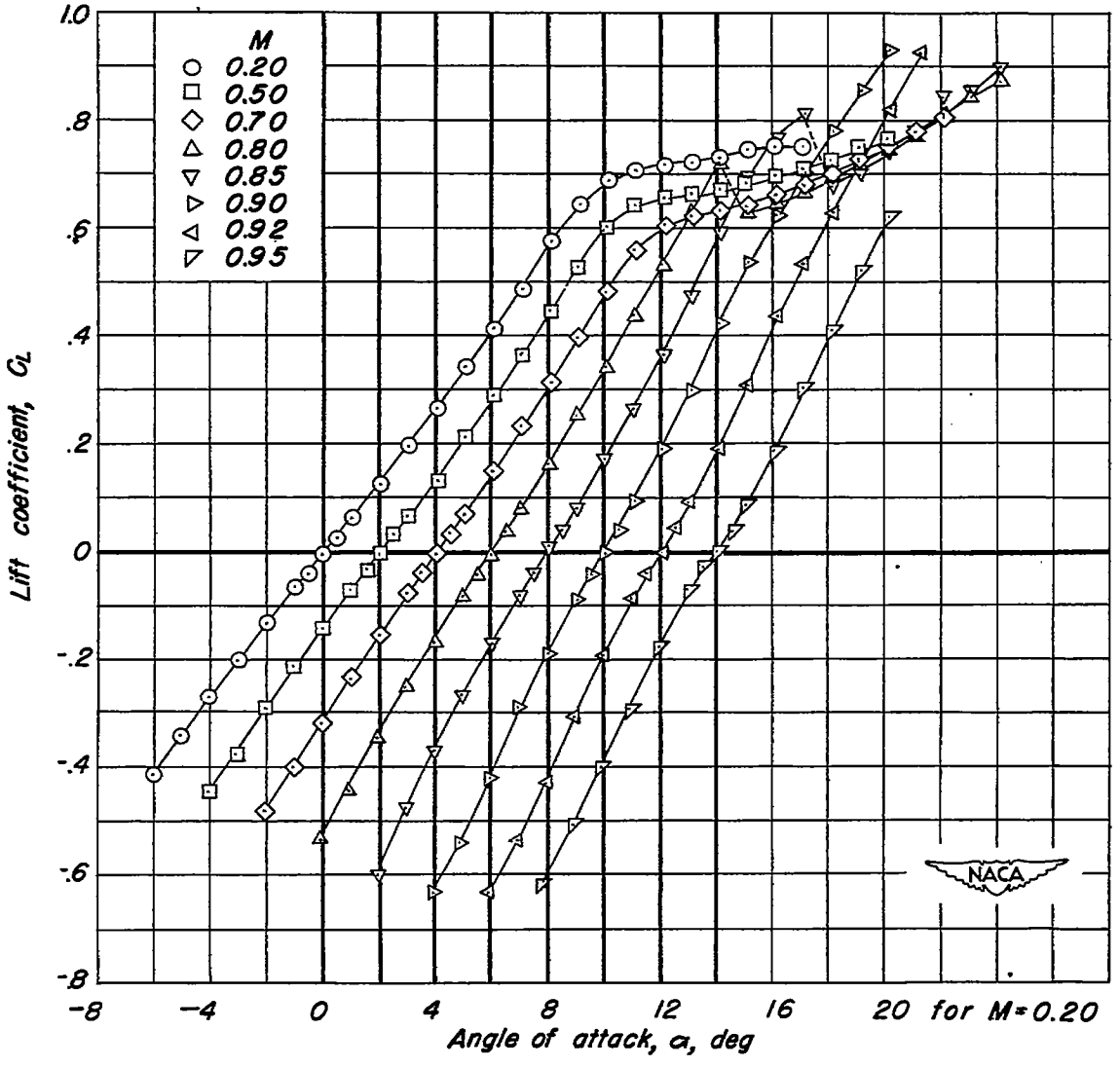

Figure 16.— The lift characteristics of the wing and fuselage with the bracket for mounting the horizontal tail above the fuselage. R, 2,000,000.

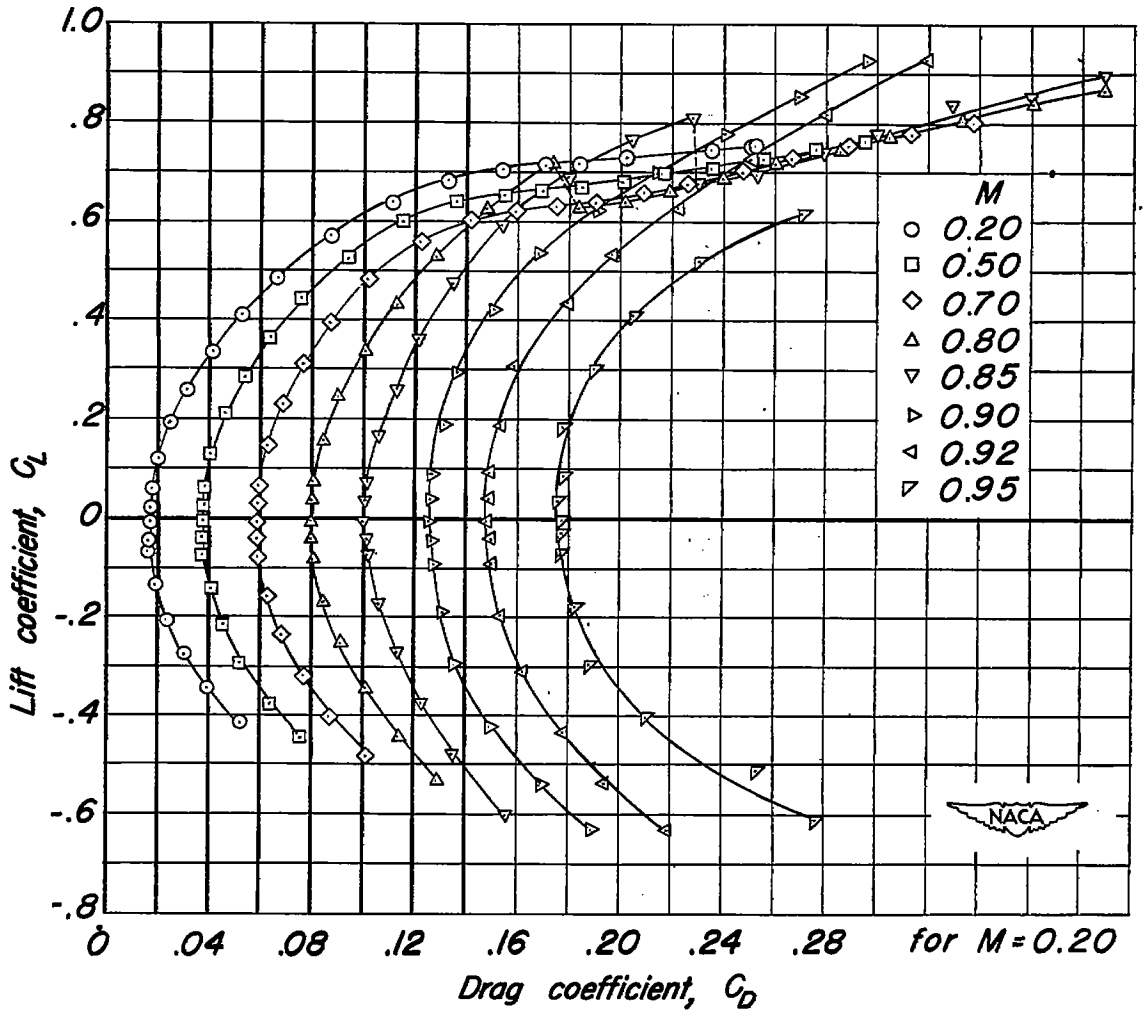

Figure 17.- The drag characteristics of the wing and fuselage with the bracket for mounting the horizontal tail above the fuselage. R, 2,000,000.

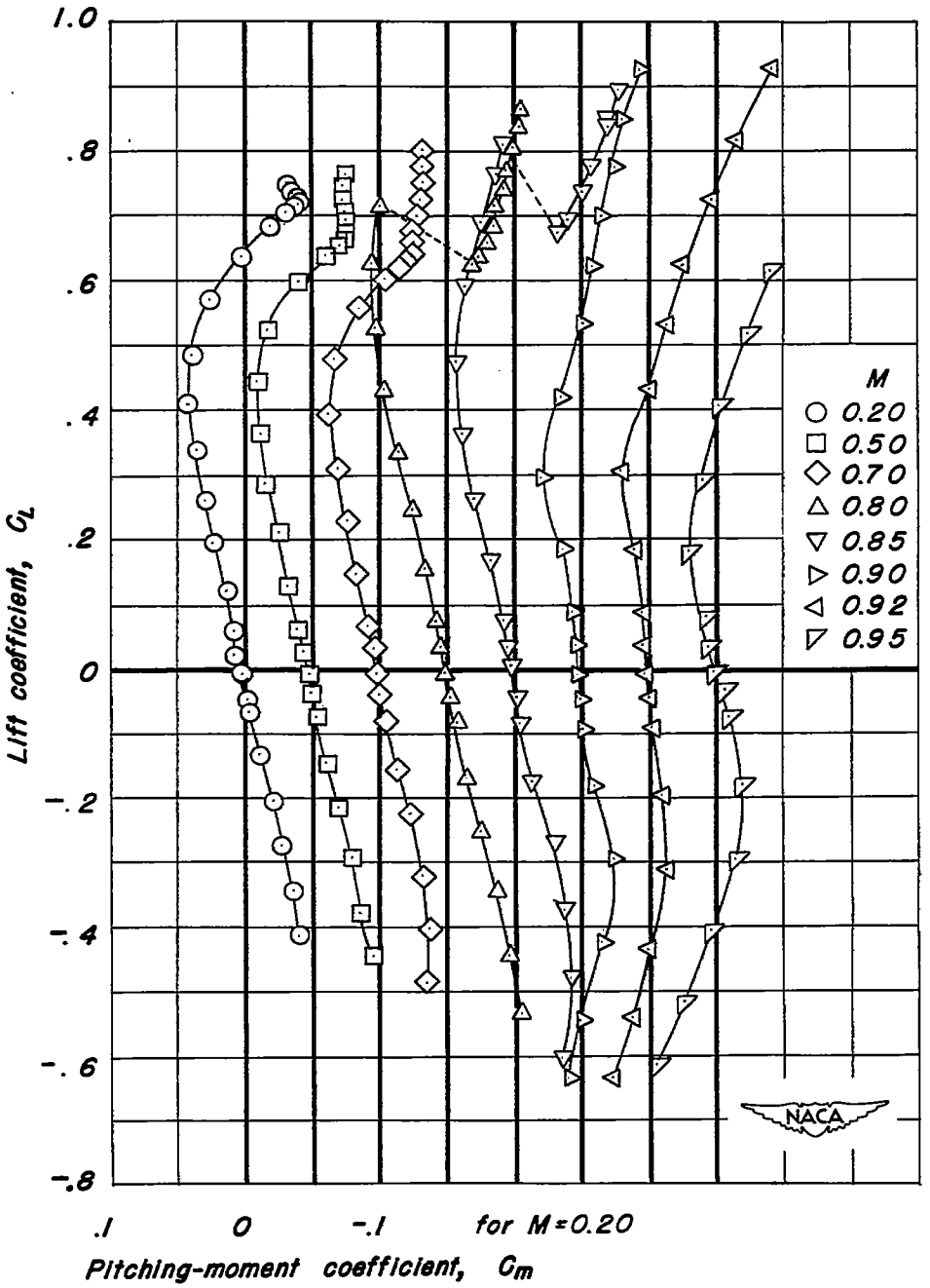

Figure 18.— The pitching-moment characteristics of the wing and fuselage with the bracket for mounting the horizontal tail above the fuselage. R, 2,000,000.

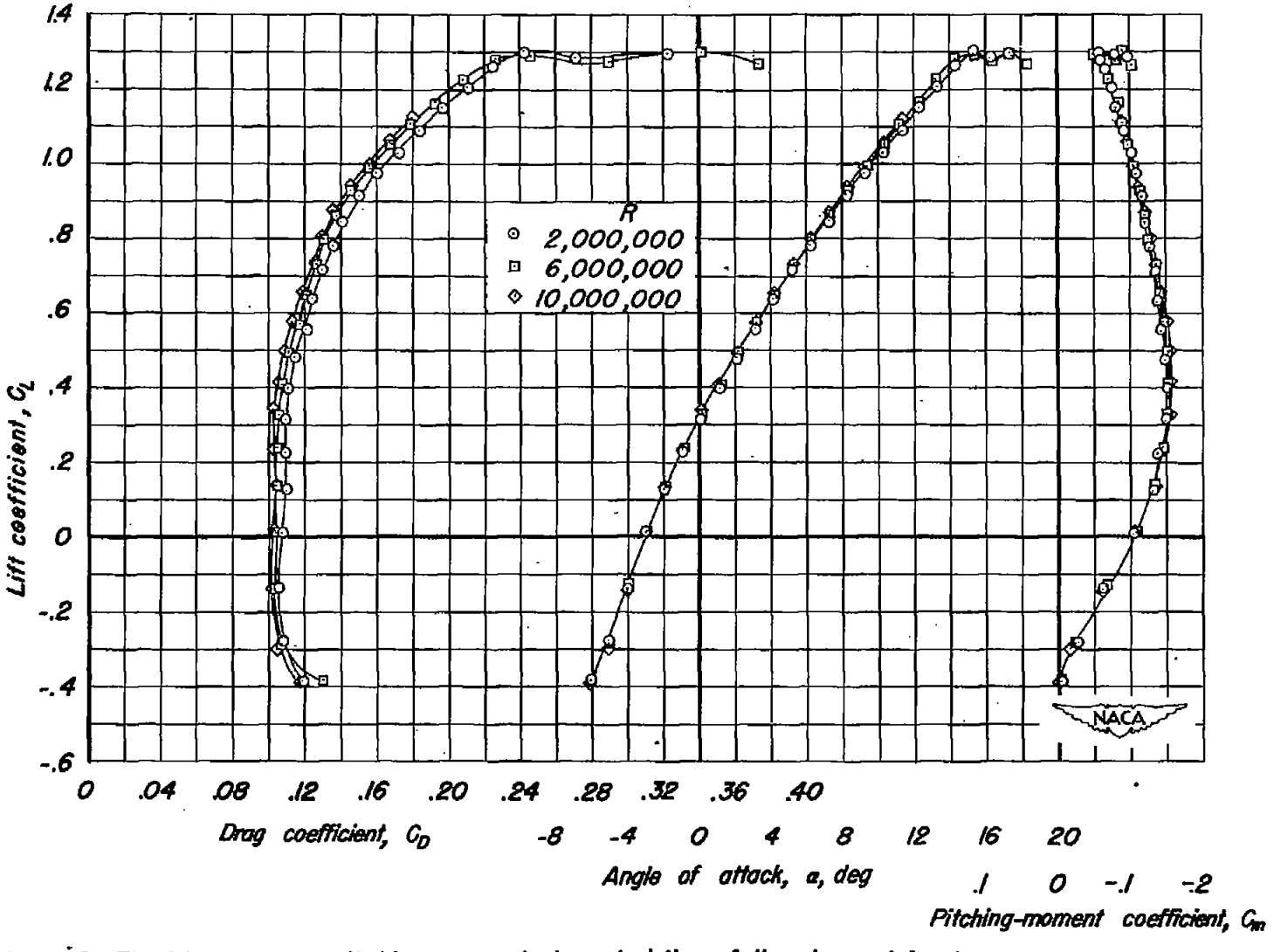

Figure 19.- The lift, drag, and pitching-moment characteristics of the wing and fuselage with the bracket for mounting the horizontal tail above the fuselage, flaps deflected δ_f, 30°; δ_n, 50°; M, 0.20.

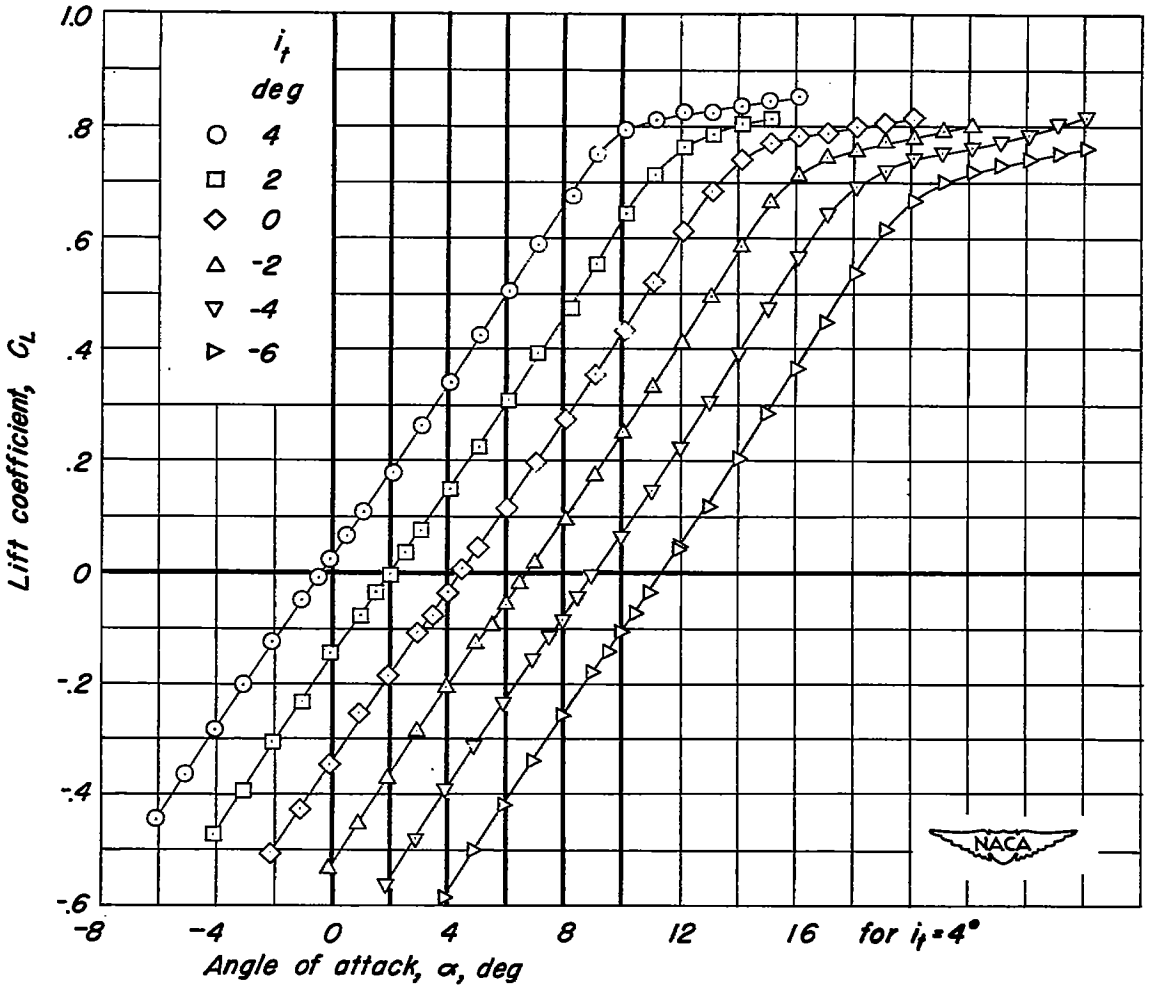

(a) M , 0.20.

Figure 20.— The lift characteristics of the airplane model with the horizontal tail mounted above the fuselage. R, 2,000,000.

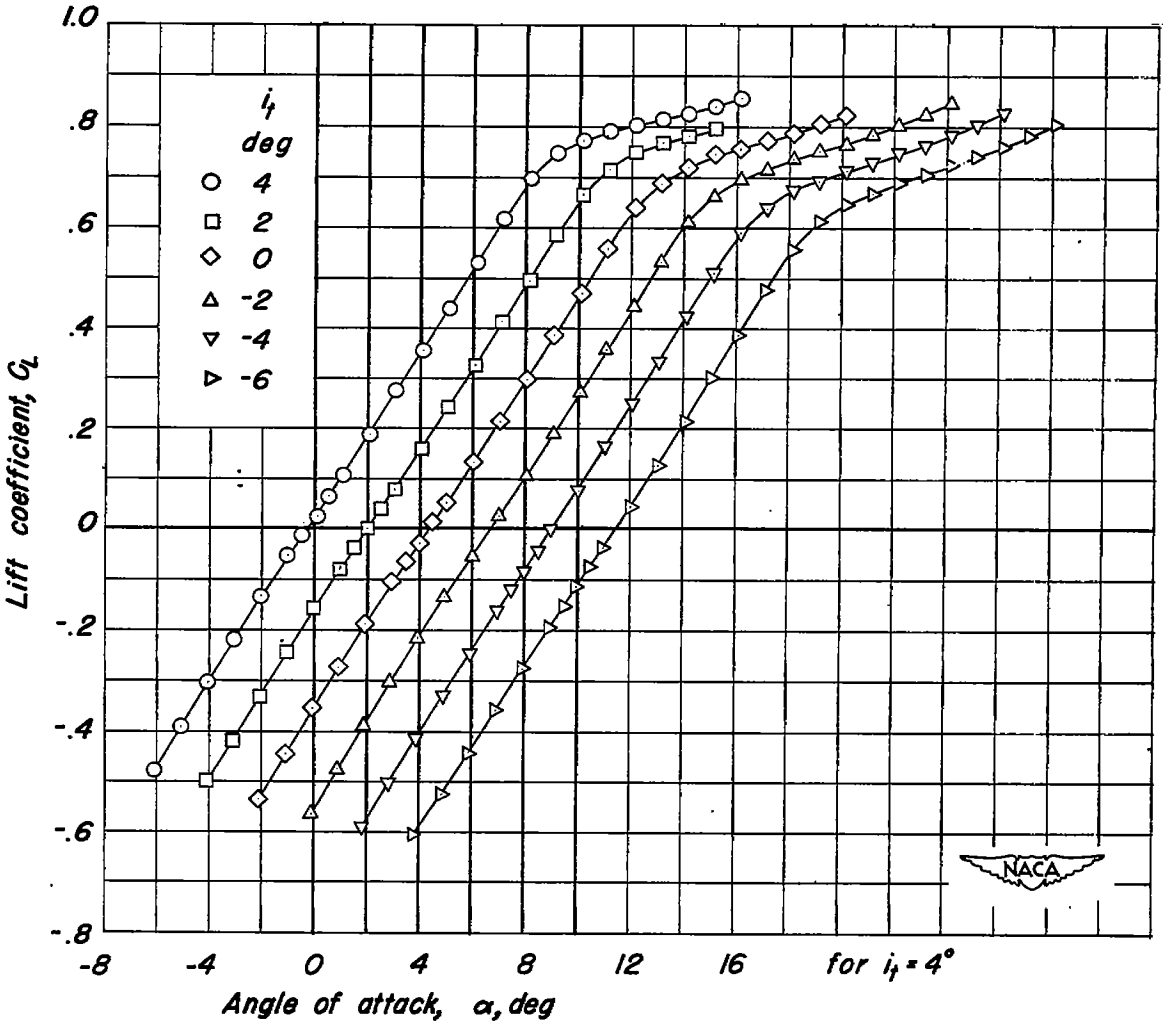

(b) M, 0.50.

Figure 20.— Continued.

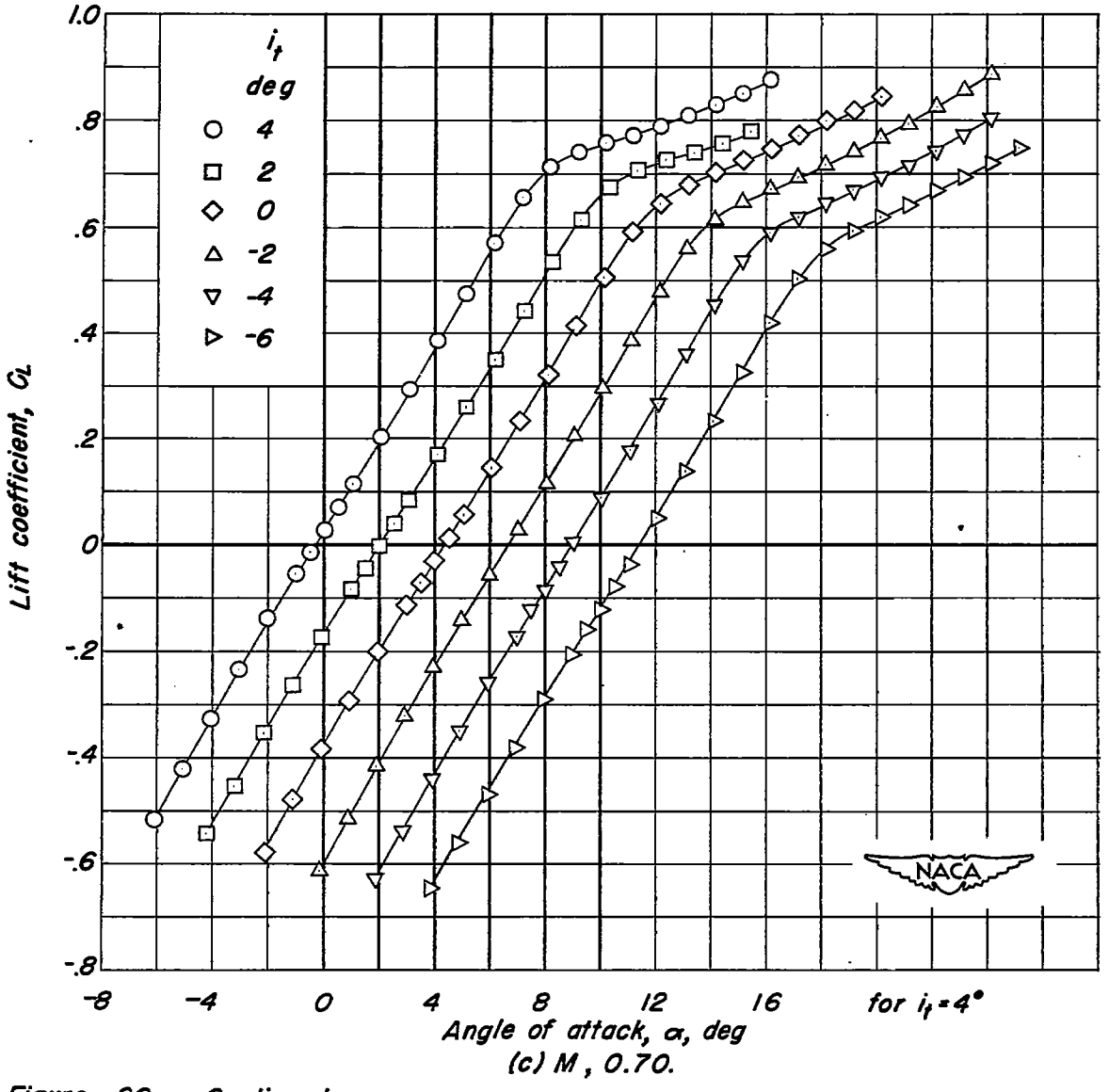

(c) M, 0.70.

Figure 20.— Continued.

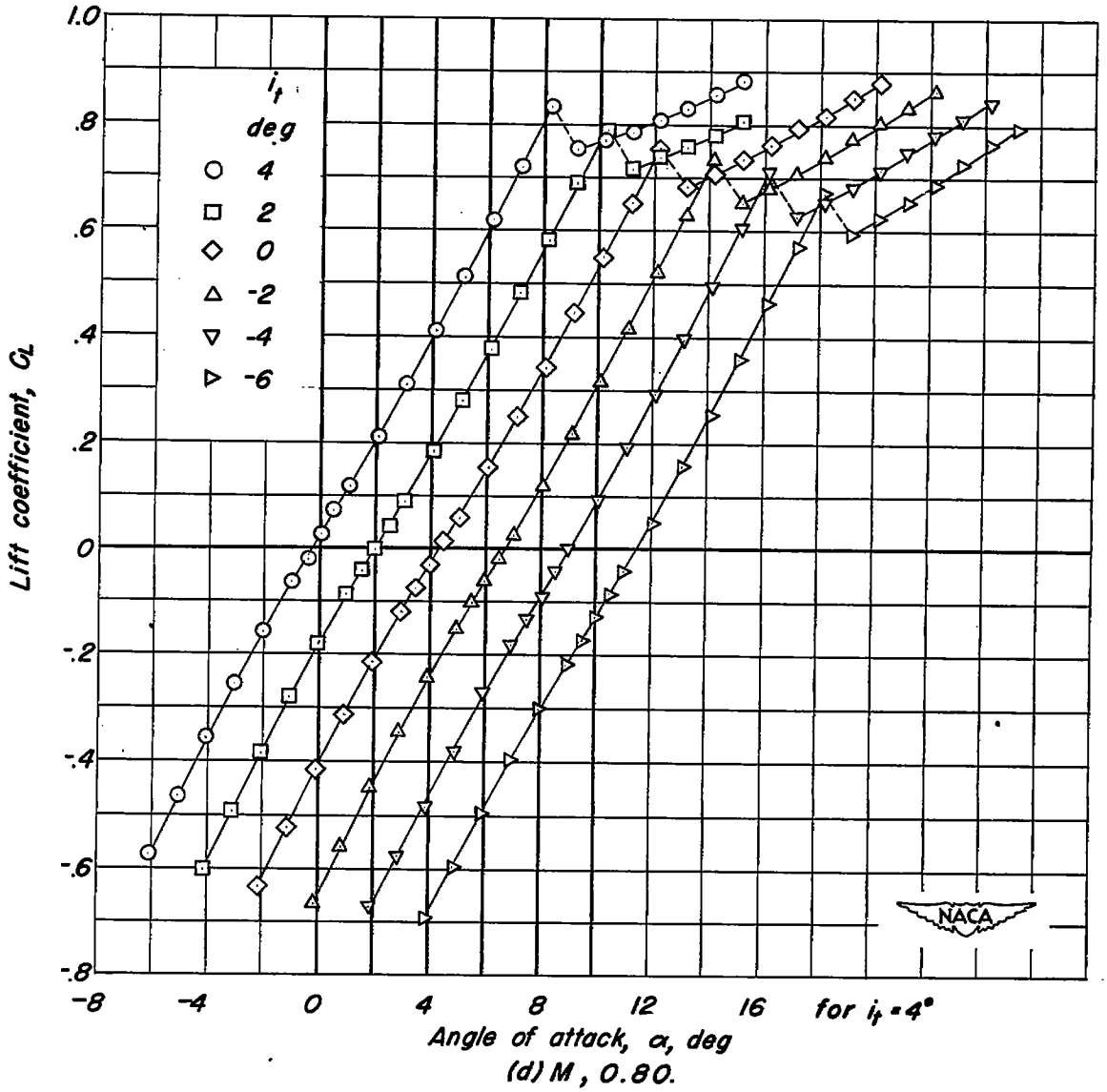

(d) M, 0.80.

Figure 20.— Continued.

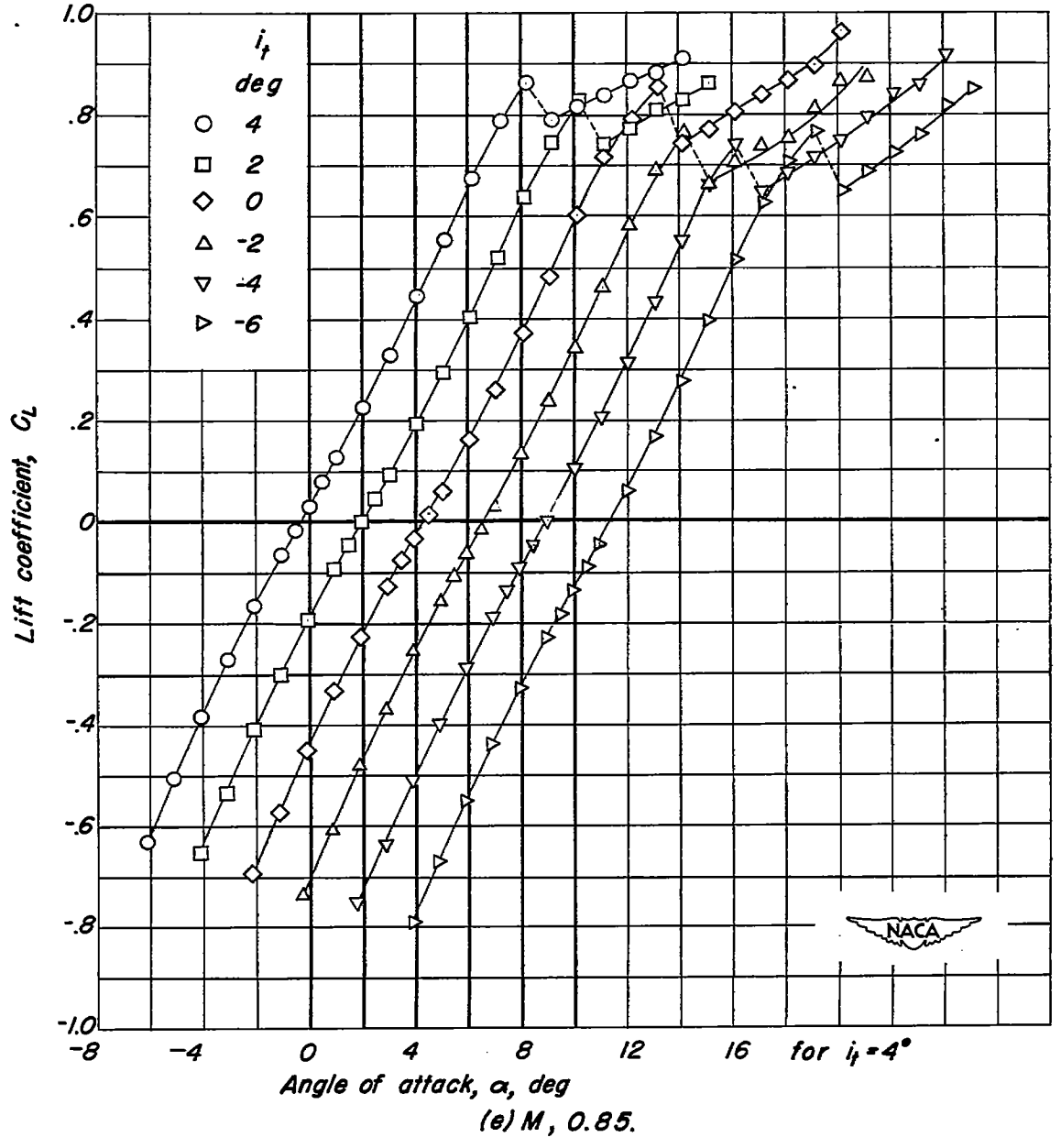

(e) M, 0.85.

Figure 20.— Continued.

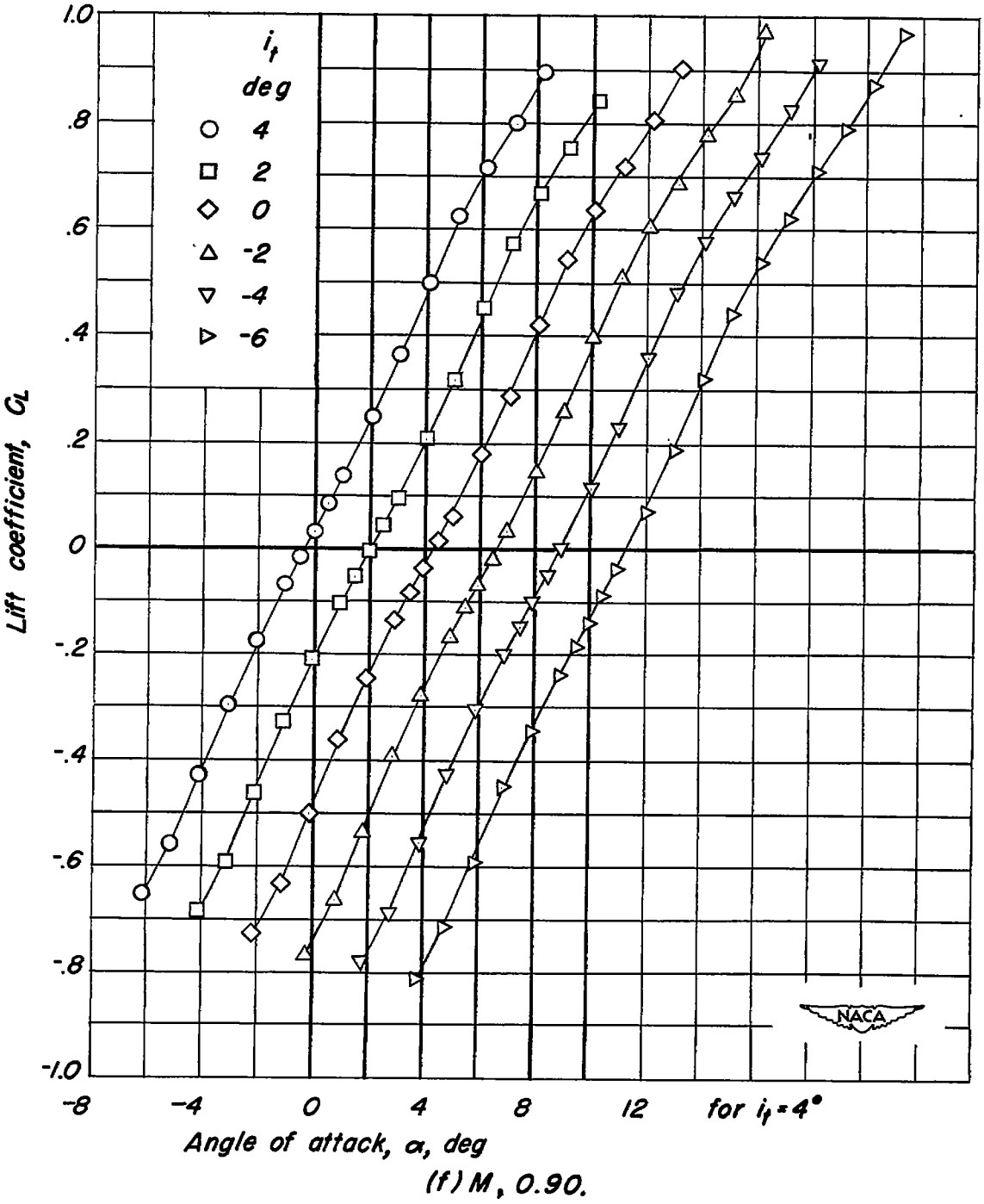

(f) M, 0.90.

Figure 20.— Continued.

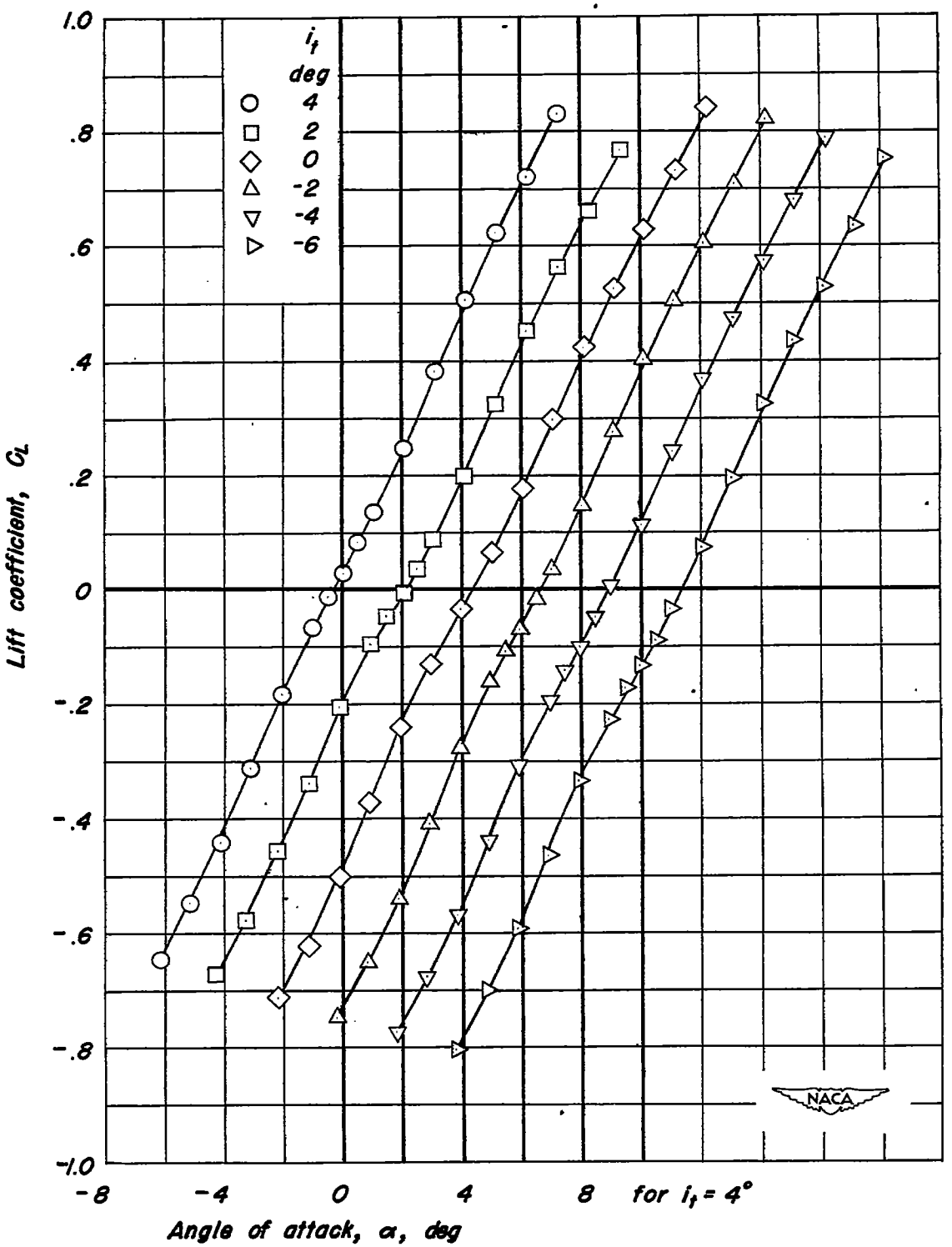

(g) M, 0.92.

Figure 20.— Continued.

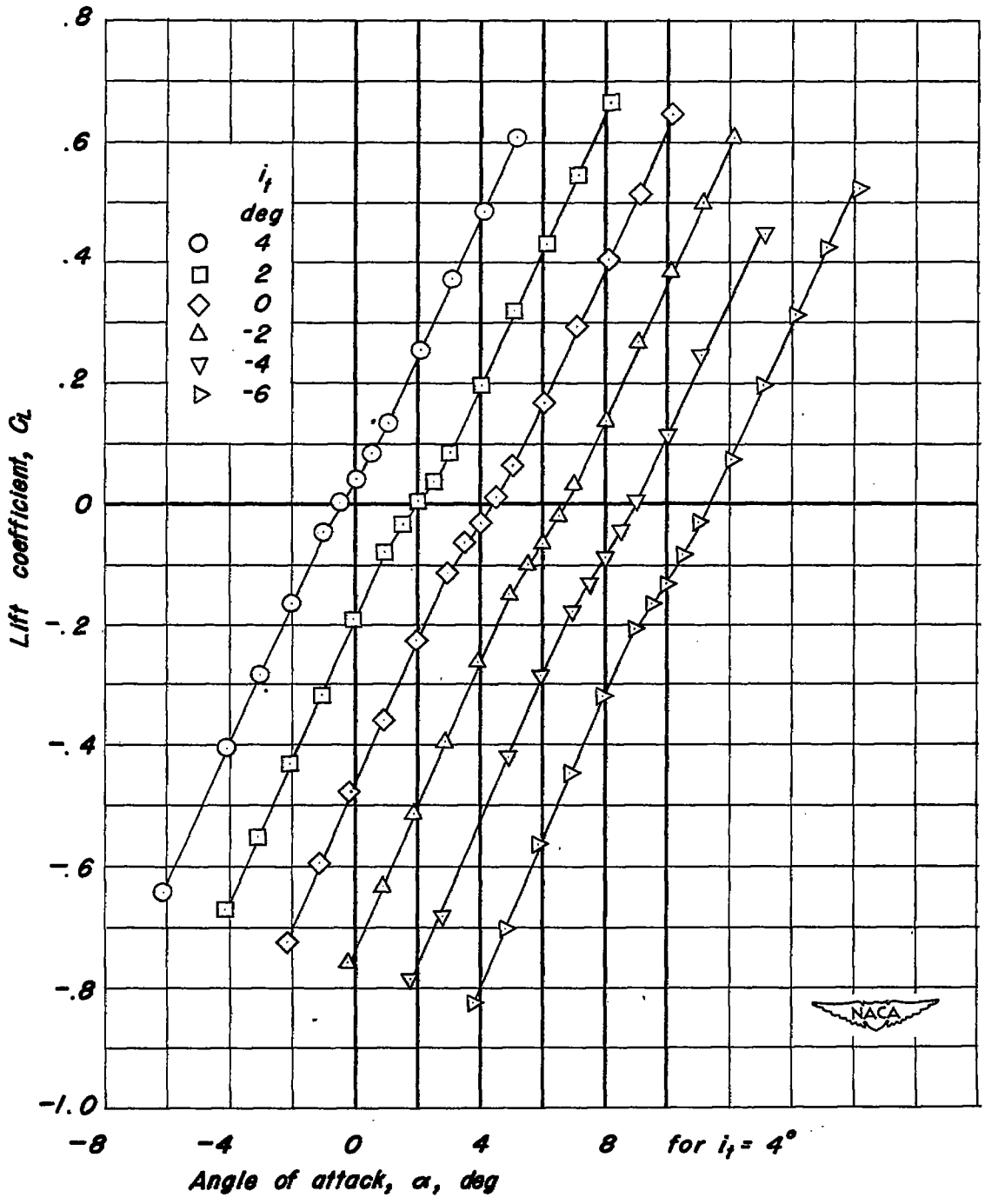

(h) M, 0.95.

Figure 20.— Concluded.

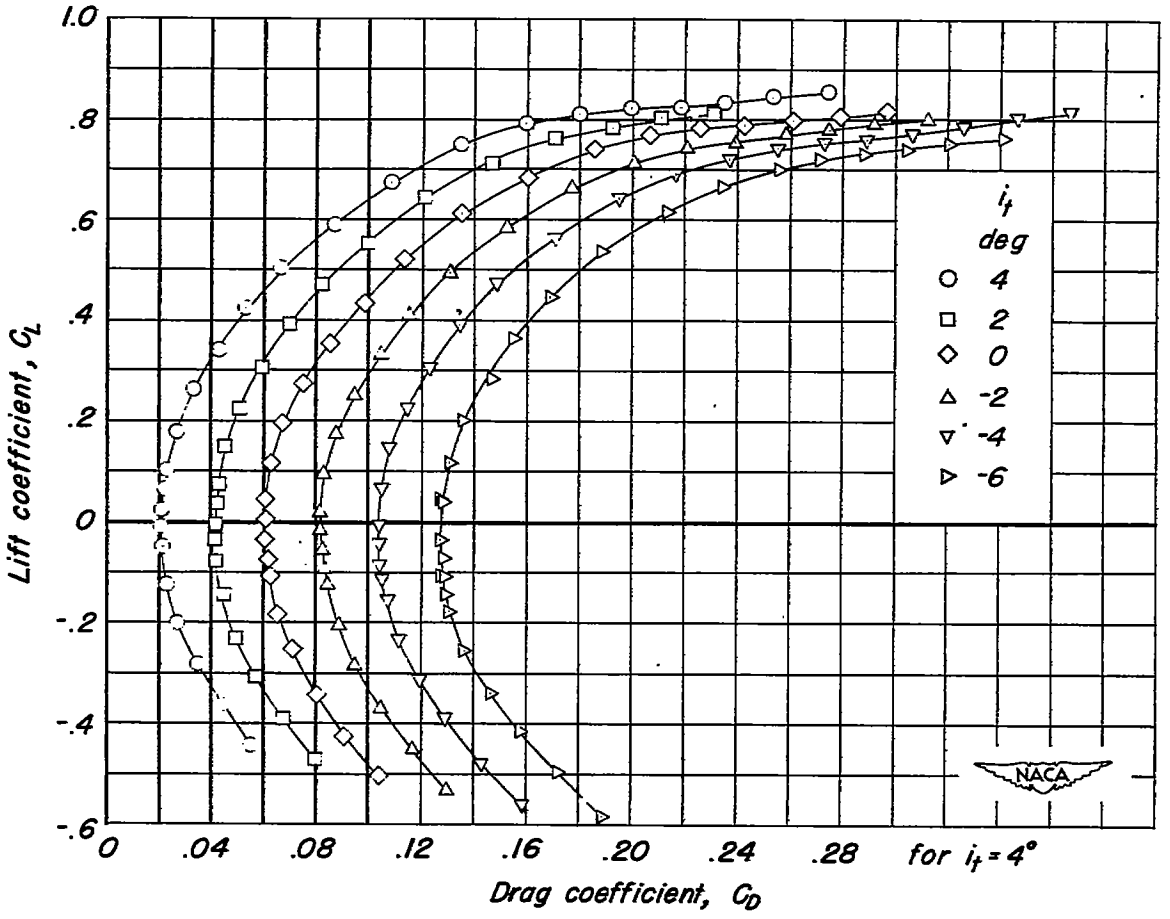

(a) M, 0.20.

Figure 21.— The drag characteristics of the airplane model with the horizontal tail mounted above the fuselage. R, 2,000,000.

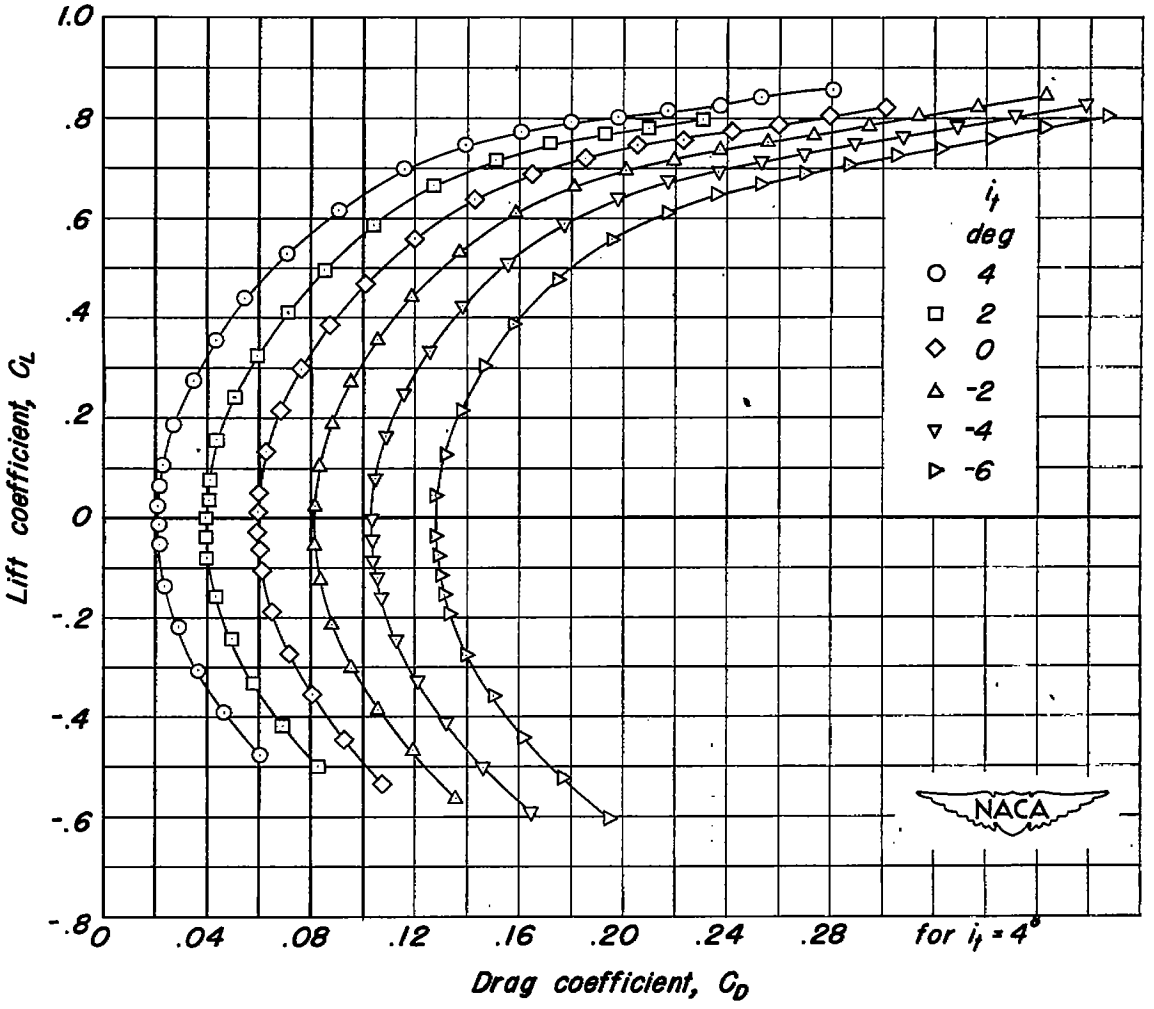

(b) M, 0.50.

Figure 21.— Continued.

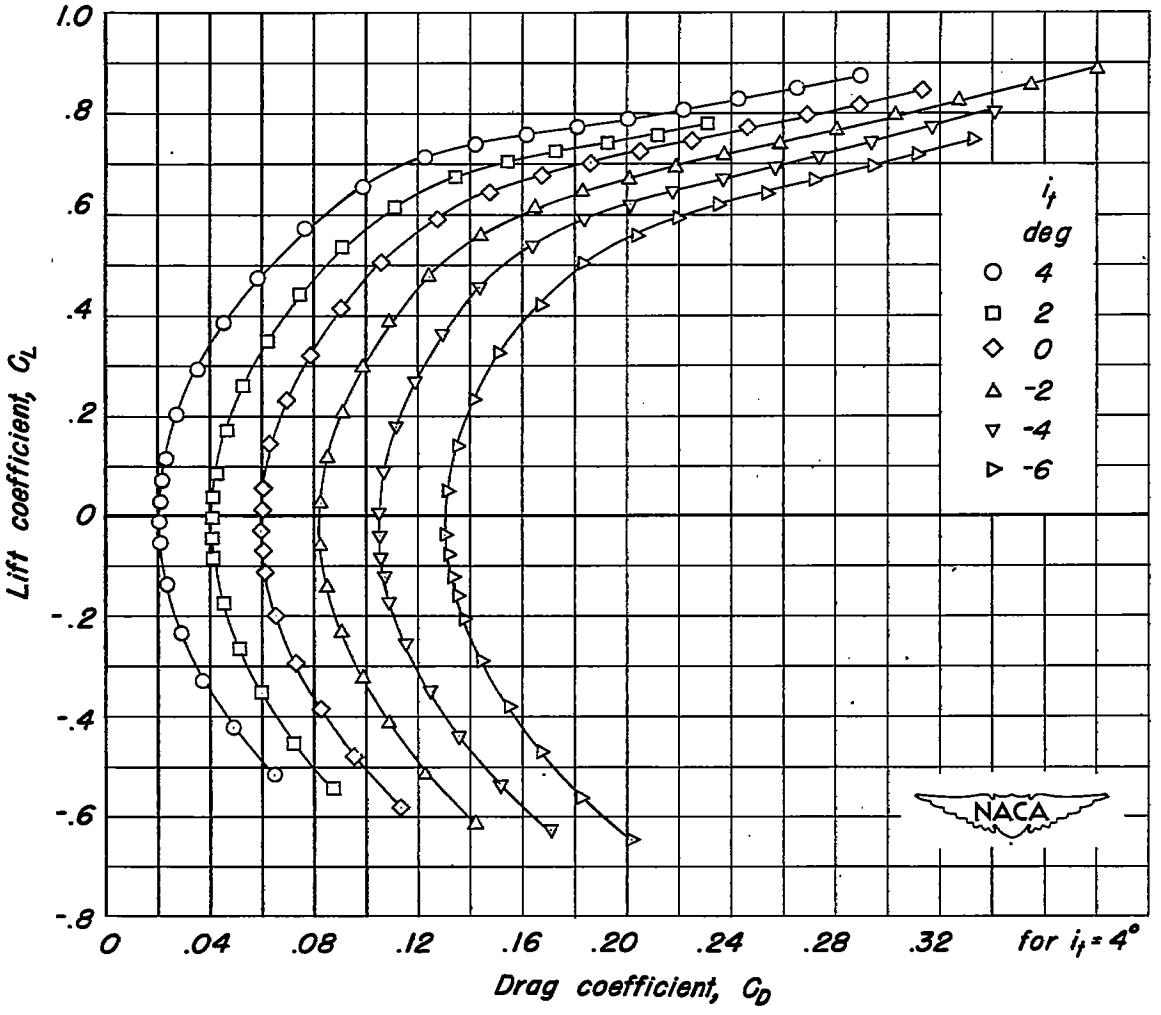

(c) M, 0.70.

Figure 21.— Continued.

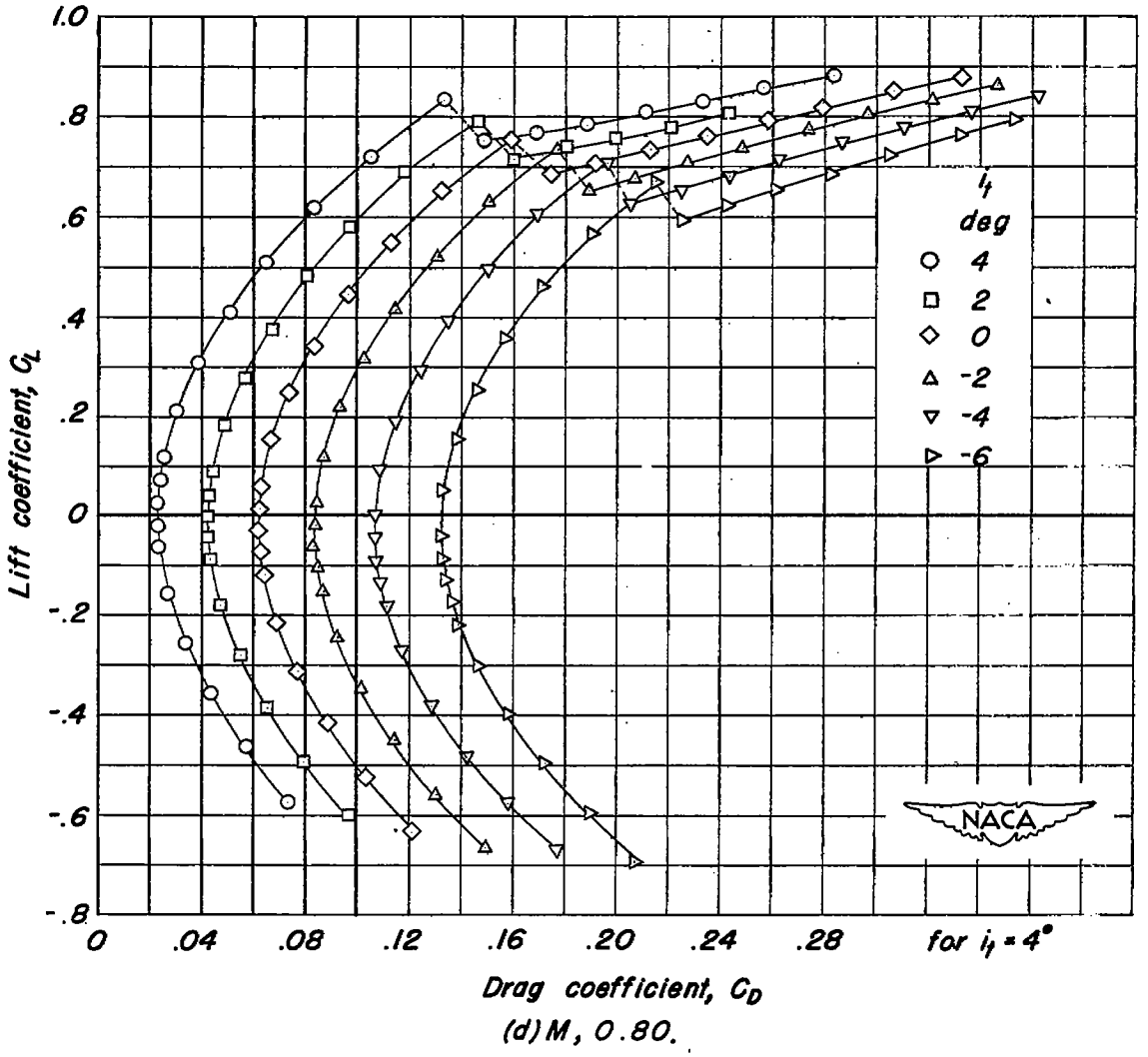

(d) M, 0.80.

Figure 21.— Continued.

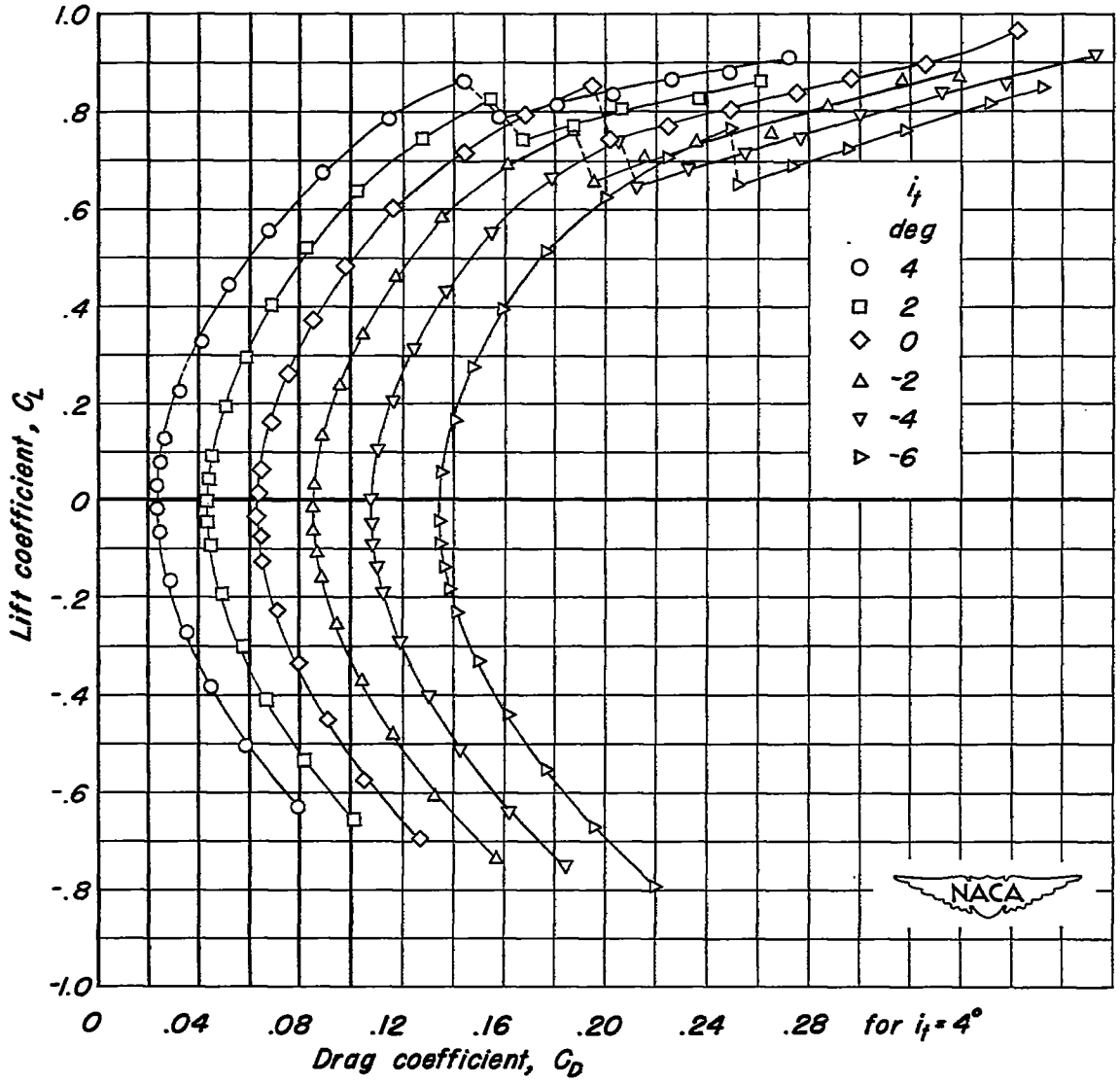

(e) M, 0.85.

Figure 21.— Continued.

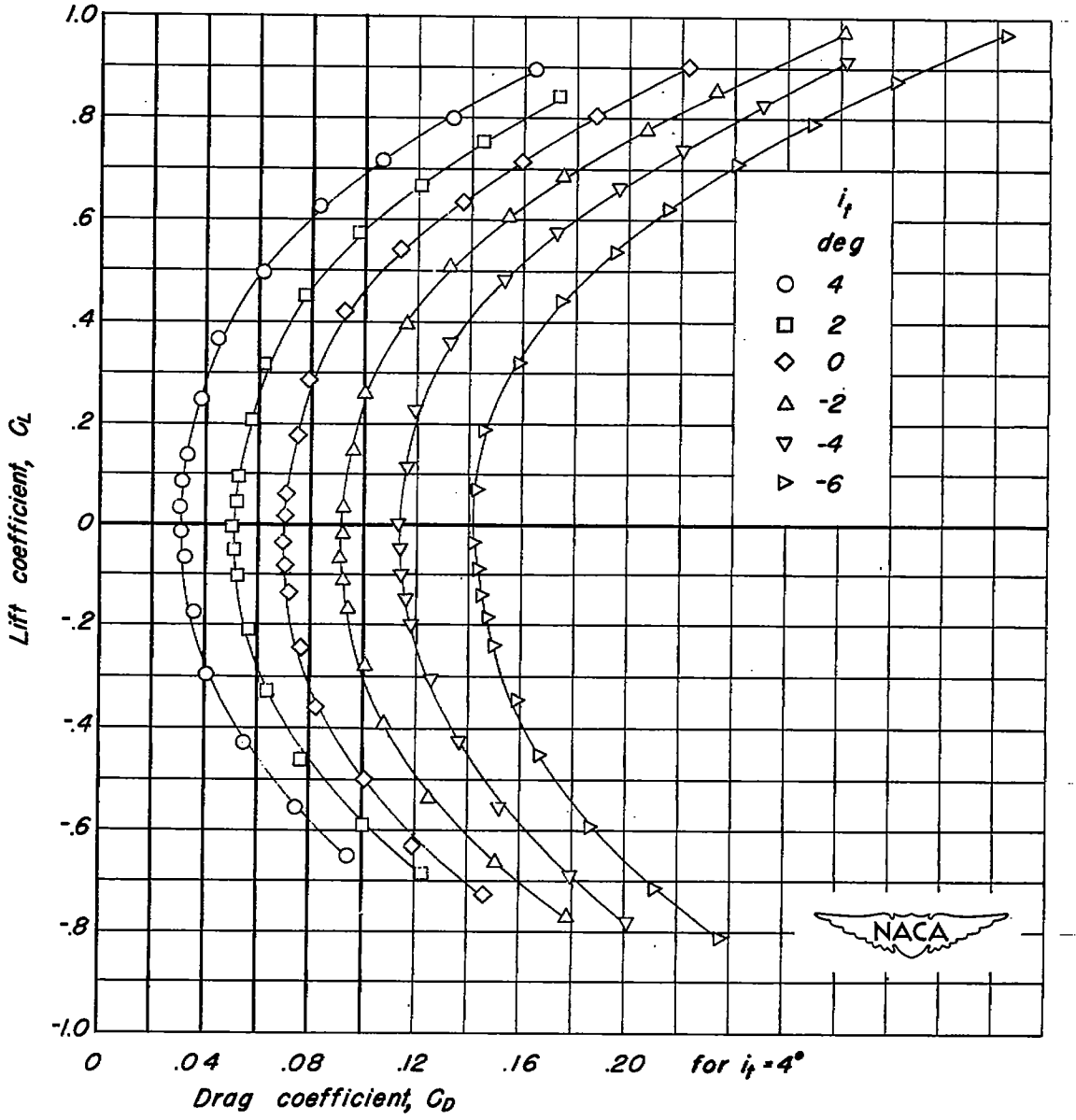

(f) M, 0.90.

Figure 21.— Continued.

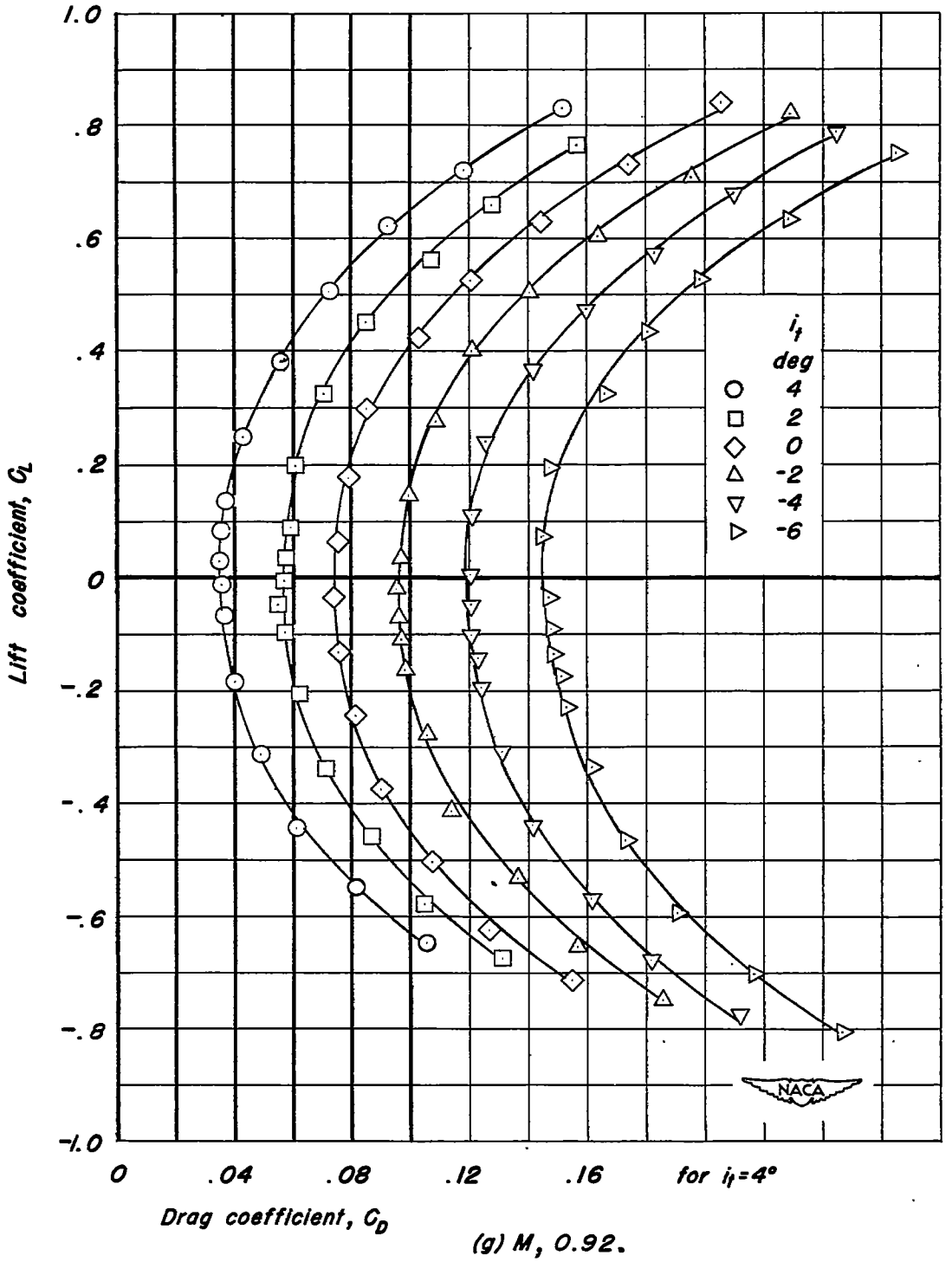

(g) M, 0.92.

Figure 21.- Continued.

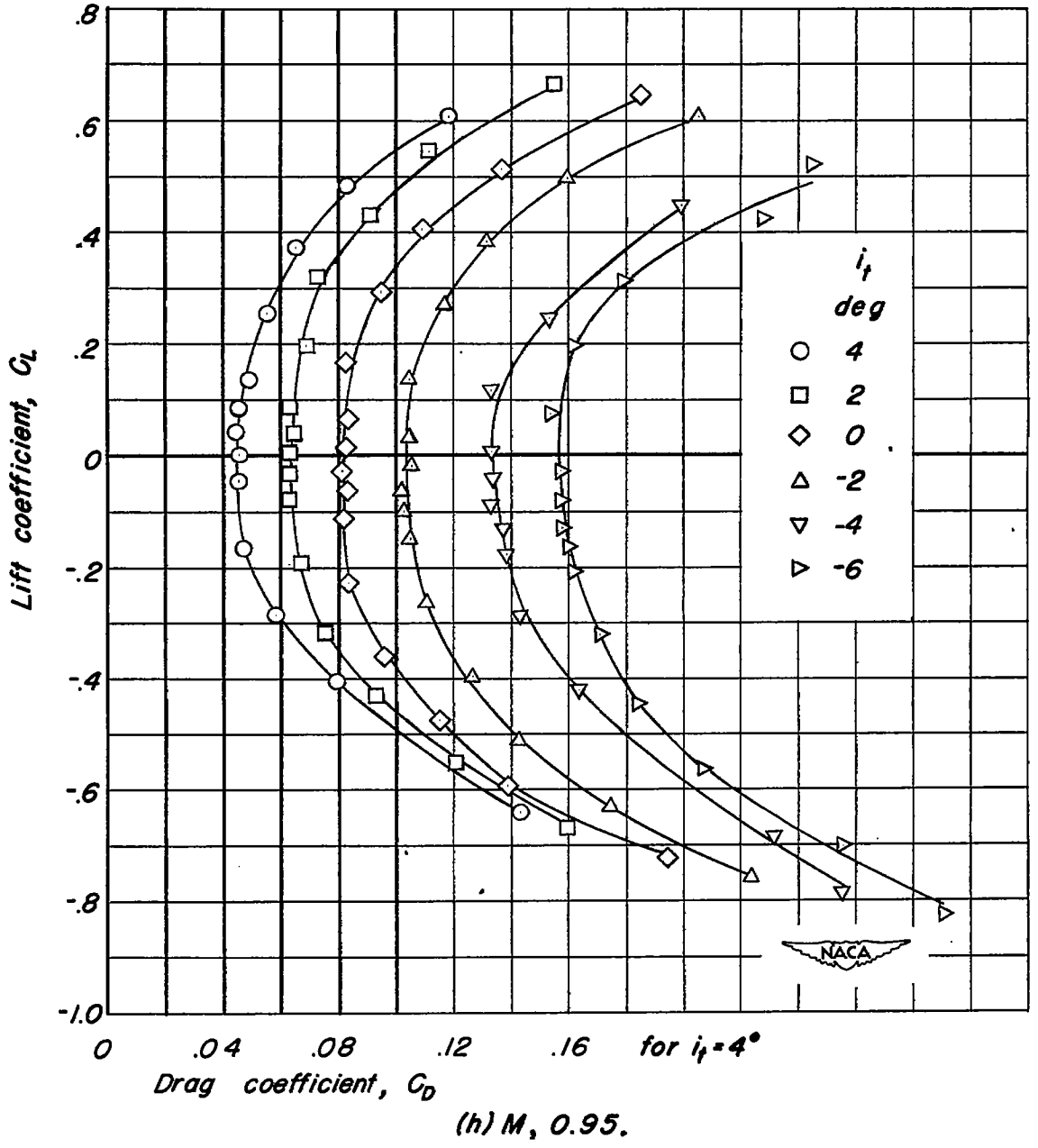

Figure 21.— Concluded.

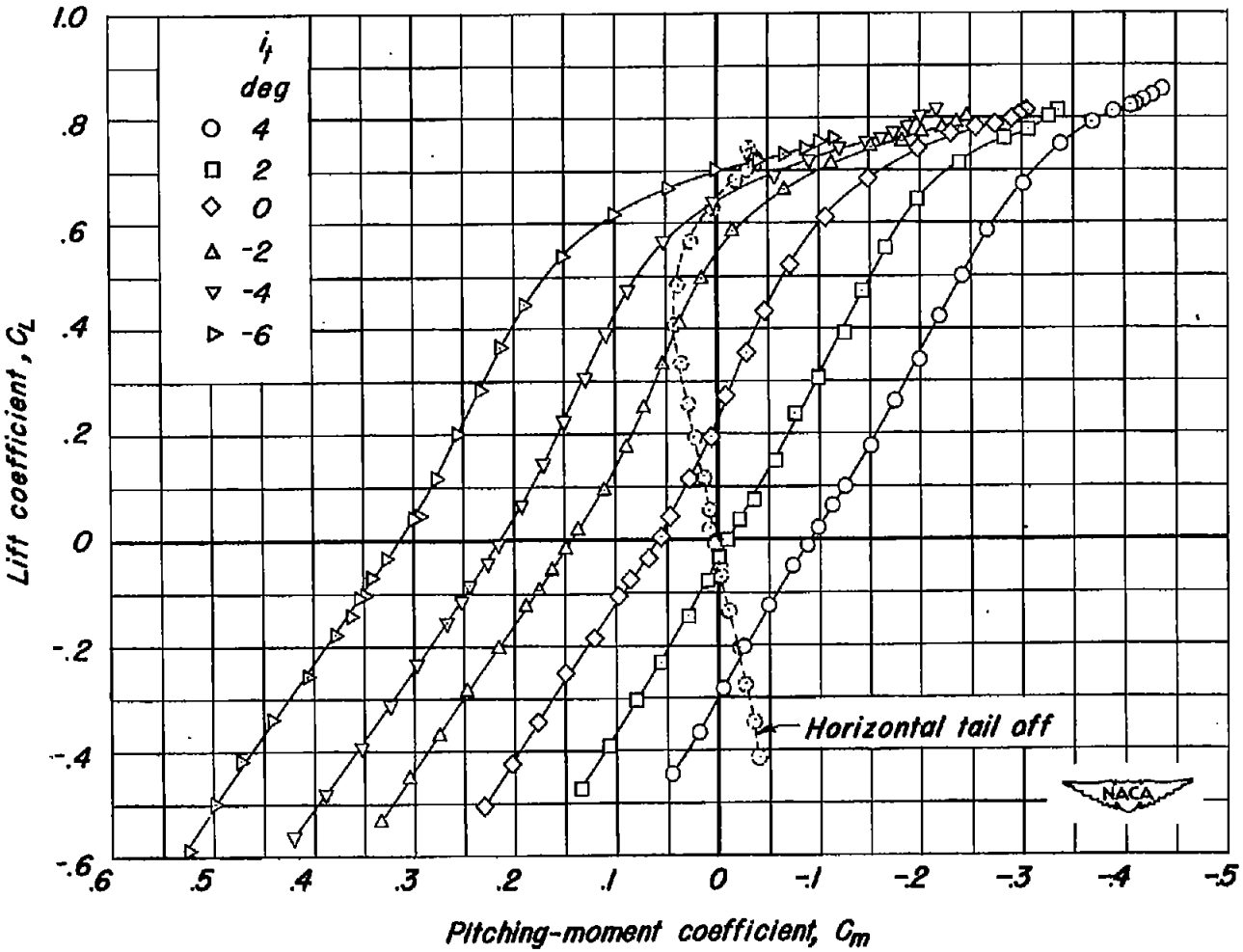

(a) M, 0.20.

Figure 22.— The pitching-moment characteristics of the airplane model with the horizontal tail mounted above the fuselage. R, 2,000,000.

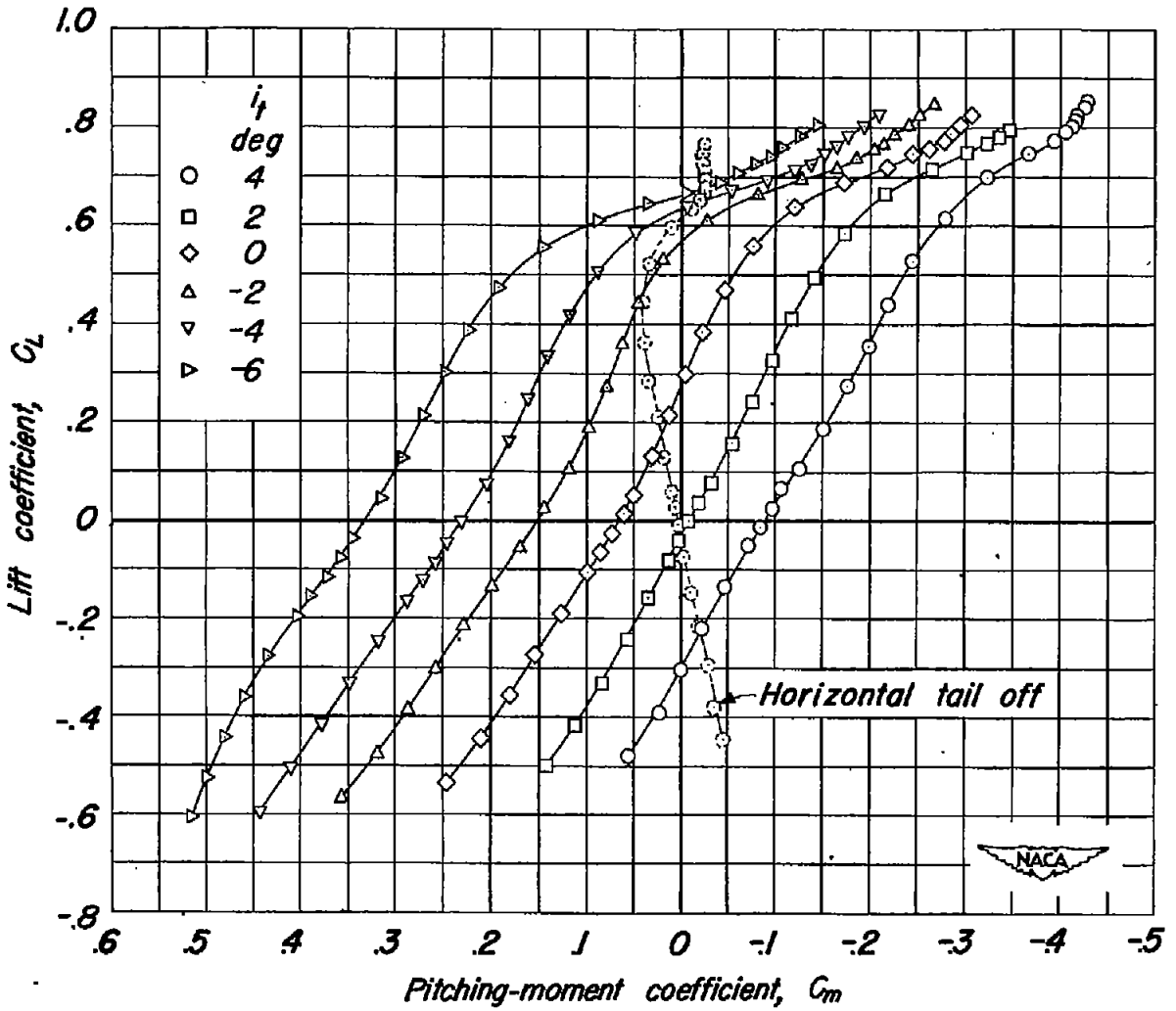

(b) M, 0.50.

Figure 22.— Continued.

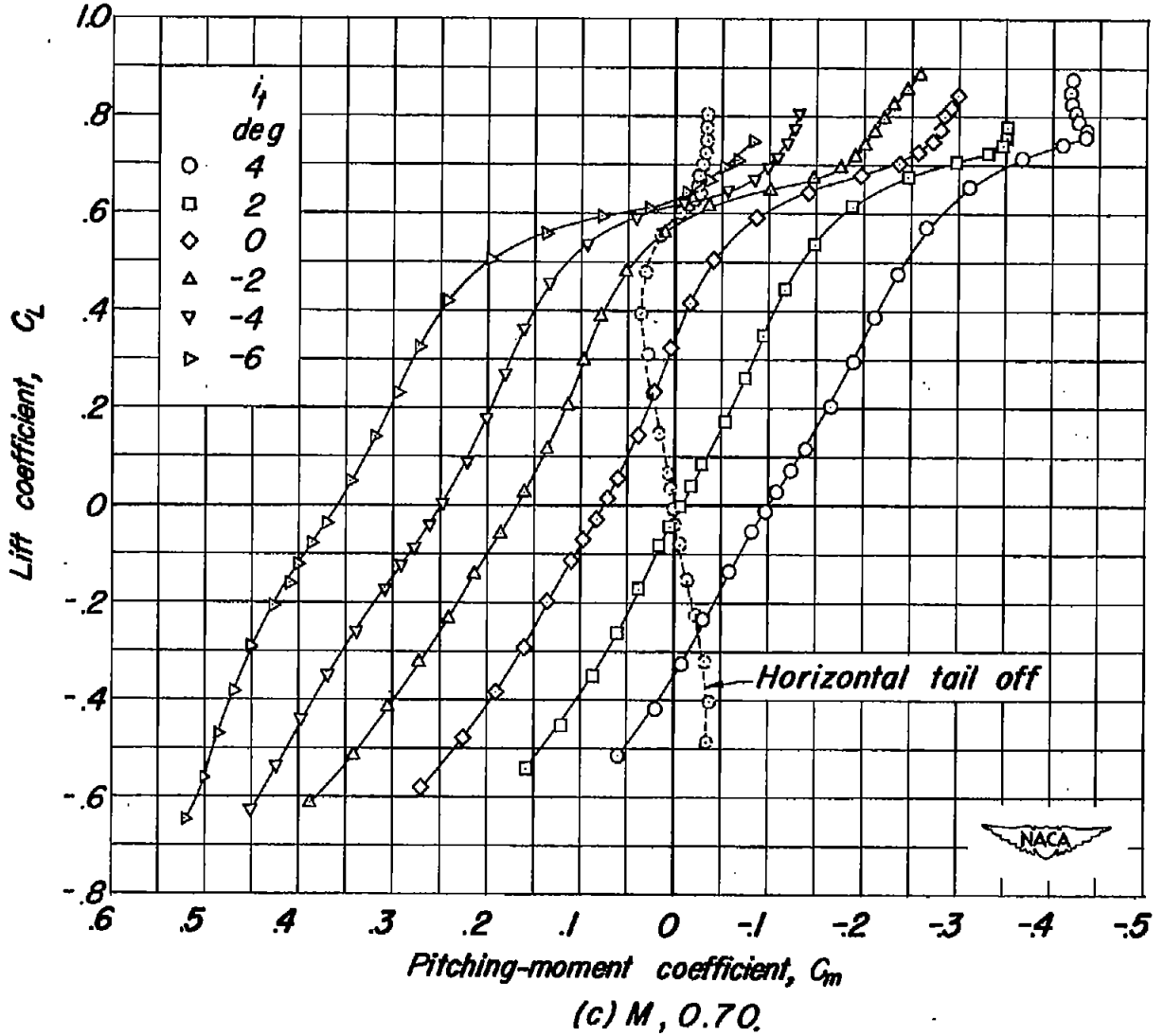

(c) M, 0.70.

Figure 22.— Continued.

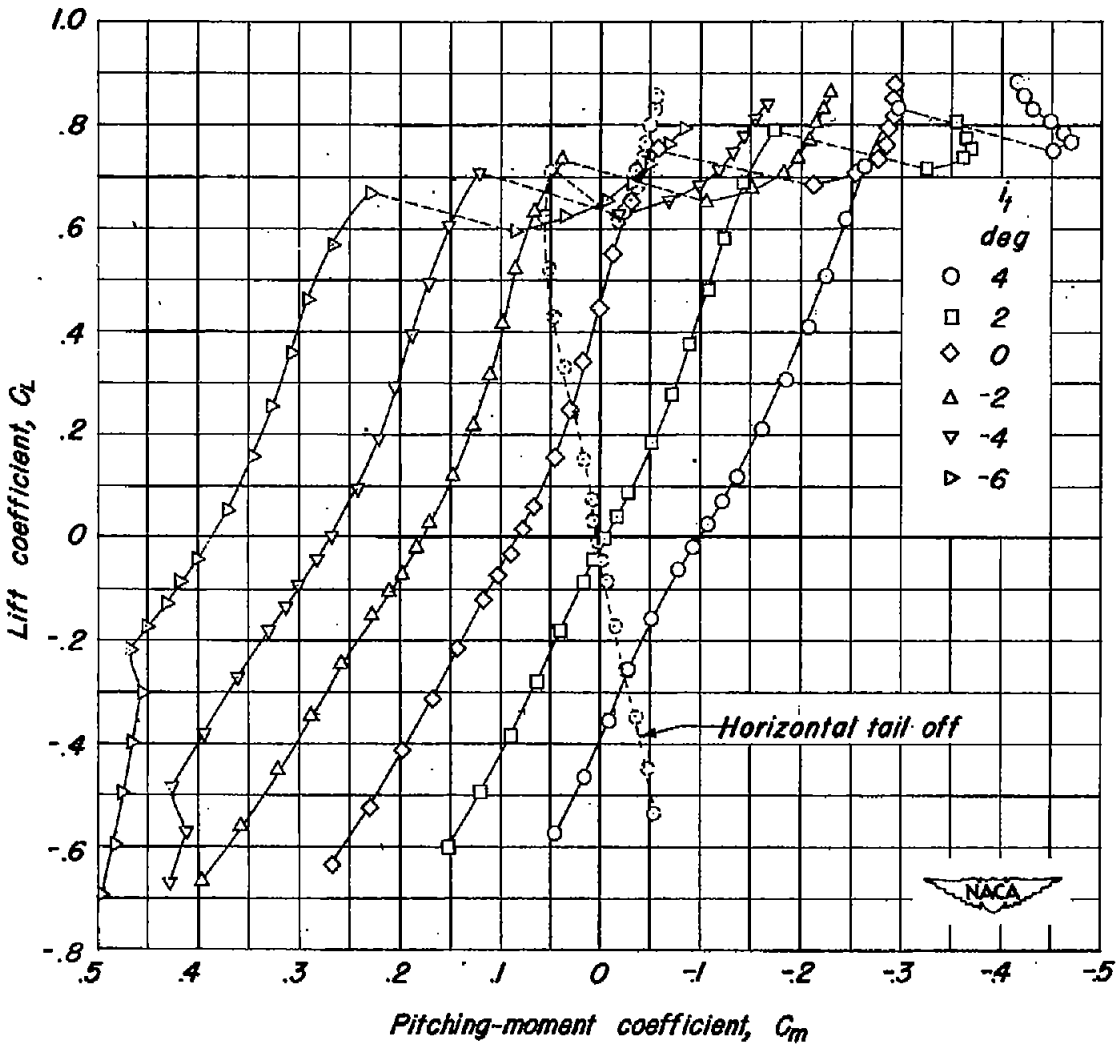

(d) M, 0.80.

Figure 22.- Continued.

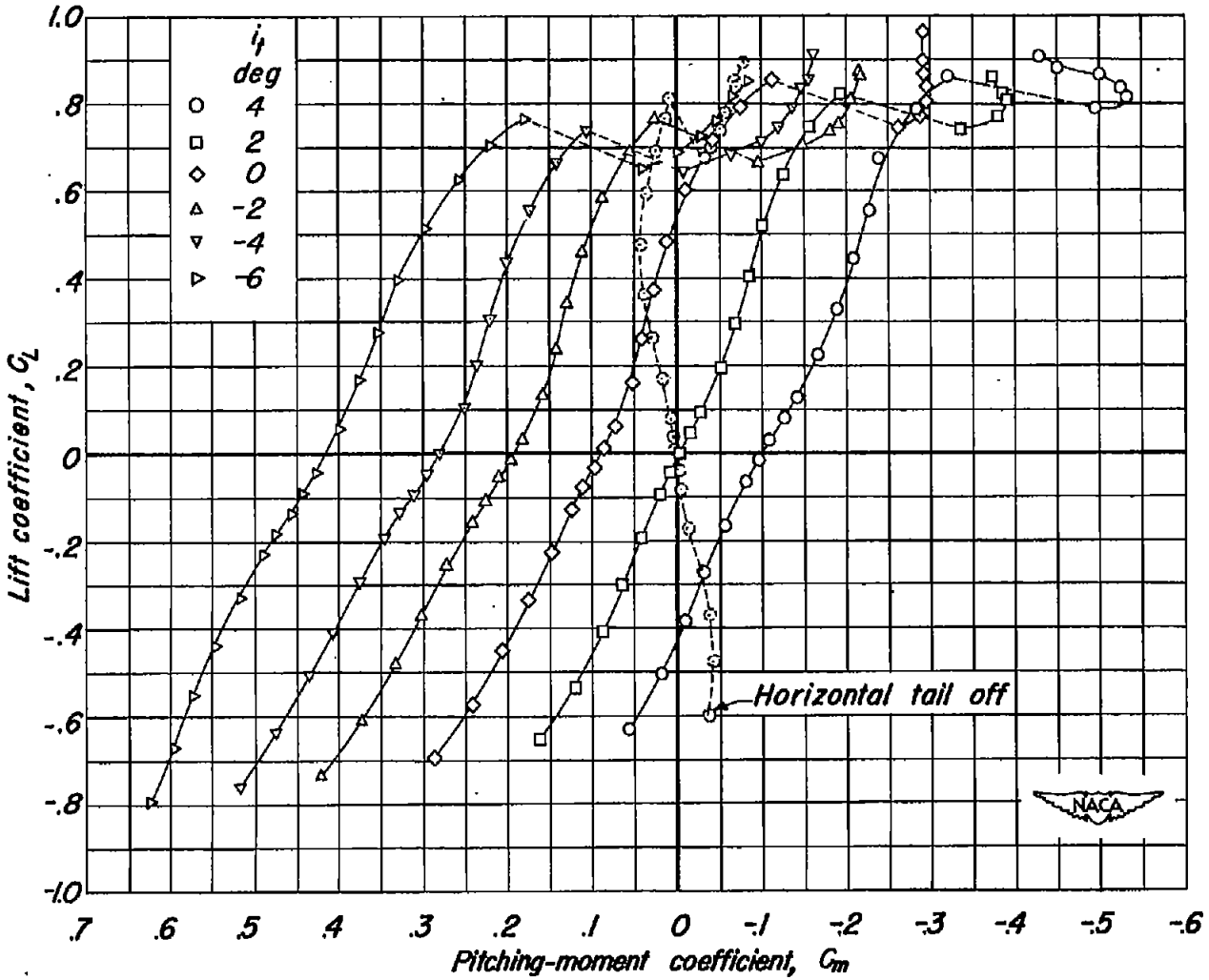

(e) M, 0.85.

Figure 22.— Continued.

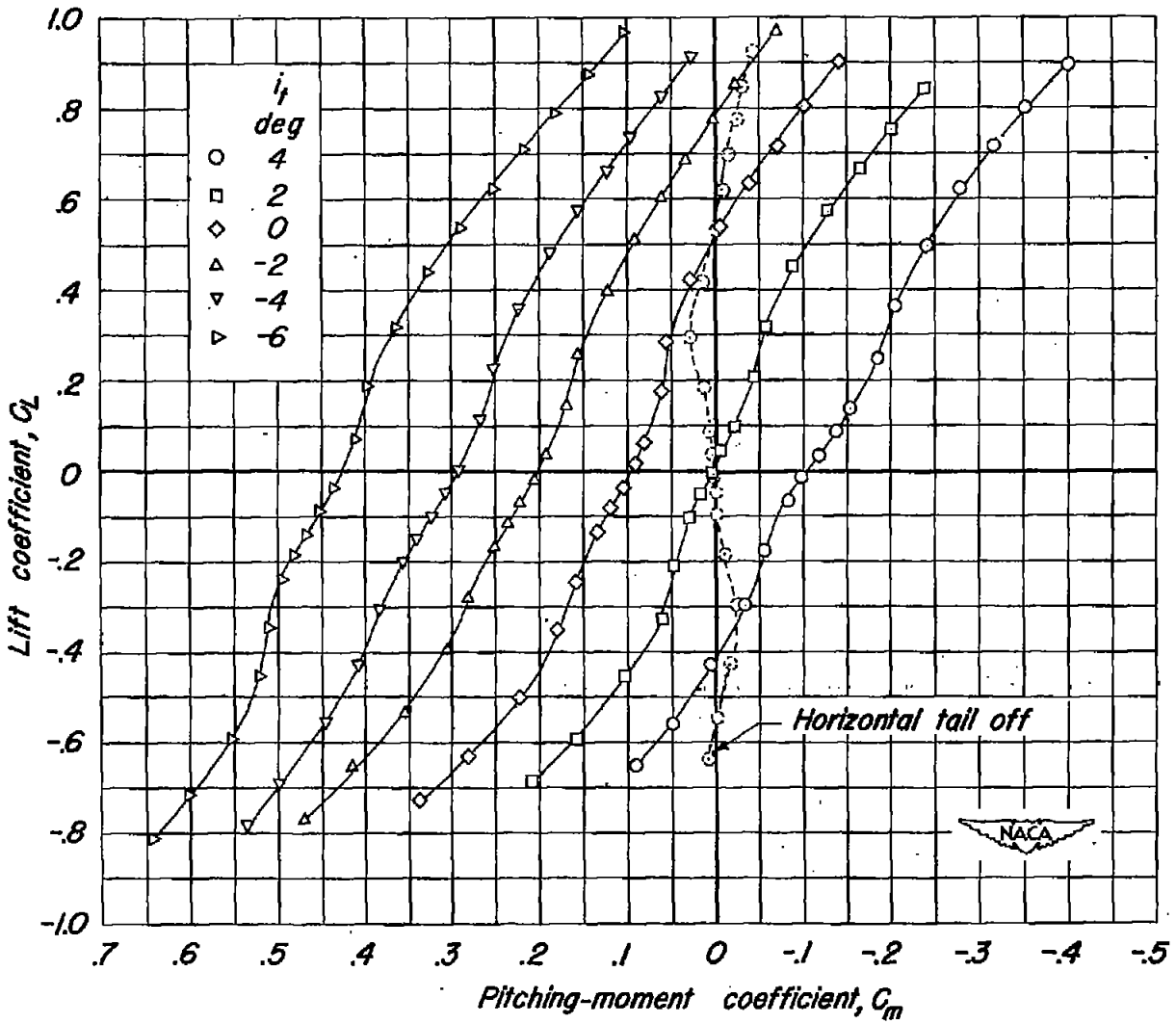

(f) M, 0.90.

Figure 22.- Continued.

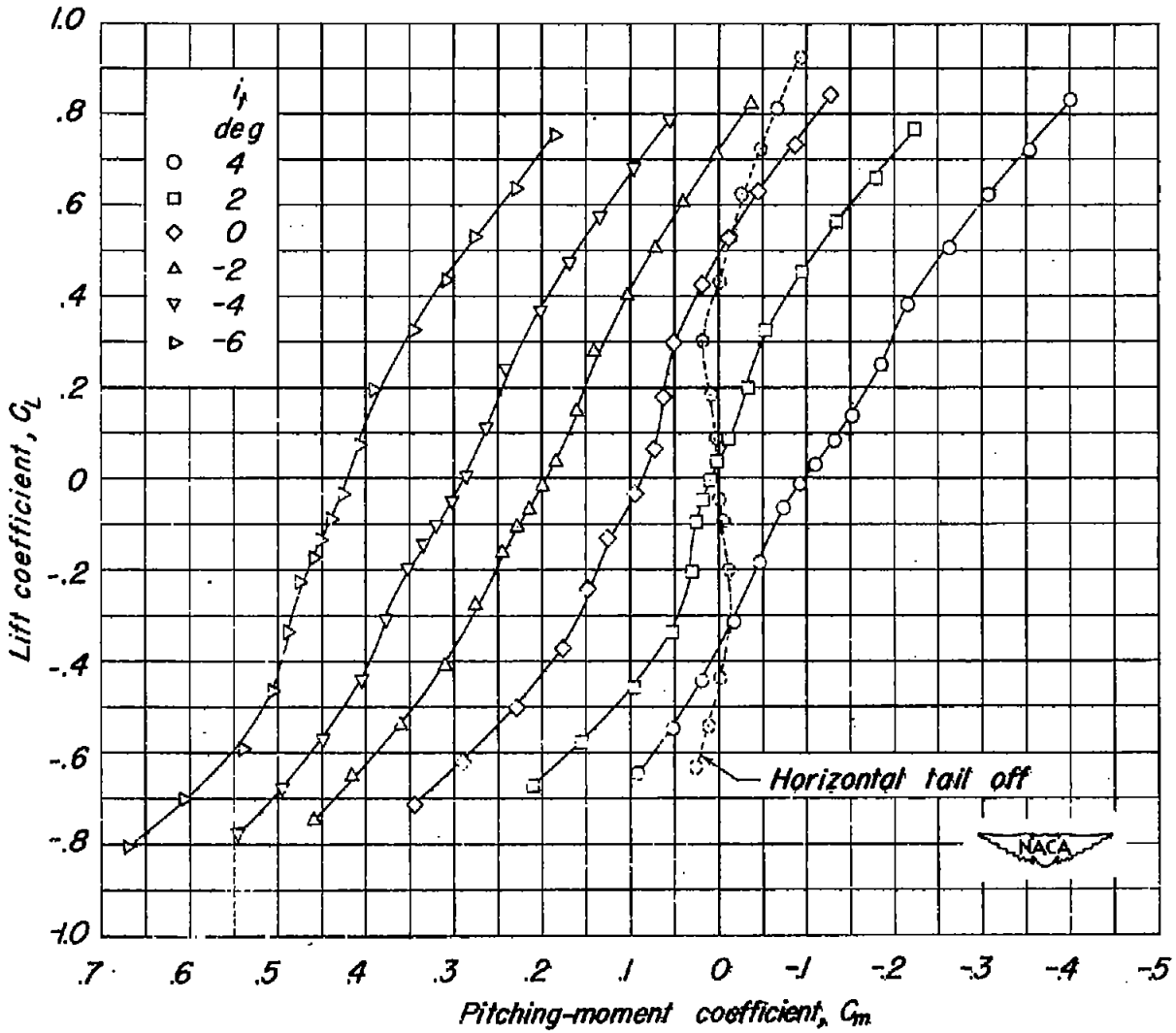

(g) M, 0.92.

Figure 22.- Continued.

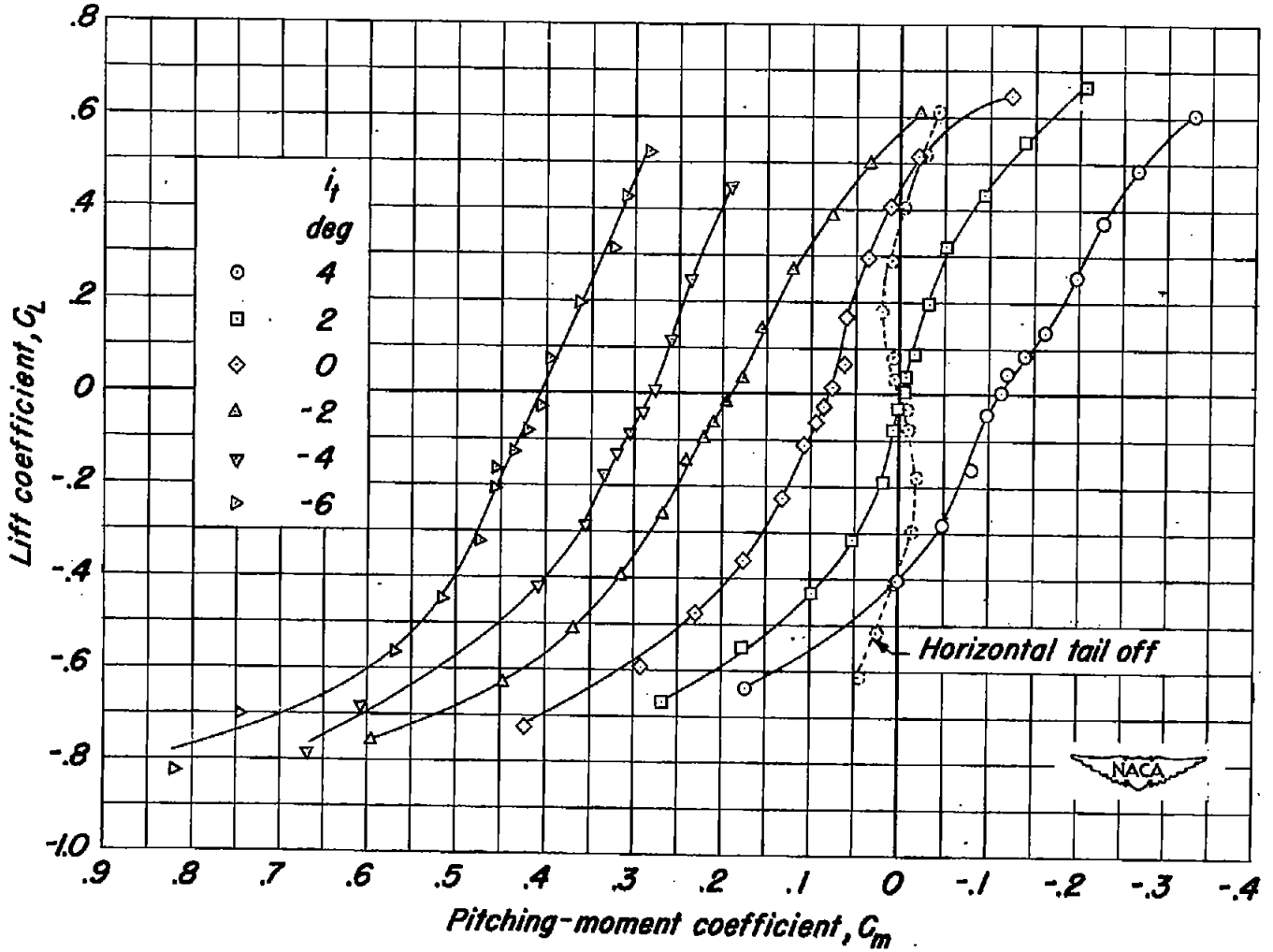

(h) M, 0.95.

Figure 22.- Concluded.

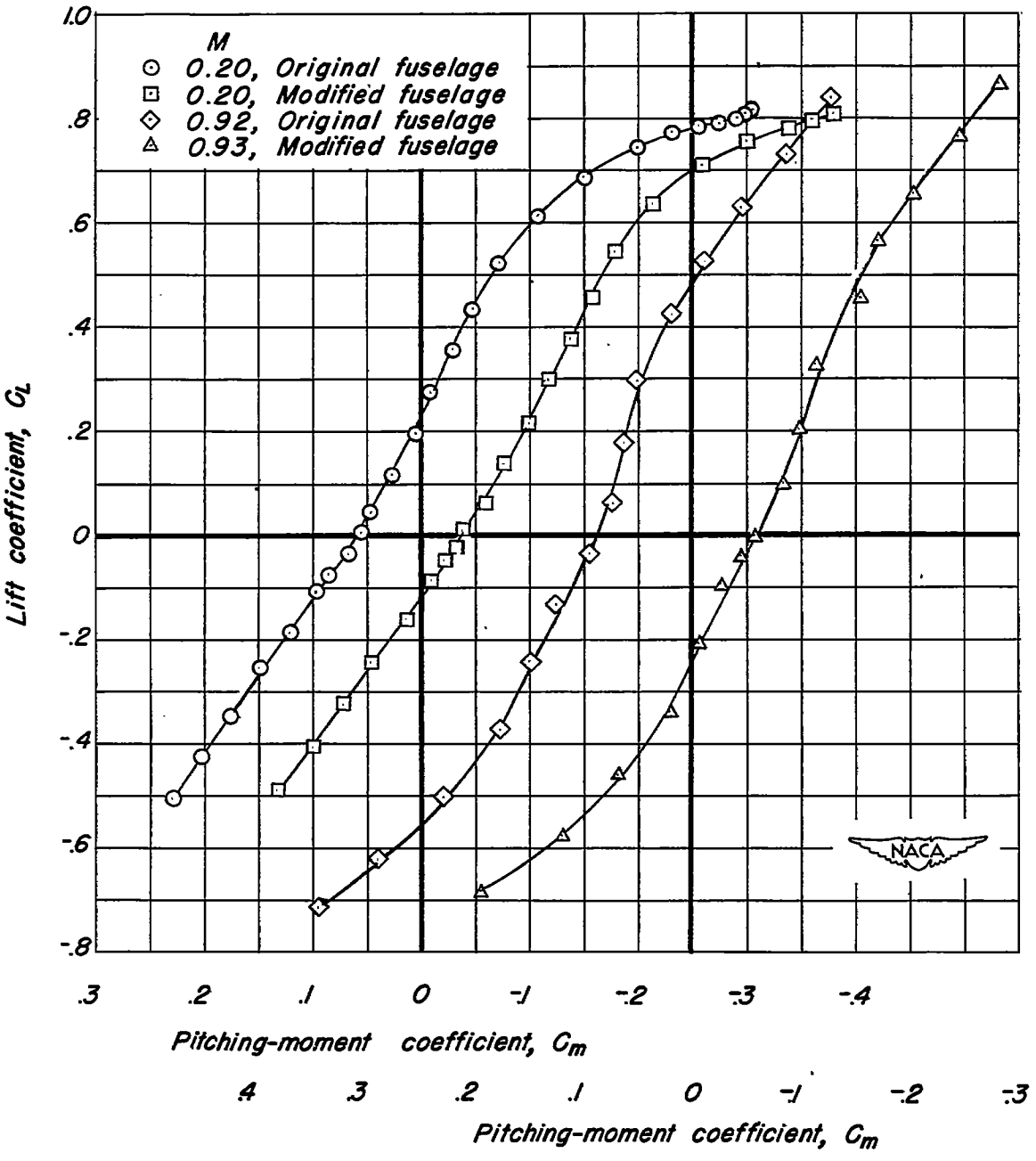

Figure 23.- The effect on the pitching-moment characteristics of modifying the fuselage of the airplane model with the horizontal tail above the fuselage. R, 2,000,000; i_t, 0°.

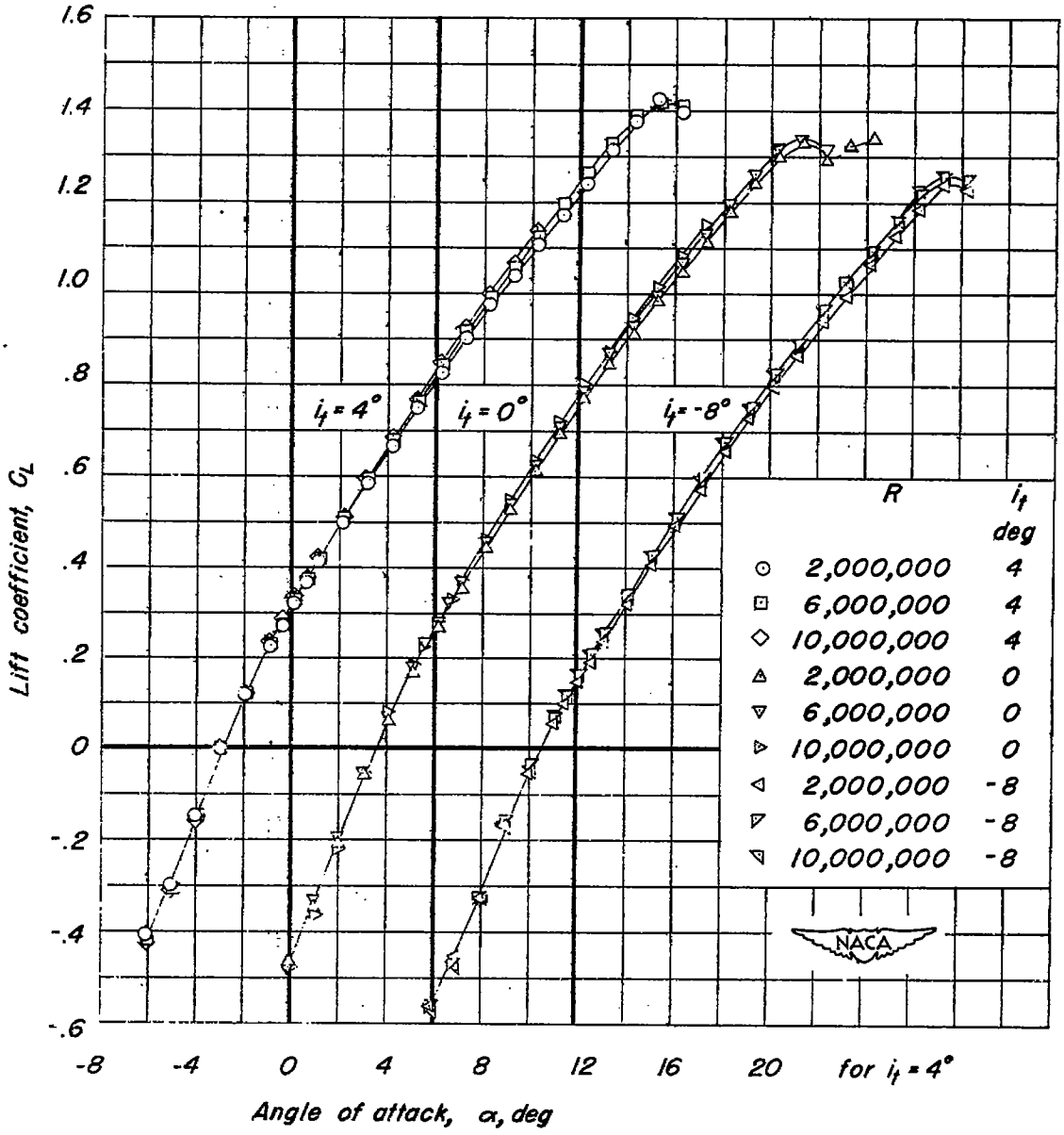

Figure 24— The lift characteristics of the airplane model with the horizontal tail mounted above the fuselage and with the flaps deflected. δ_n, 30°; δ_f 50°; M, 0.20.

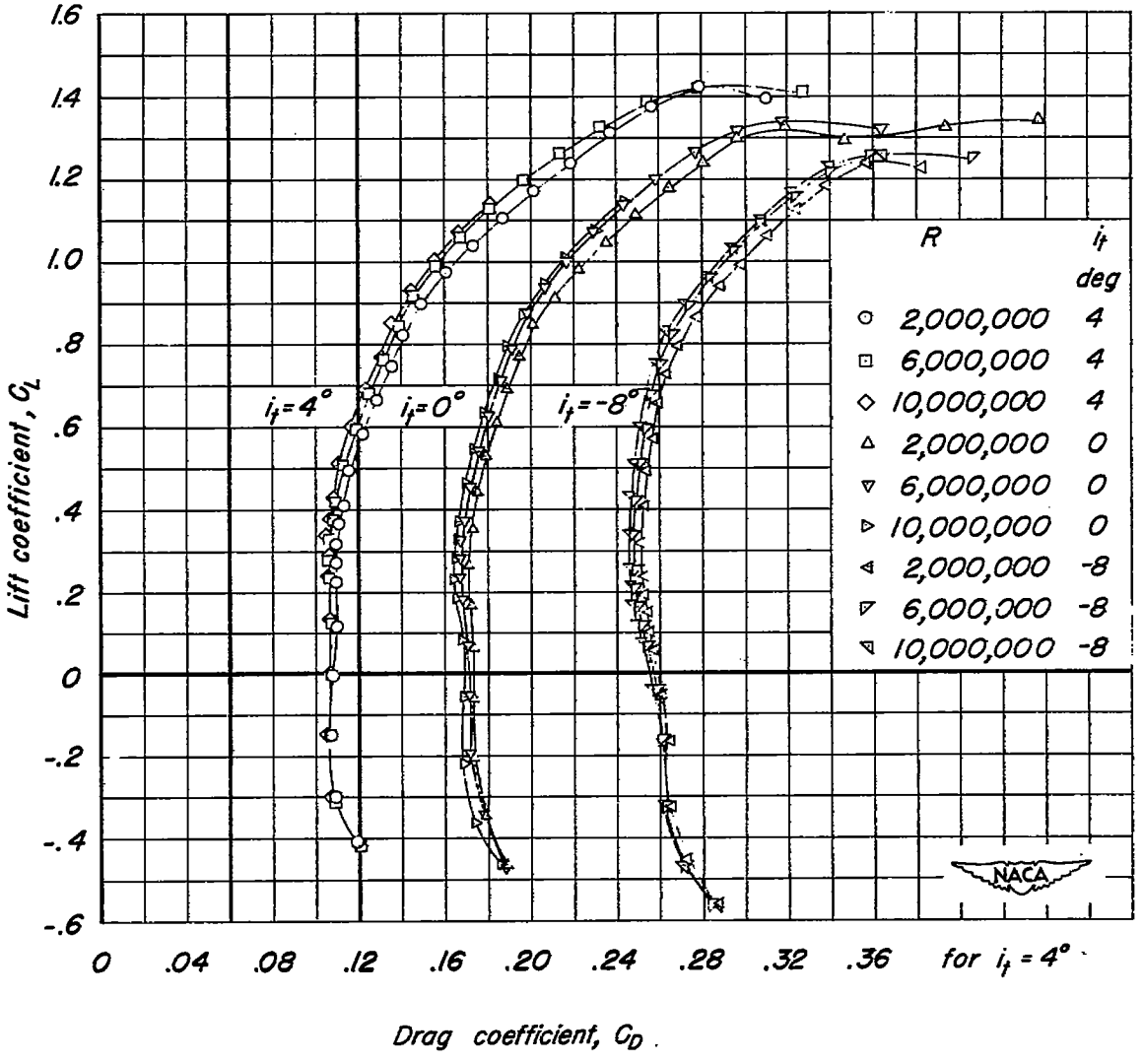

Figure 25.- The drag characteristics of the airplane model with the horizontal tail mounted above the fuselage and with the flaps deflected. δ_n, 30°; δ_f, 50°; M, 0.20.

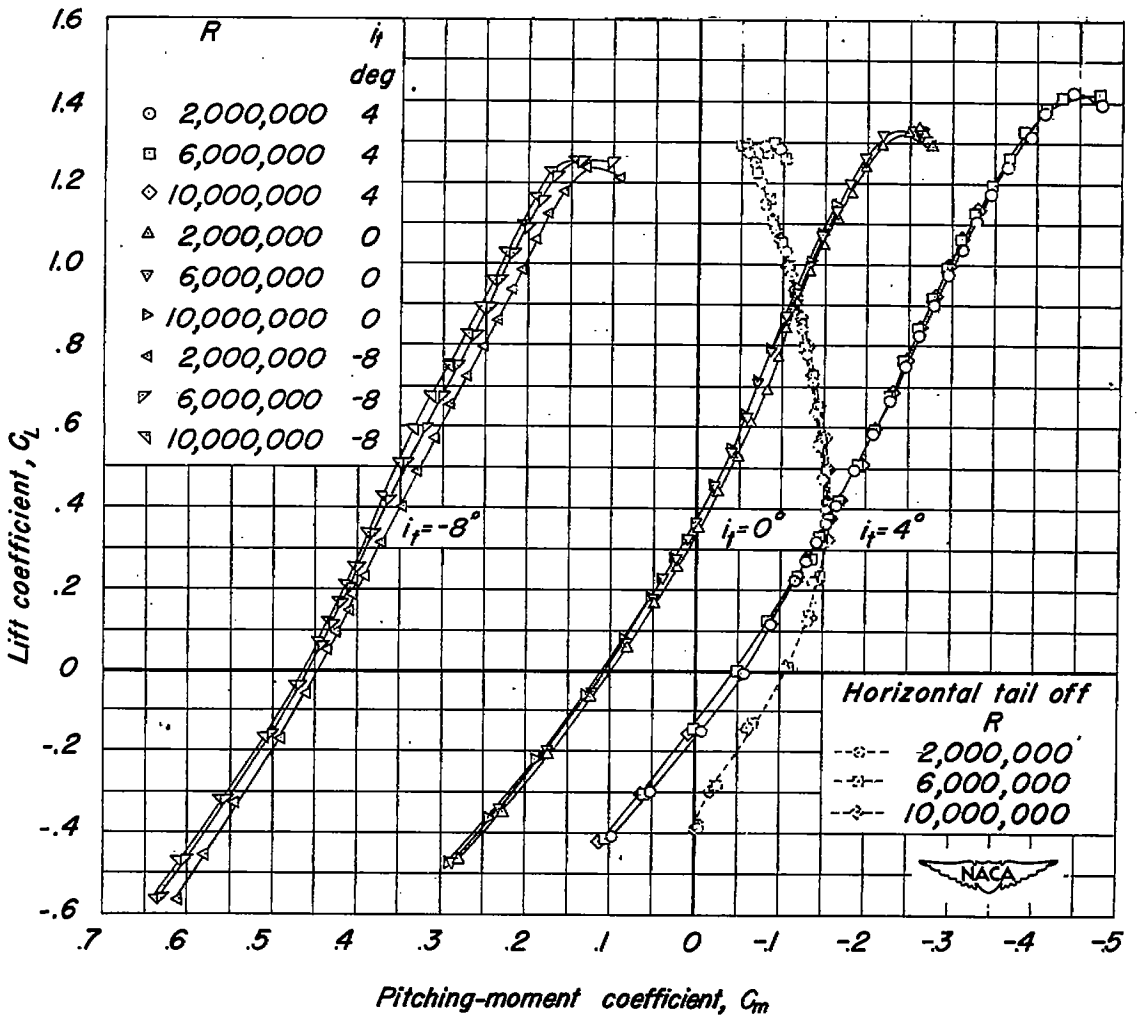

Figure 26.- The pitching-moment characteristics of the airplane model with the horizontal tail mounted above the fuselage and with the flaps deflected. δ_n, 30°; δ_f, 50°; M, 0.20.

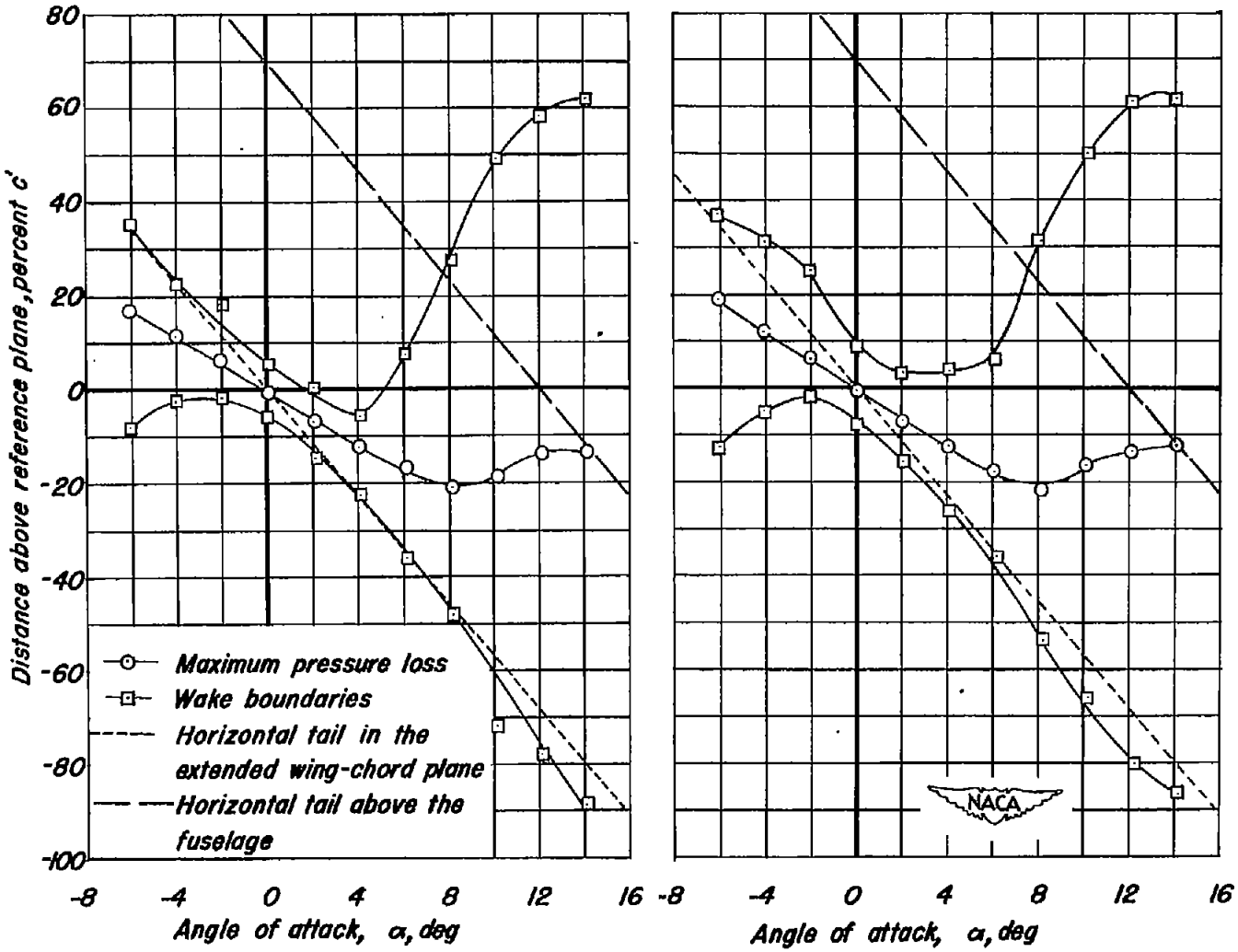

(a) M, 0.20. (b) M, 0.50.

Figure 27.- The variation with angle of attack of the wake-boundary, maximum-pressure-loss locations and horizontal-tail positions with reference to the wing-chord plane at α = 0°. Wing and fuselage. R, 2,000,000.

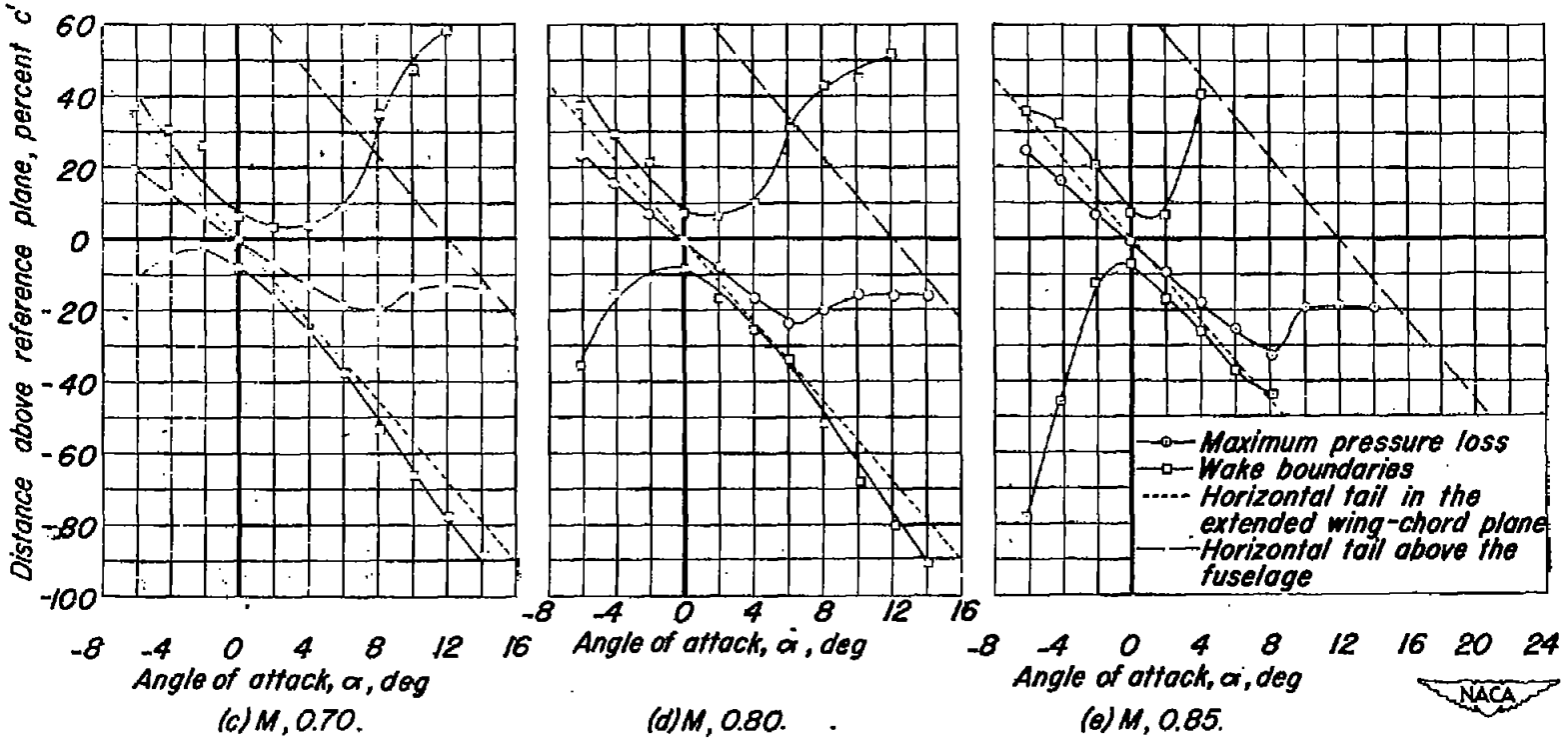

Figure 27.-Continued.

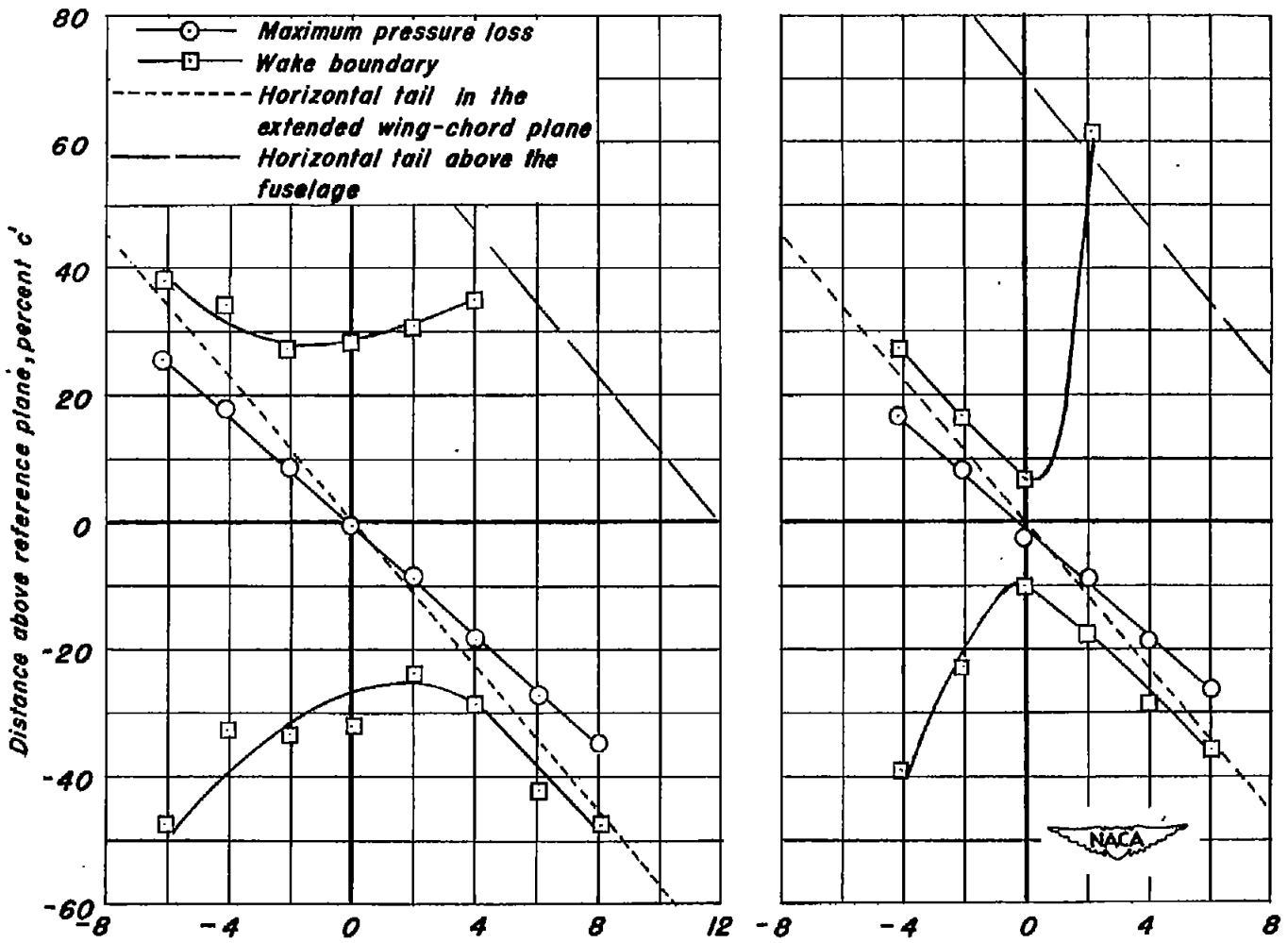

(f) M, 0.90.

(g) M, 0.95.

Figure 27.— Concluded.

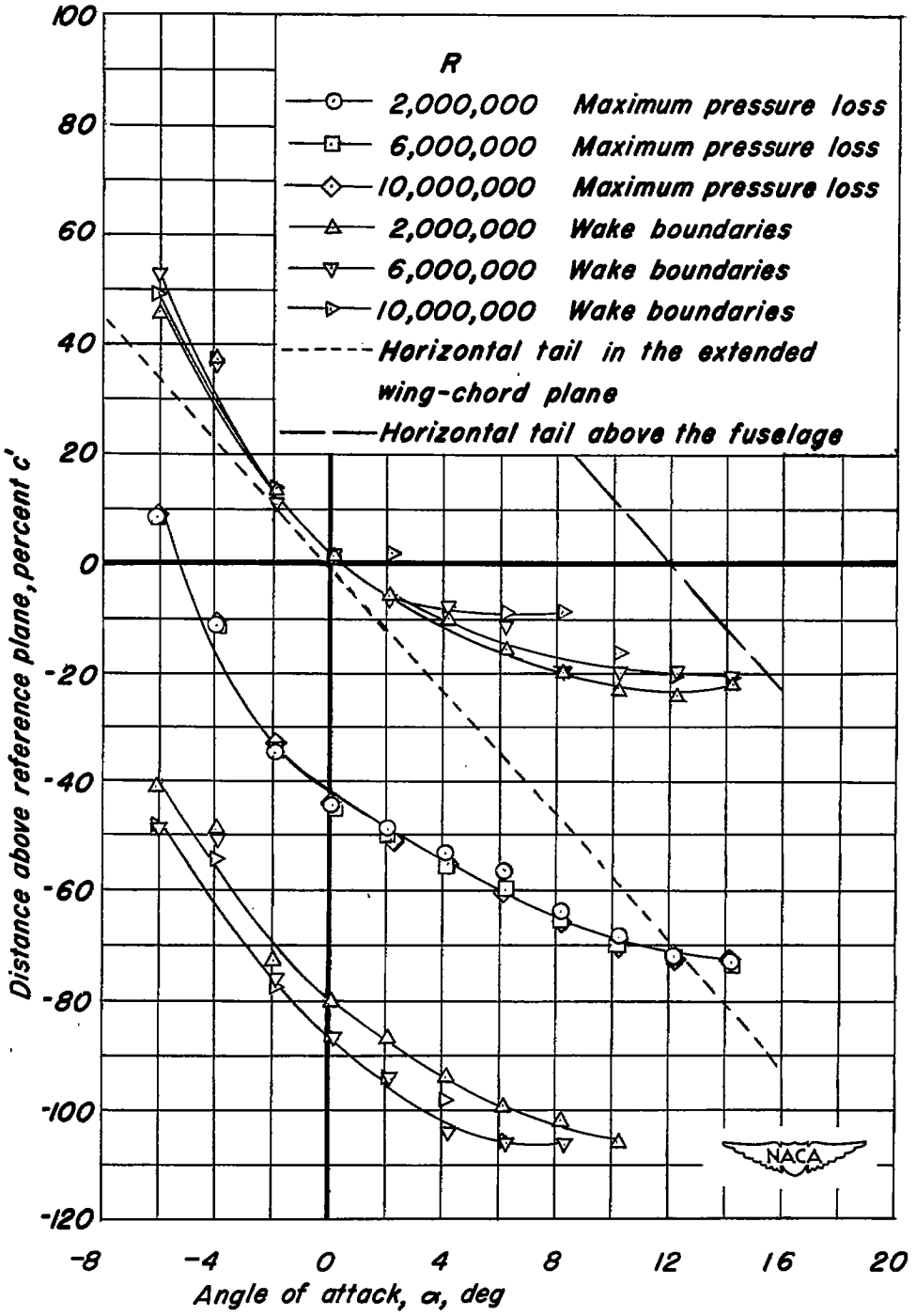

Figure 28.- The variation with angle of attack of the wake-boundary, maximum-pressure-loss locations and horizontal-tail positions with reference to the wing-chord plane at $\alpha = 0°$. Wing and fuselage with the flaps deflected. δ_n, 30°; δ_f, 50°; M, 0.20.

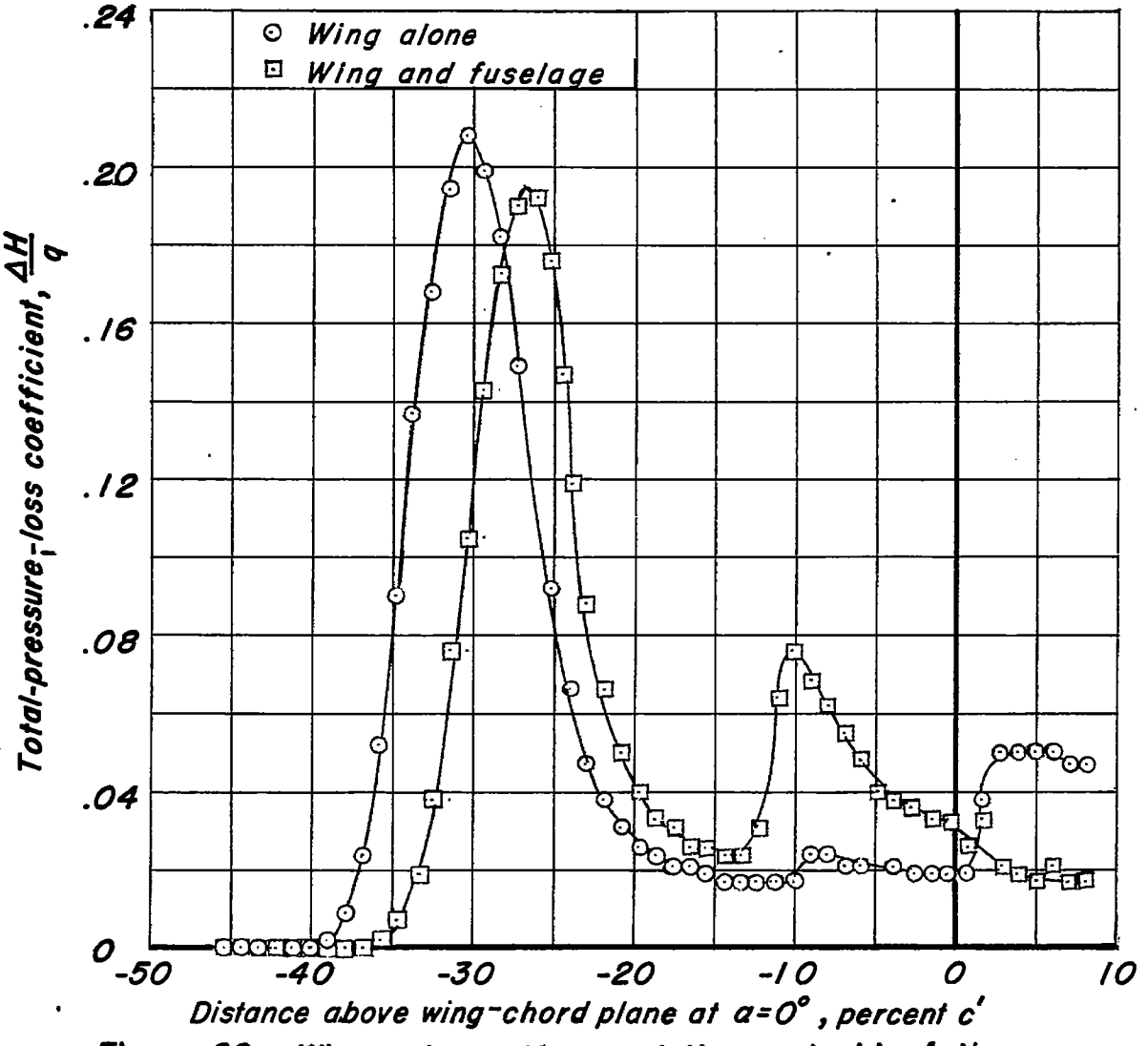

Figure 29.- Wing wake patterns at the centroid of the semitail area. α, 6°; M, 0.85; R, 2,000,000.

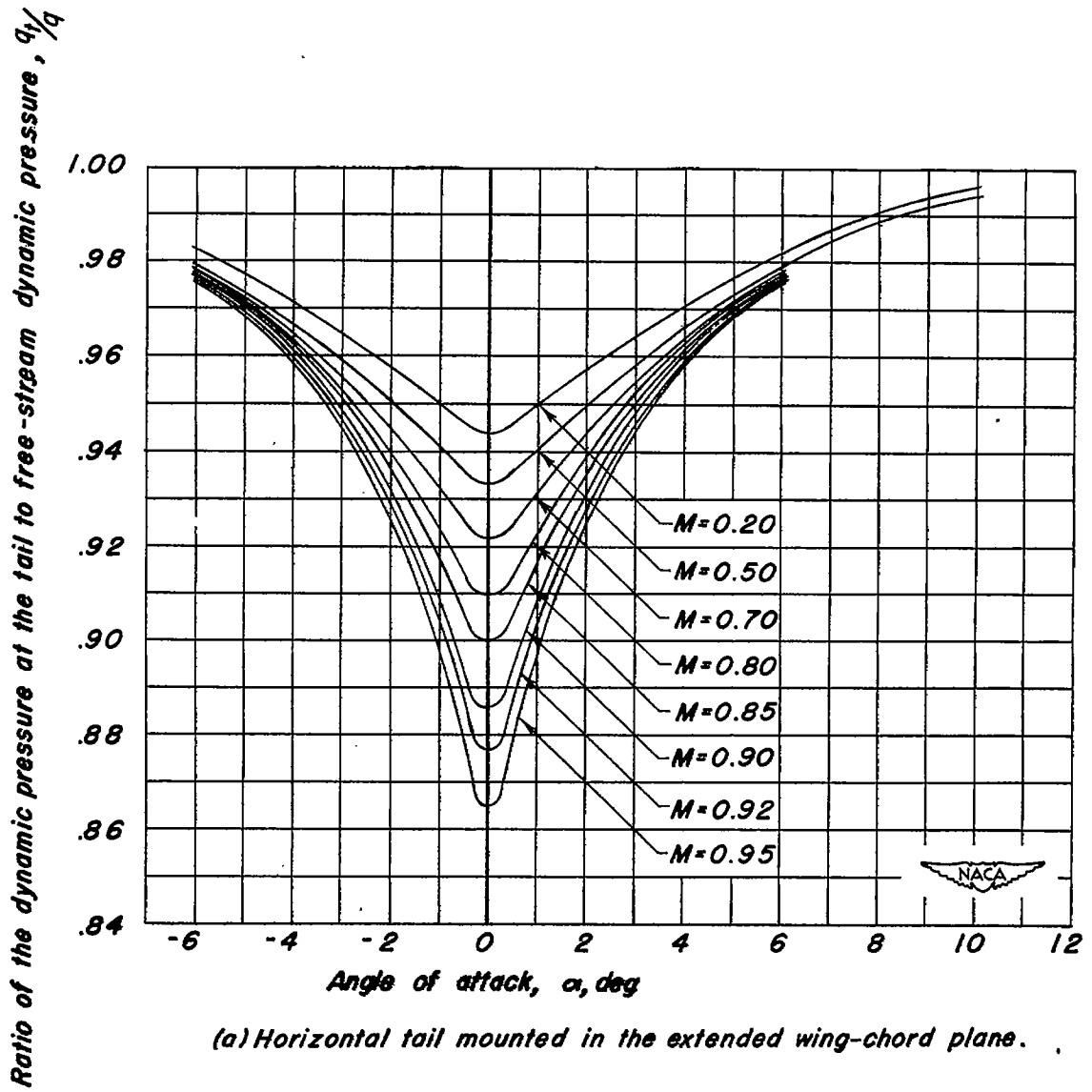

(a) Horizontal tail mounted in the extended wing-chord plane.

Figure 30.- The variation with angle of attack of the ratio of the dynamic pressure at the tail to free-stream dynamic pressure. R, 2,000,000.

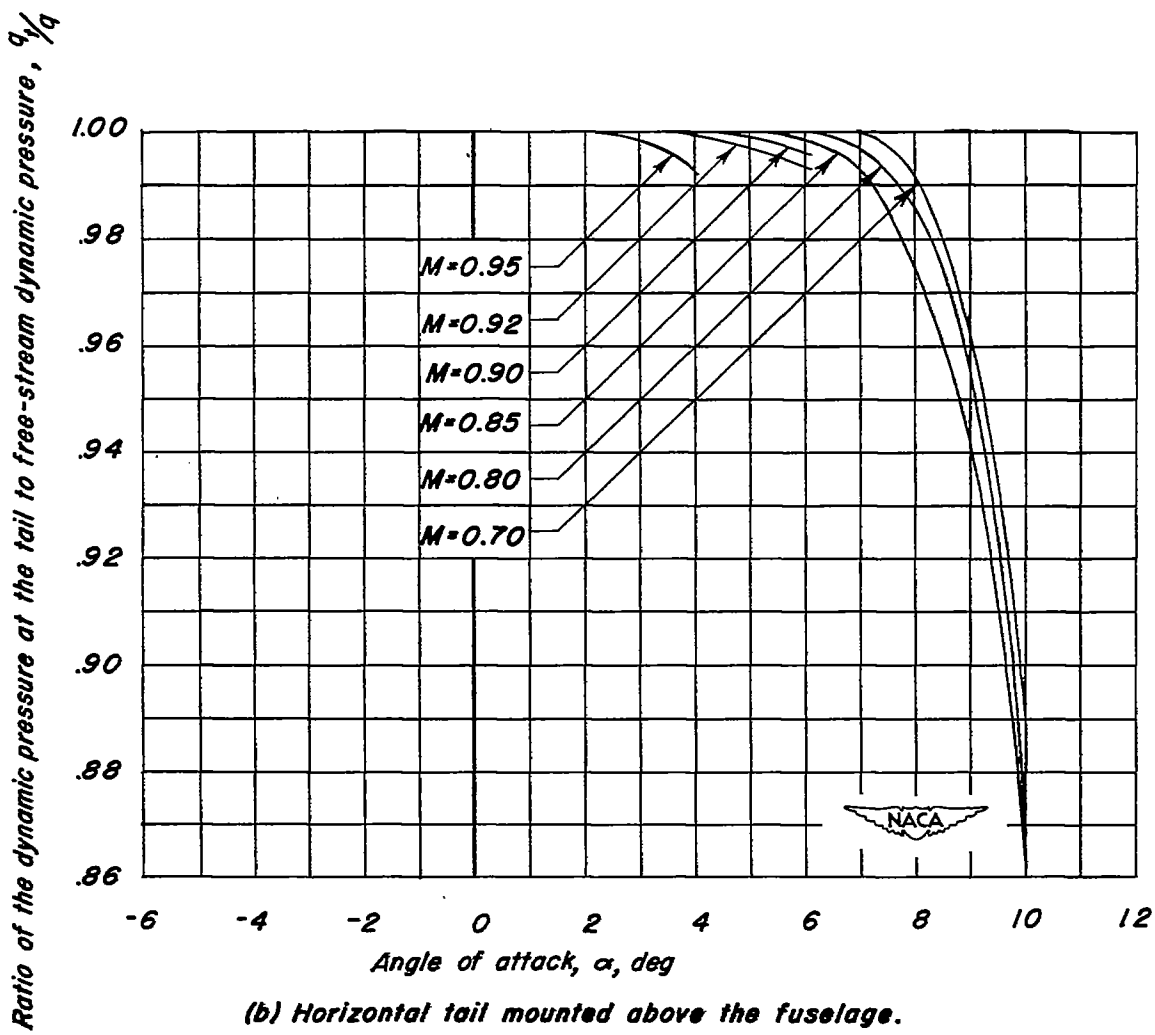

(b) Horizontal tail mounted above the fuselage.

Figure 30.- Concluded.

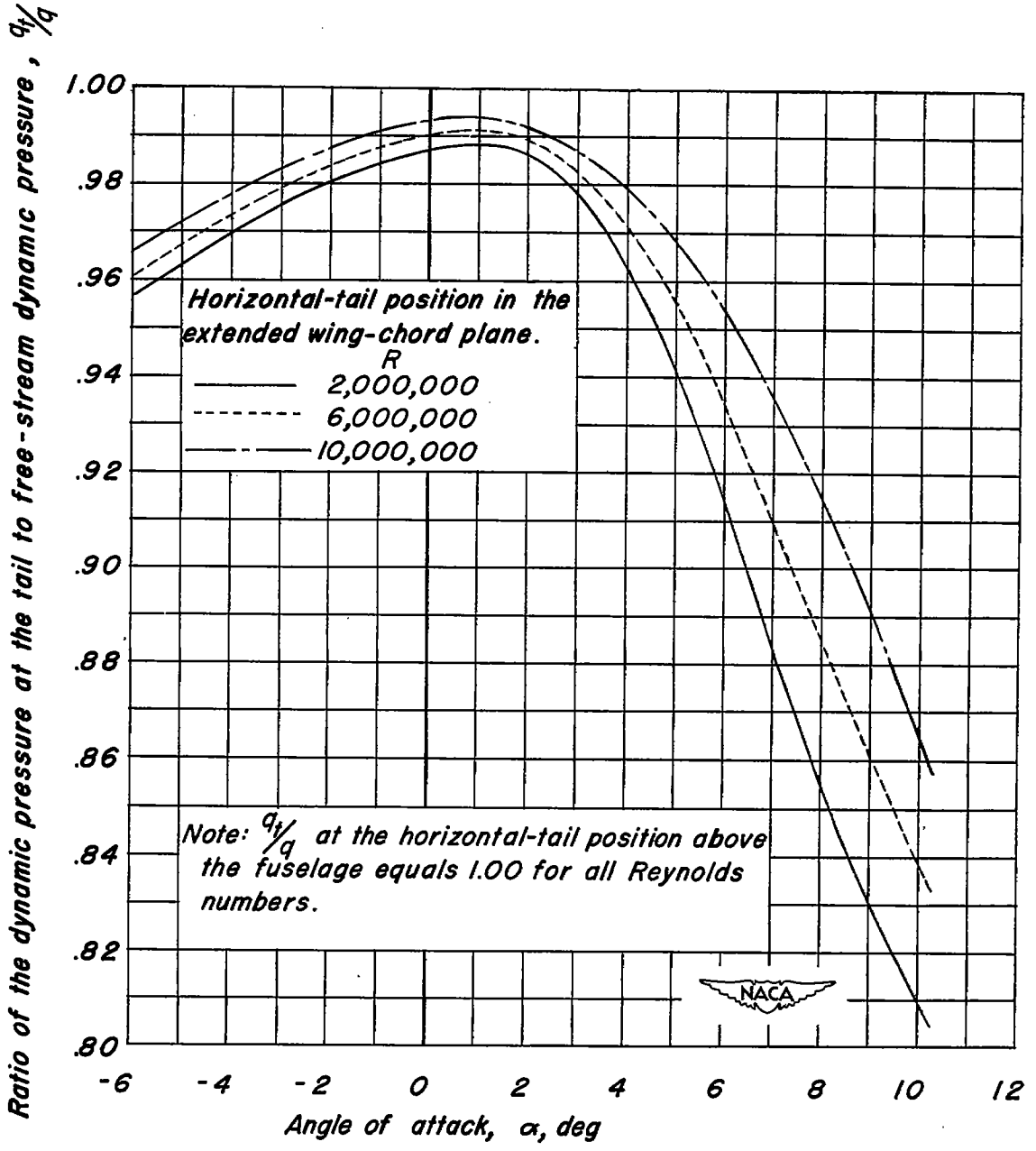

Figure 31 .-The variation with angle of attack of the ratio of the dynamic pressure at the tail to free-stream dynamic pressure. Flaps deflected. δ_n, 30°; δ_f, 50°; M, 0.20.

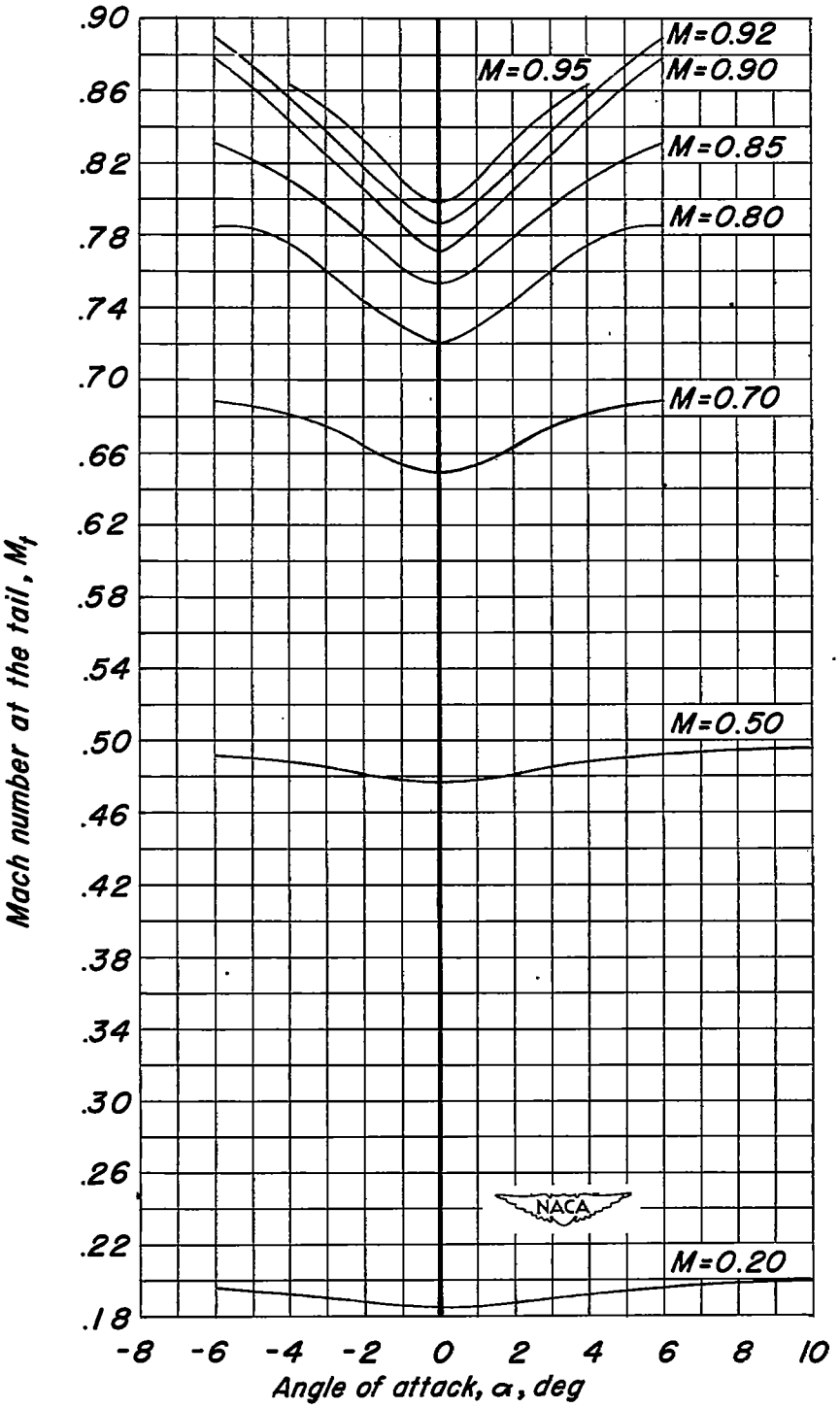

(a) Horizontal tail mounted in the extended wing-chord plane.

Figure 32.- The variation of Mach number at the tail with angle of attack.

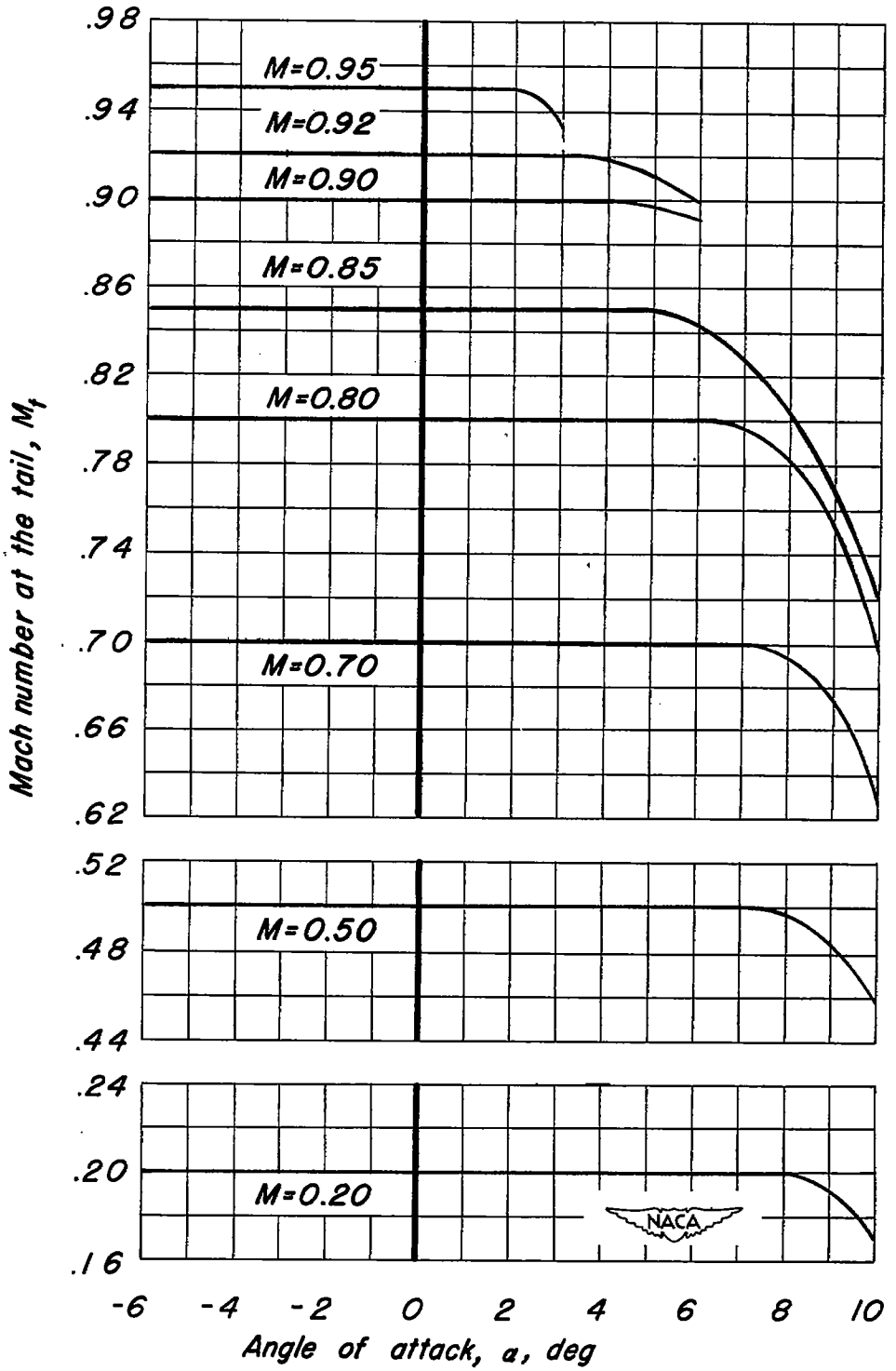

(b) Horizontal tail mounted above the fuselage.

Figure 32.— Concluded.

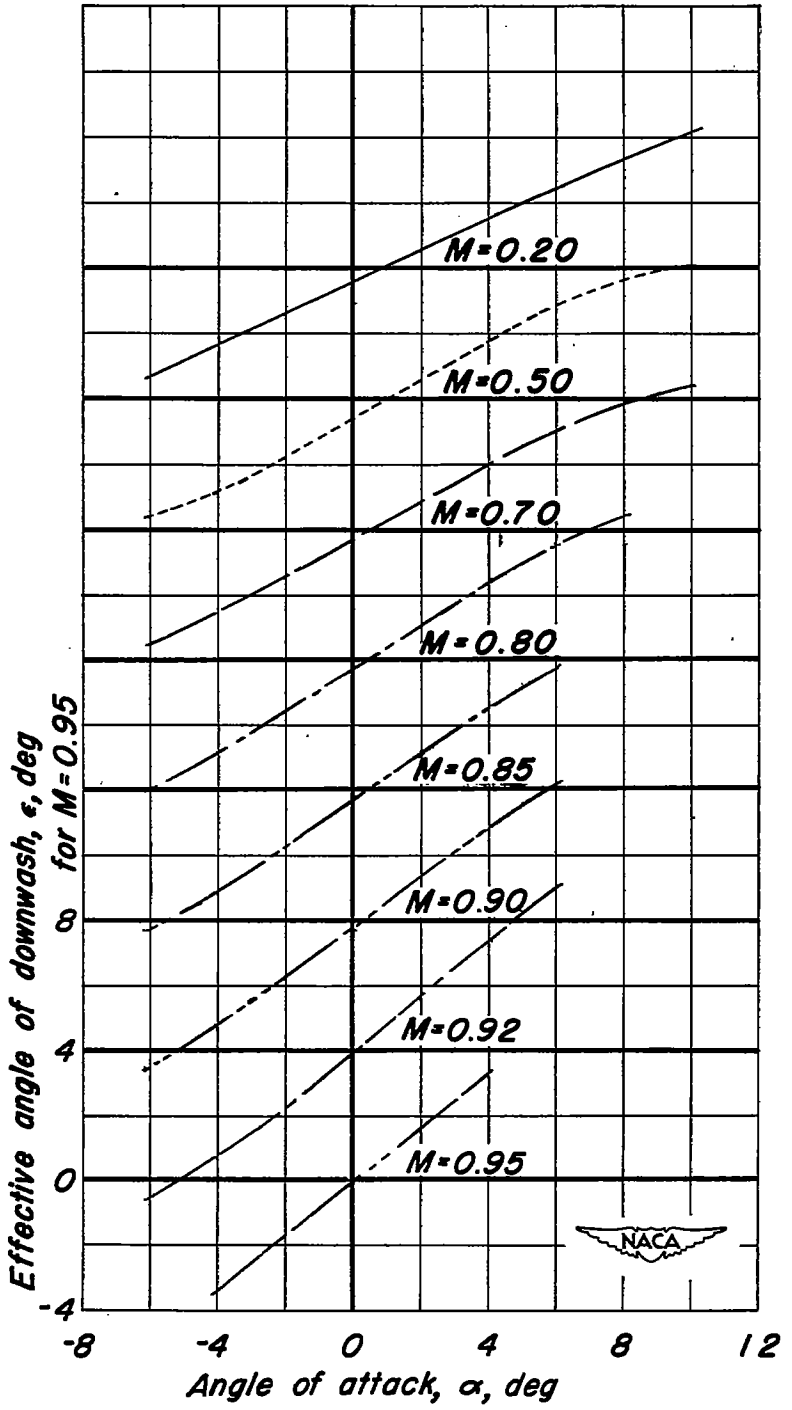

(a) Horizontal tail mounted in the extended wing-chord plane.

Figure 33.— The variation with angle of attack of the effective angle of downwash at a position corresponding to the centroid of the semitail area. R, 2,000,000.

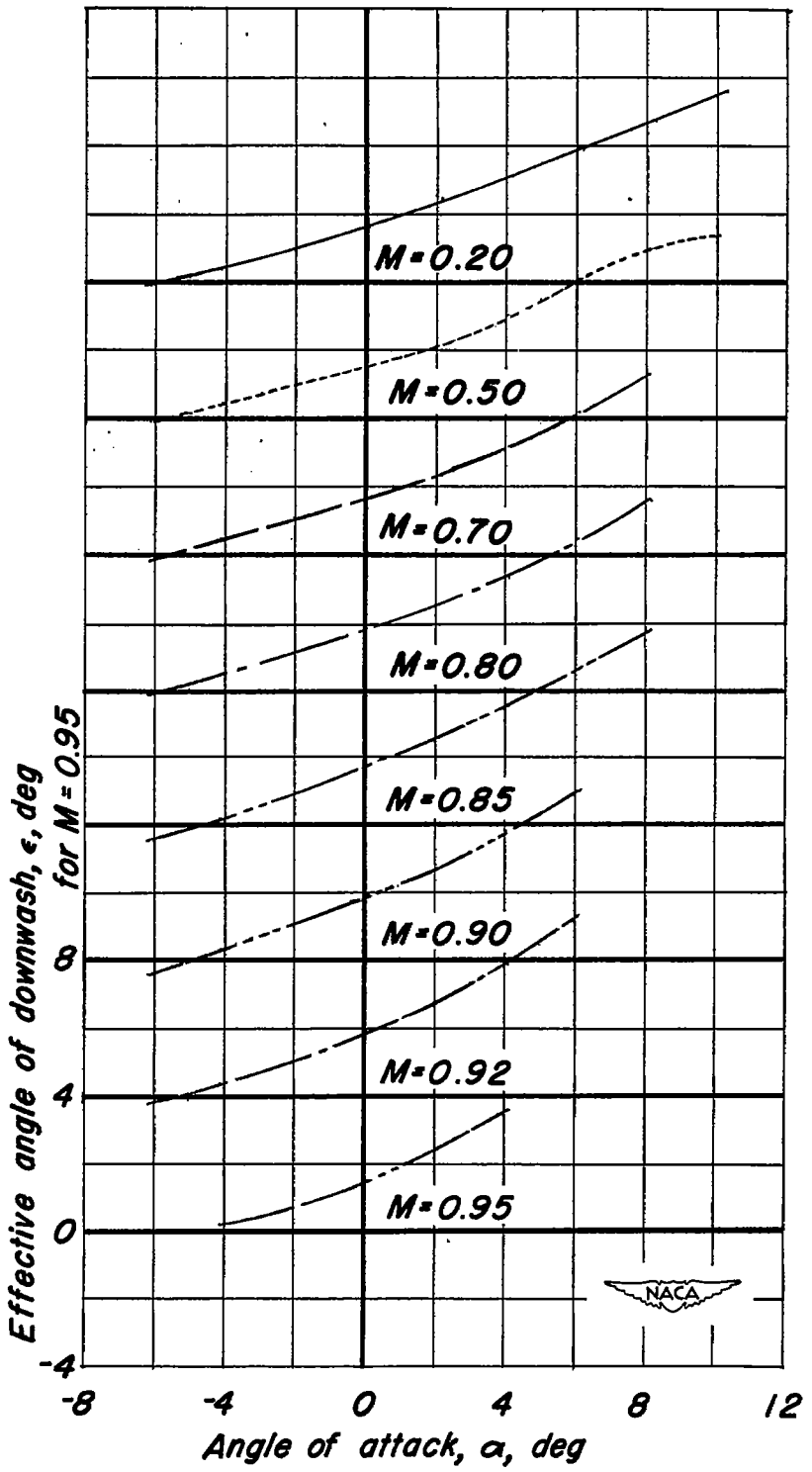

(b) Horizontal tail mounted above the fuselage.

Figure 33.-Concluded.

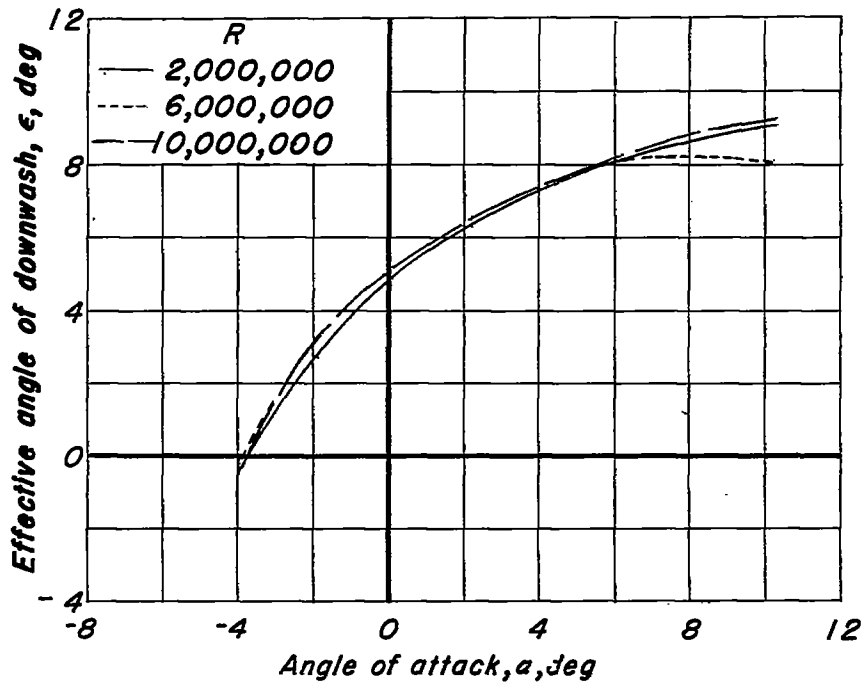

(a) Horizontal tail mounted in the extended wing-chord plane.

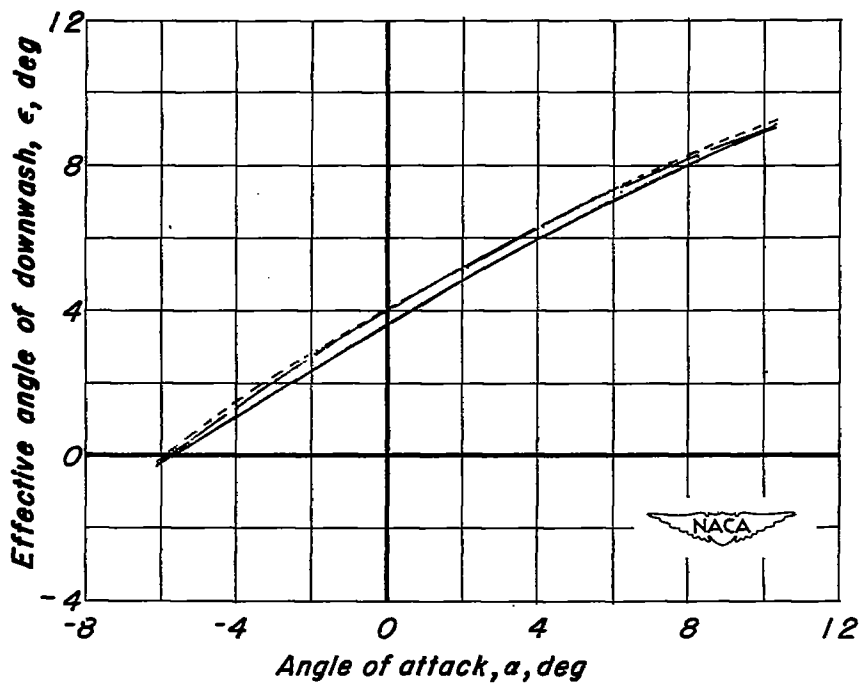

(b) Horizontal tail mounted above the fuselage.

Figure 34.- The variation with angle of attack of the effective angle of downwash at a position corresponding to the centroid of the semitail area. Flaps deflected. δ_n, 30°; δ_f, 50°; M, 0.20.

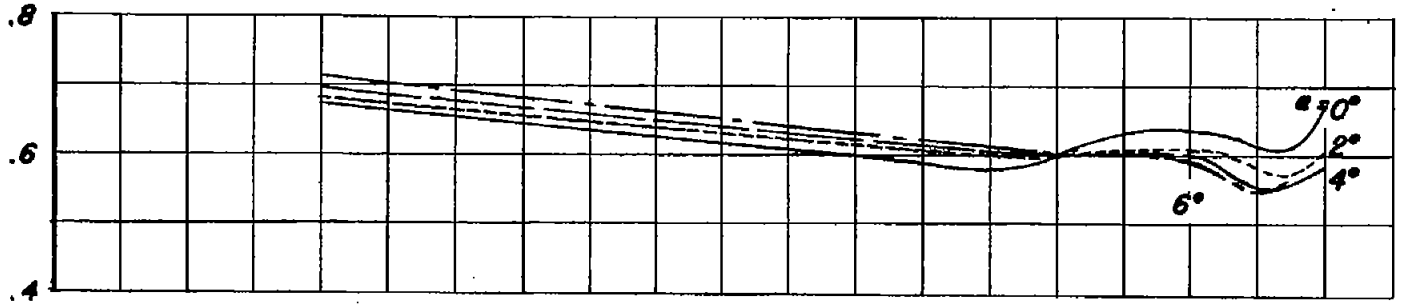

(a) Horizontal tail mounted in the extended wing-chord plane.

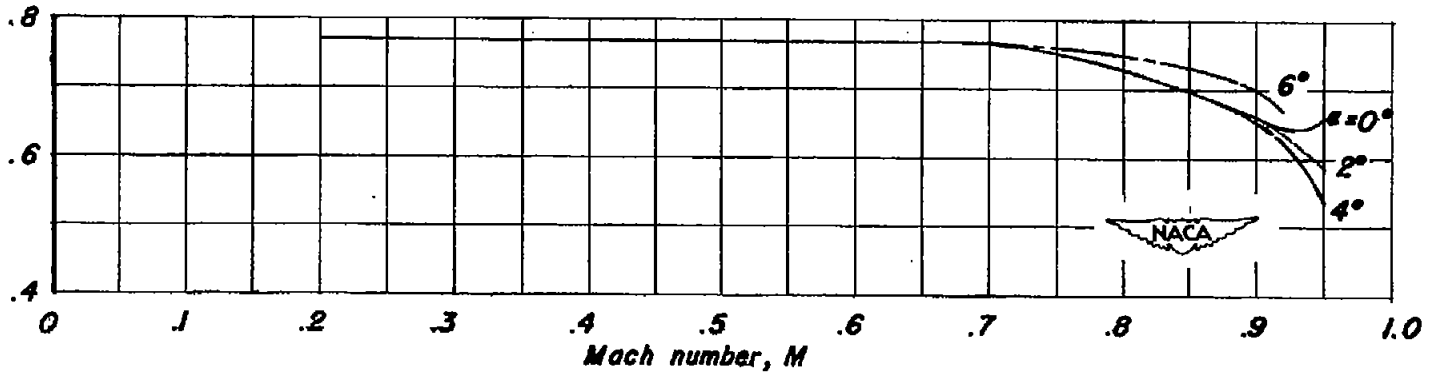

(b) Horizontal tail mounted above fuselage.

Figure 35.- The variation with Mach number of the tail efficiency factor.

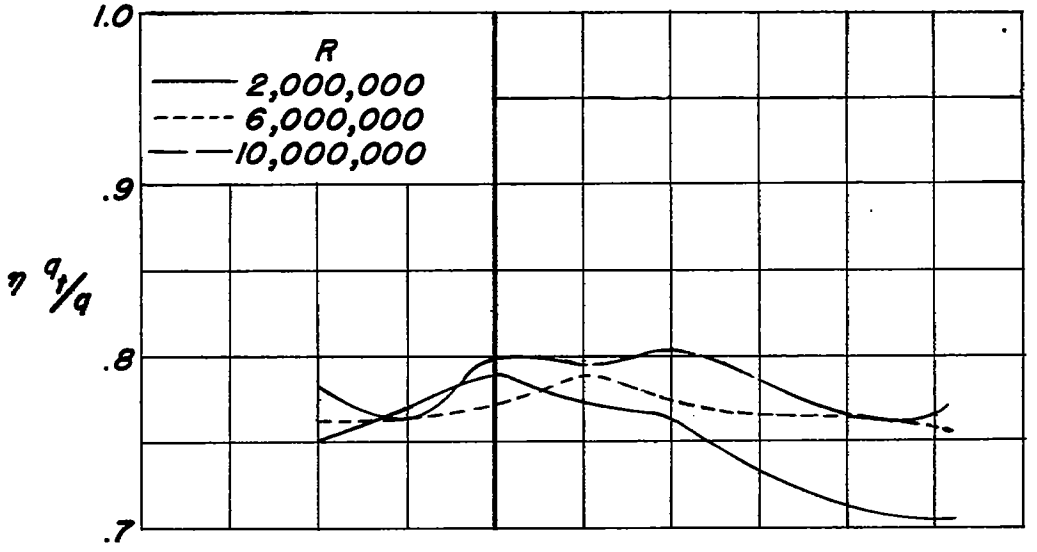

(a) Horizontal tail mounted in the extended wing-chord plane.

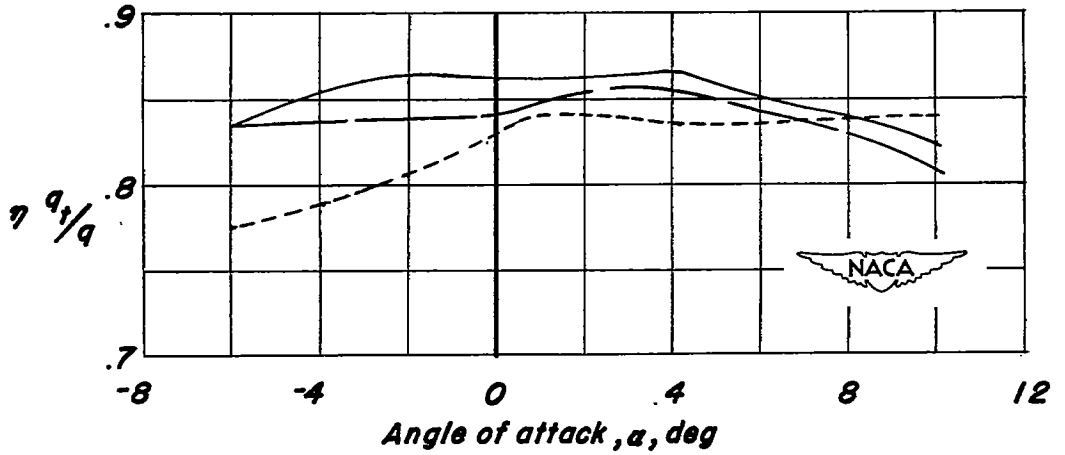

(b) Horizontal tail mounted above the fuselage.

Figure 36.- The variation of the tail efficiency factor with angle of attack. Flaps deflected, δ_n, 30°; δ_f, 50°; M, 0.20.

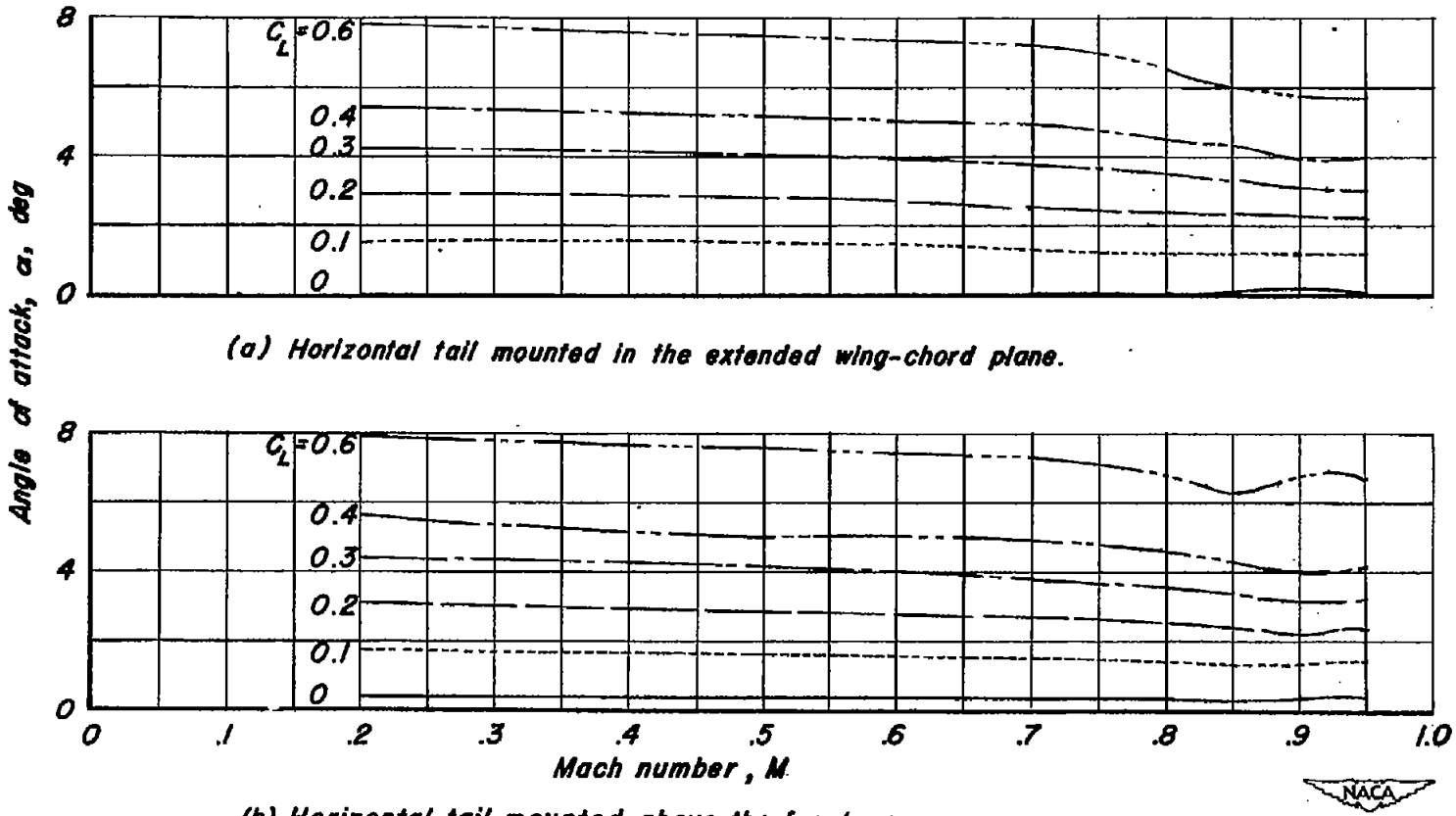

(a) Horizontal tail mounted in the extended wing-chord plane.

(b) Horizontal tail mounted above the fuselage.

Figure 37.— The variation with Mach number of the angle of attack of the airplane model for various lift coefficients. R, 2,000,000; i_t, 0°.

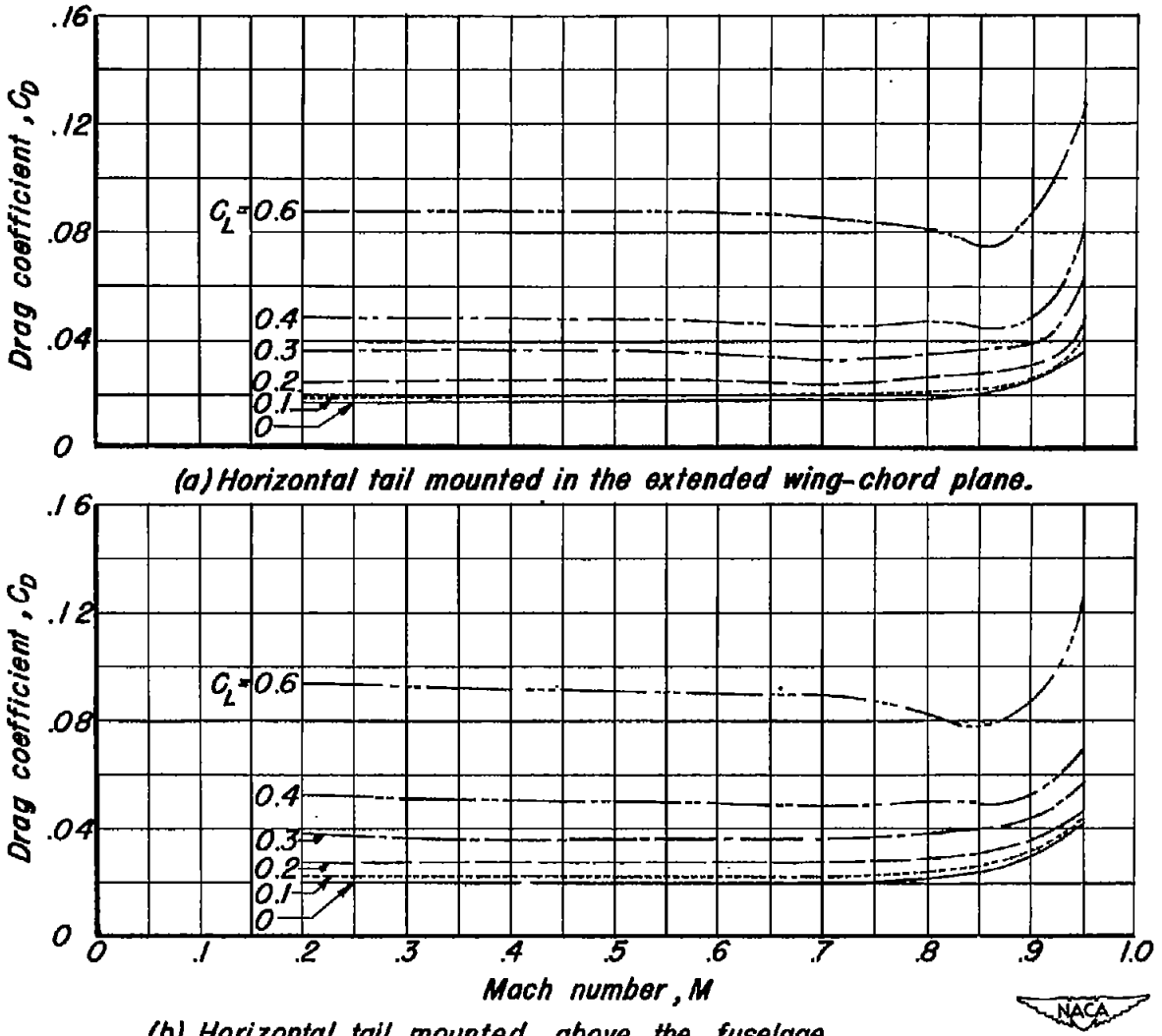

(a) Horizontal tail mounted in the extended wing-chord plane.

(b) Horizontal tail mounted above the fuselage.

Figure 38.- The variation with Mach number of the drag coefficient of the airplane model for various lift coefficients. R, 2,000,000; i_t, 0°.

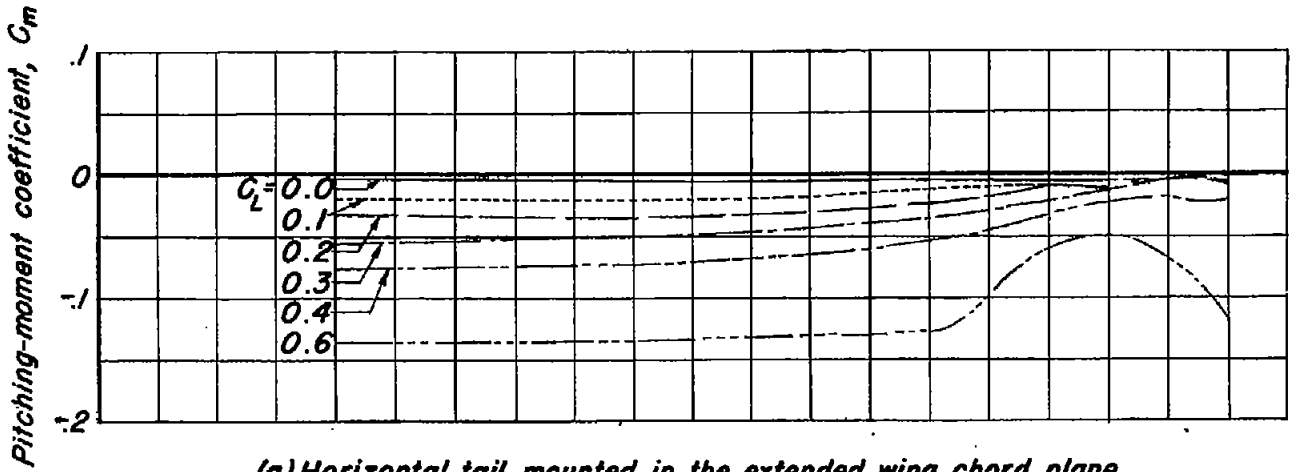

(a) Horizontal tail mounted in the extended wing-chord plane.

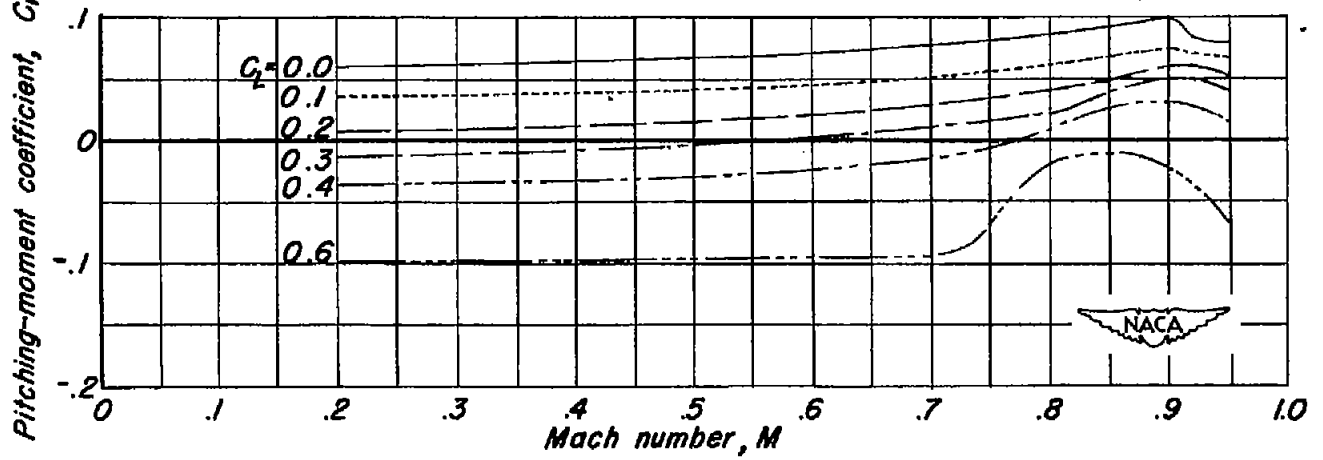

(b) Horizontal tail mounted above the fuselage.

Figure 39 .- The variation with Mach number of the pitching-moment coefficient of the airplane model for various lift coefficients. R, 2,000,000; i_t, 0°.

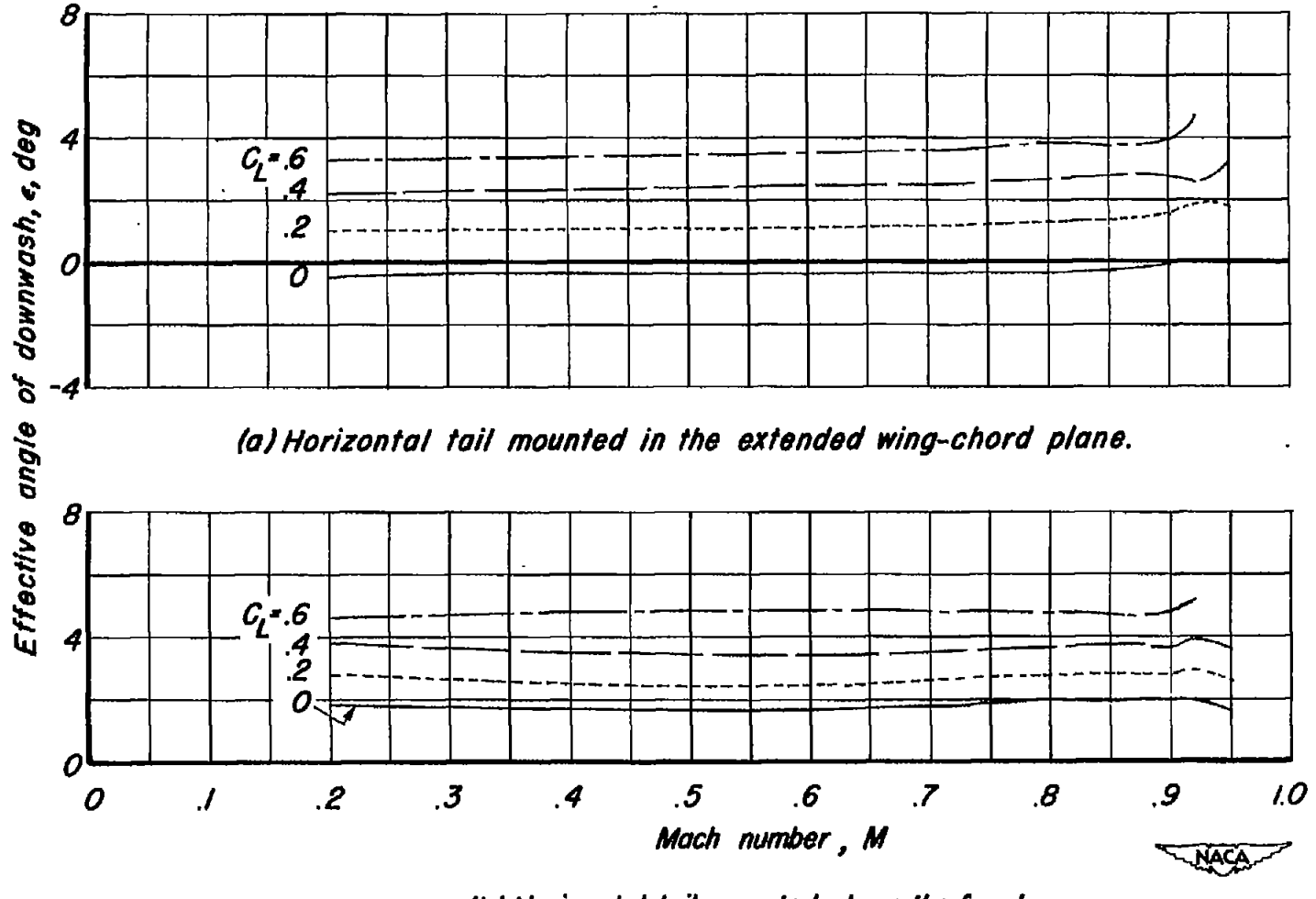

(a) Horizontal tail mounted in the extended wing-chord plane.

(b) Horizontal tail mounted above the fuselage.

Figure 40.- The variation with Mach number of the effective angle of downwash at a position corresponding to the centroid of the semitail area for various lift coefficients. R, 2,000,000.

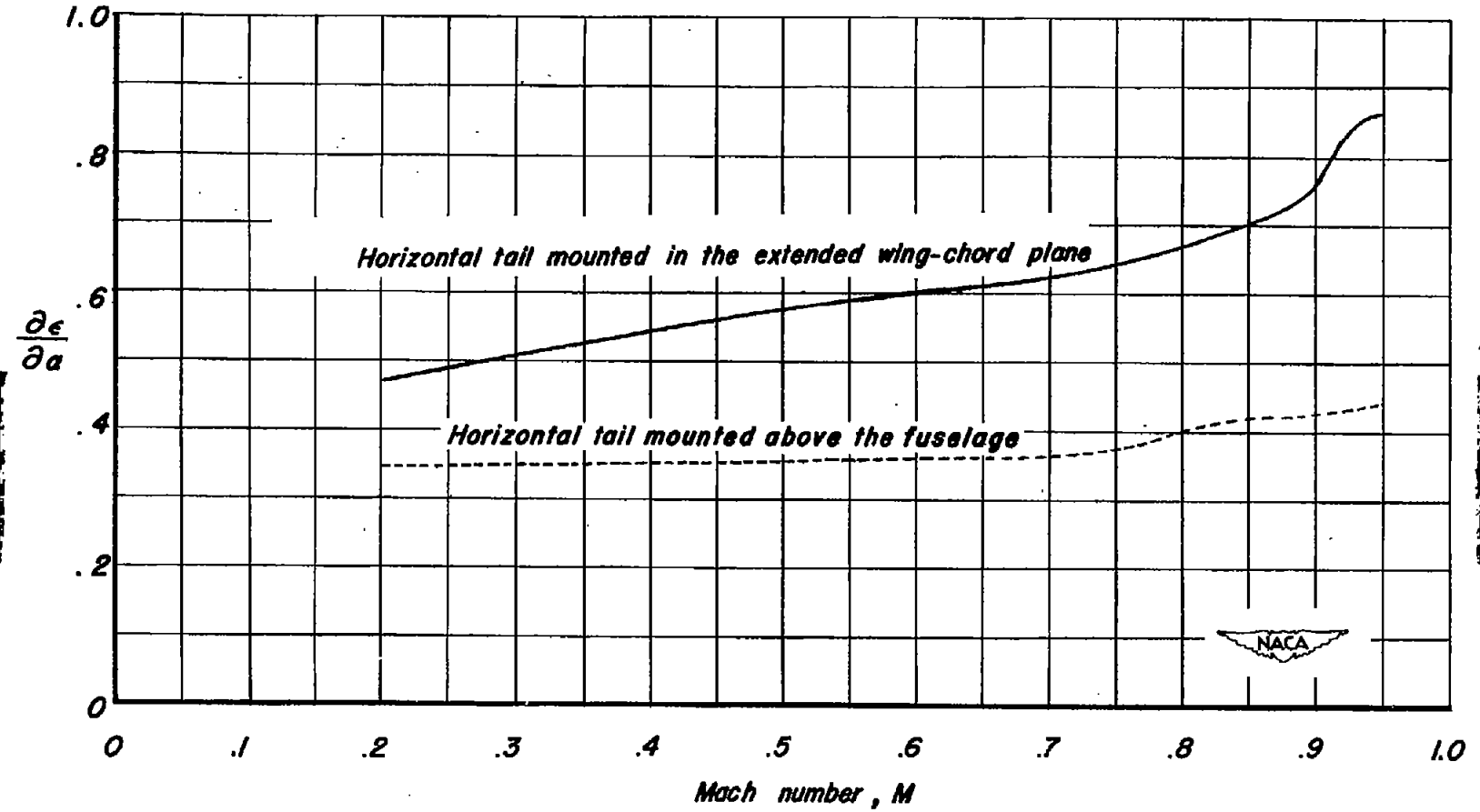

Figure 41.— The variation with Mach number of the rate of change of the effective angle of downwash with angle of attack. R, 2,000,000.

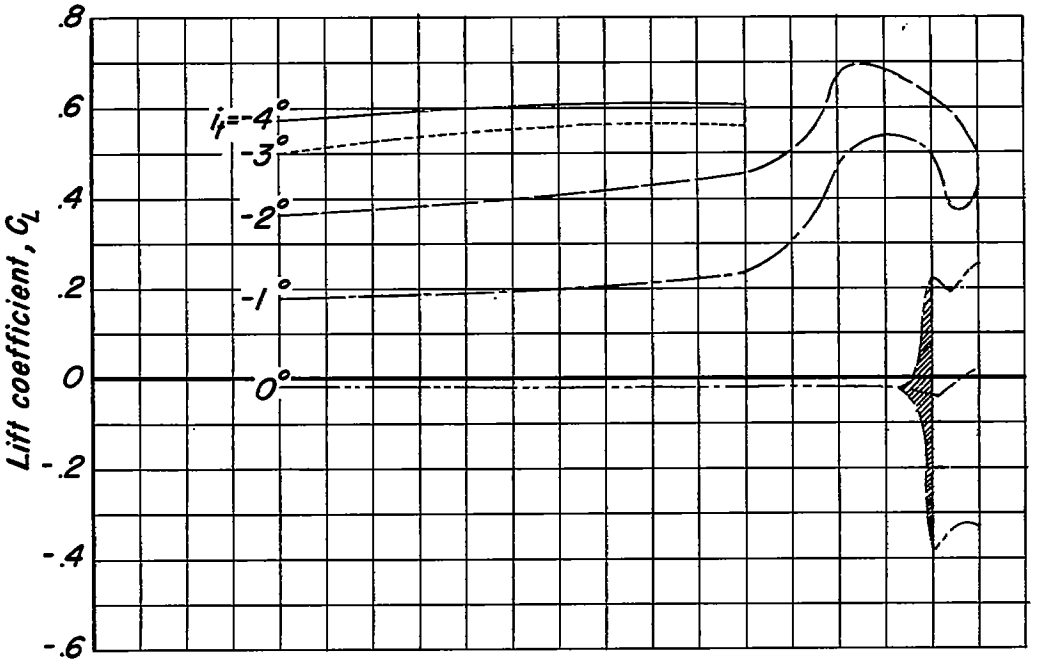

(a) Horizontal tail mounted in the extended wing-chord plane.

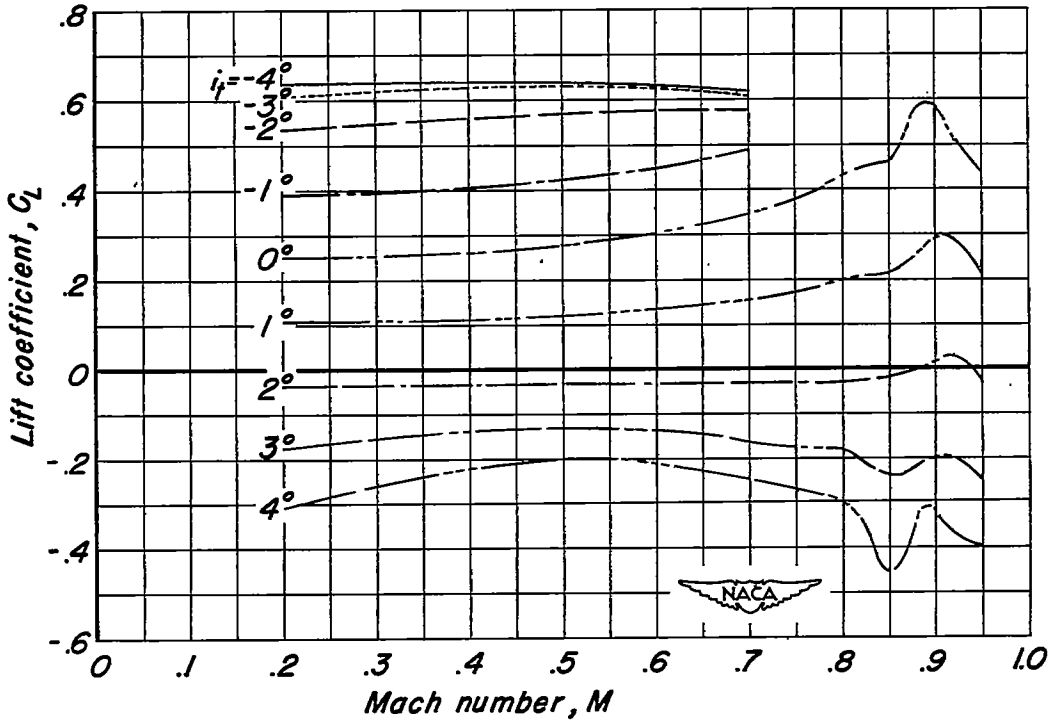

(b) Horizontal tail mounted above the fuselage.

Figure 42.— The variation of the lift coefficient for C_m=0 with Mach number. R, 2,000,000.

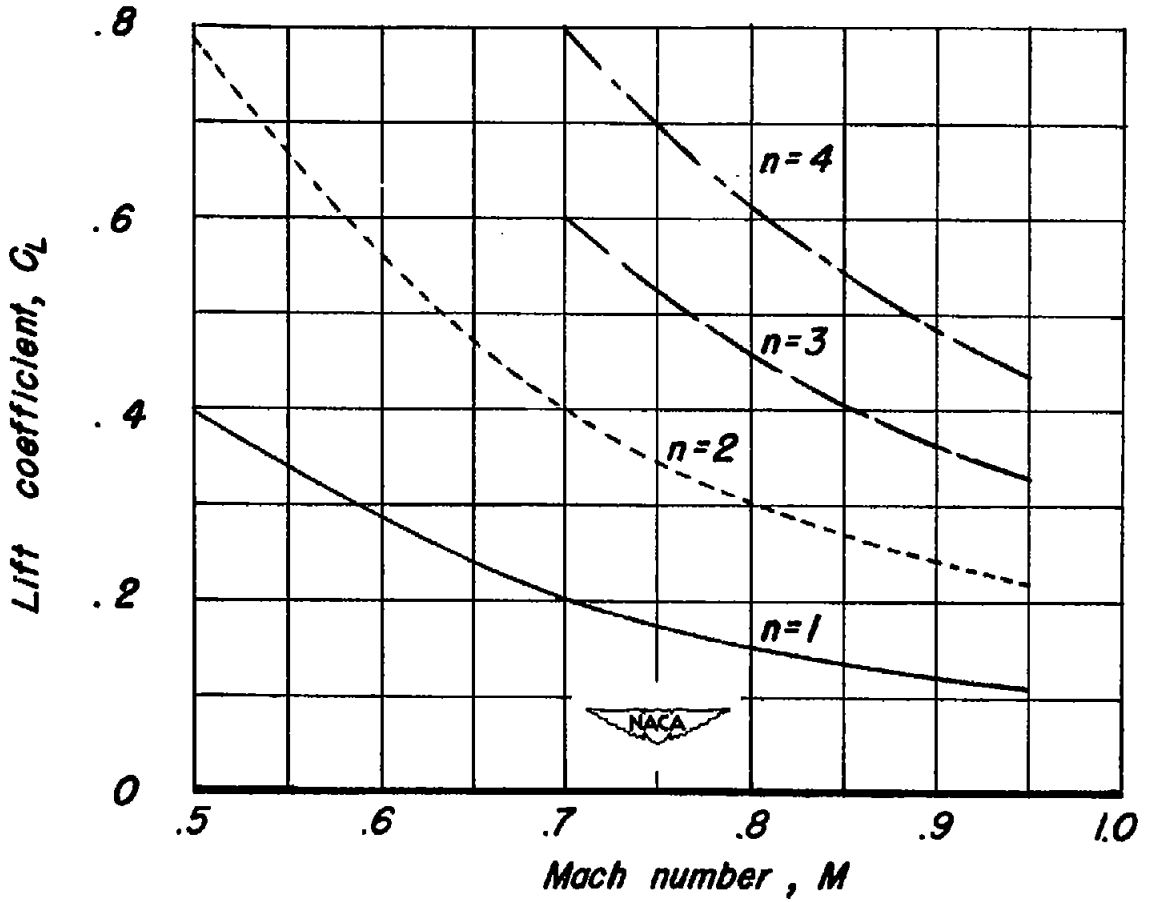

Figure 43.- The lift coefficient required for an airplane with a wing loading of 100 pounds per square foot in flight at an altitude of 10,000 feet.

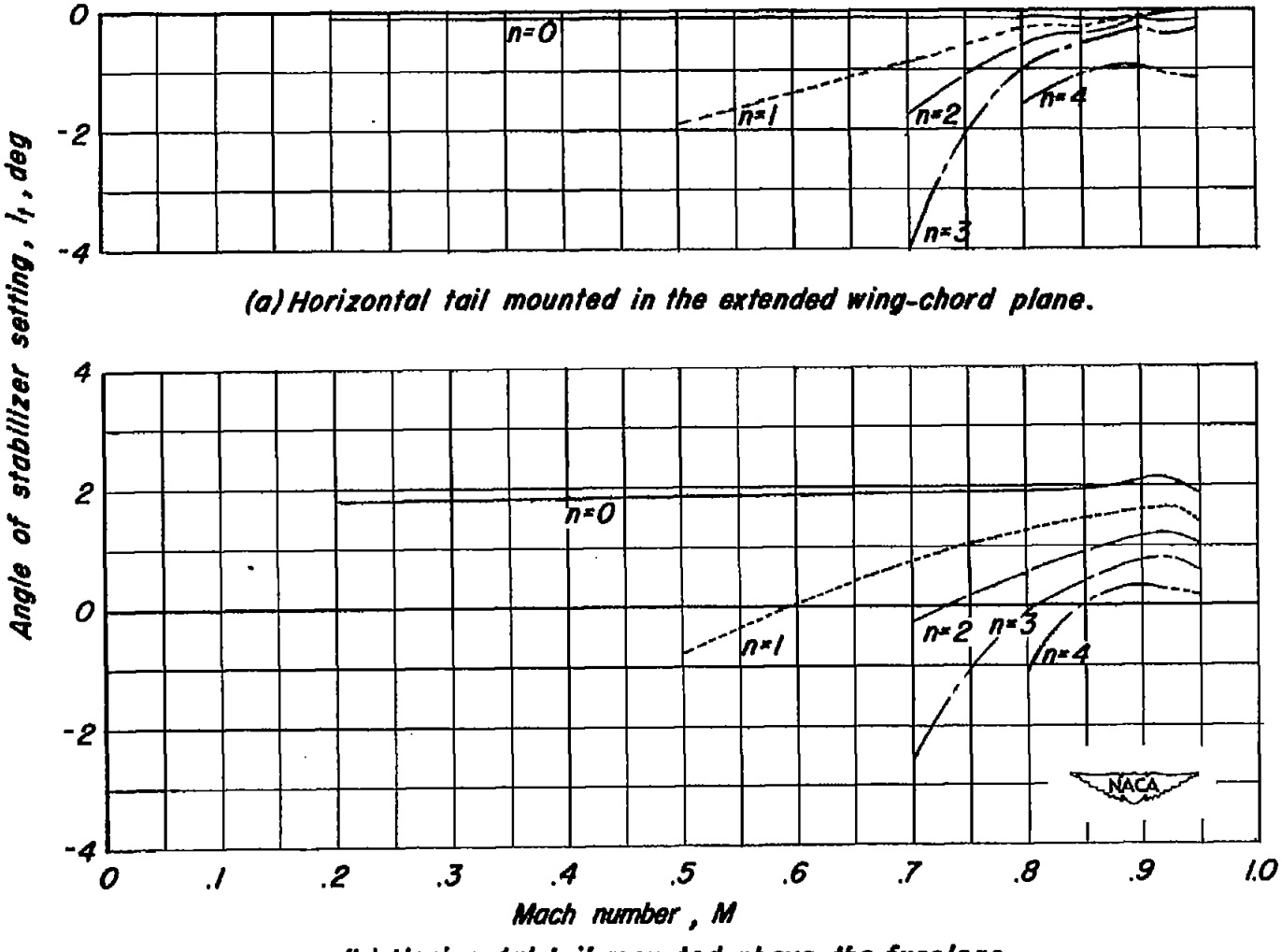

Figure 44.- Variation with Mach number of the angle of stabilizer setting to balance an airplane in flight at 10,000 feet. Wing loading 100 pounds per square foot. Center of gravity at 0.25c'.

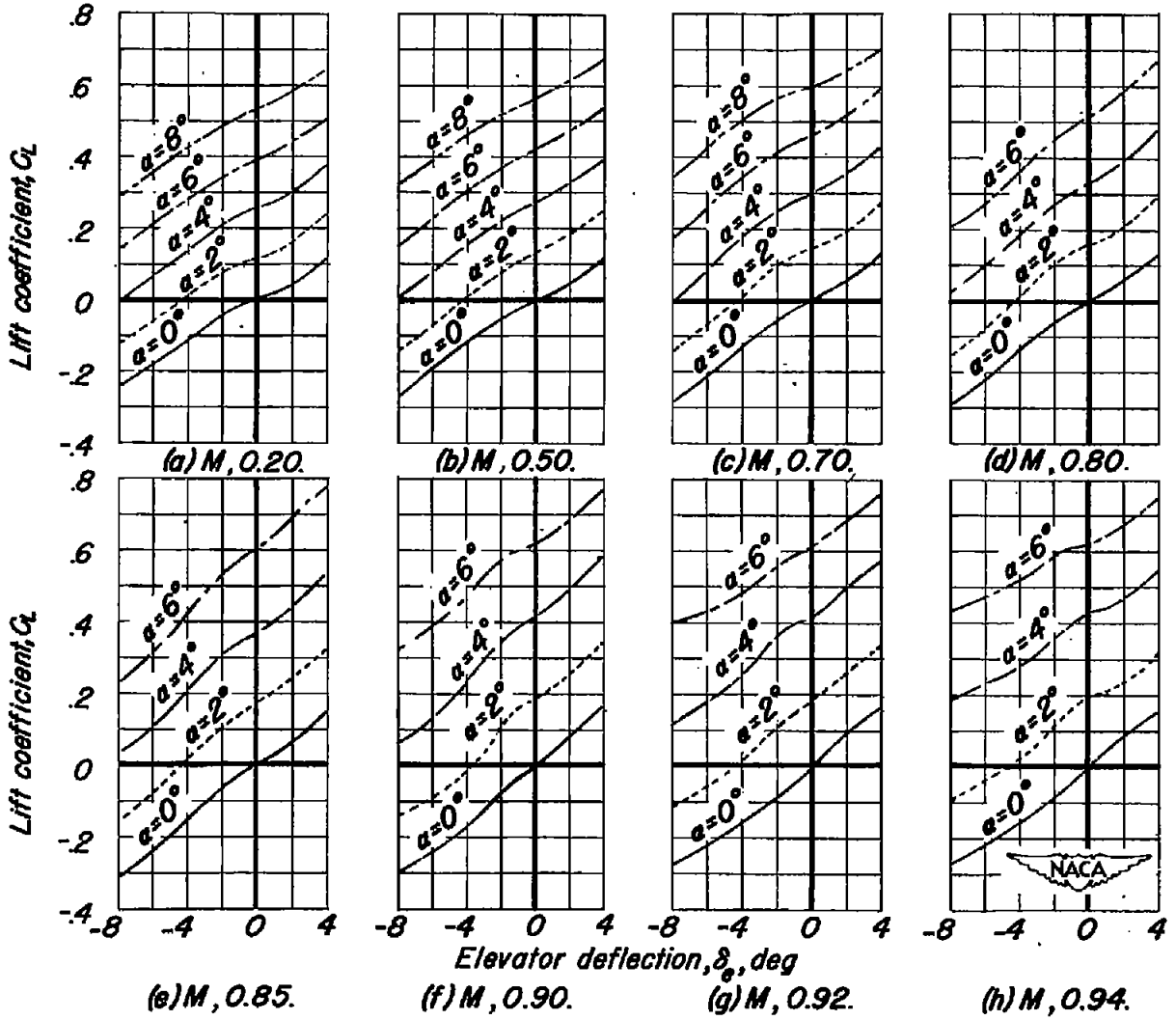

Figure 45.- The lift characteristics of the isolated tail with a 20-percent-area constant-chord elevator. R, 2,000,000.

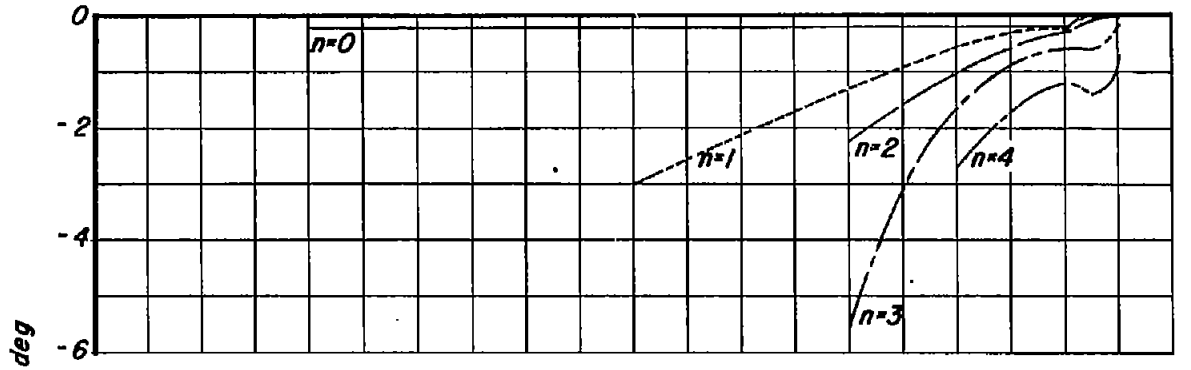

(a) Horizontal tail mounted in the extended wing-chord plane. i_t, 0°.

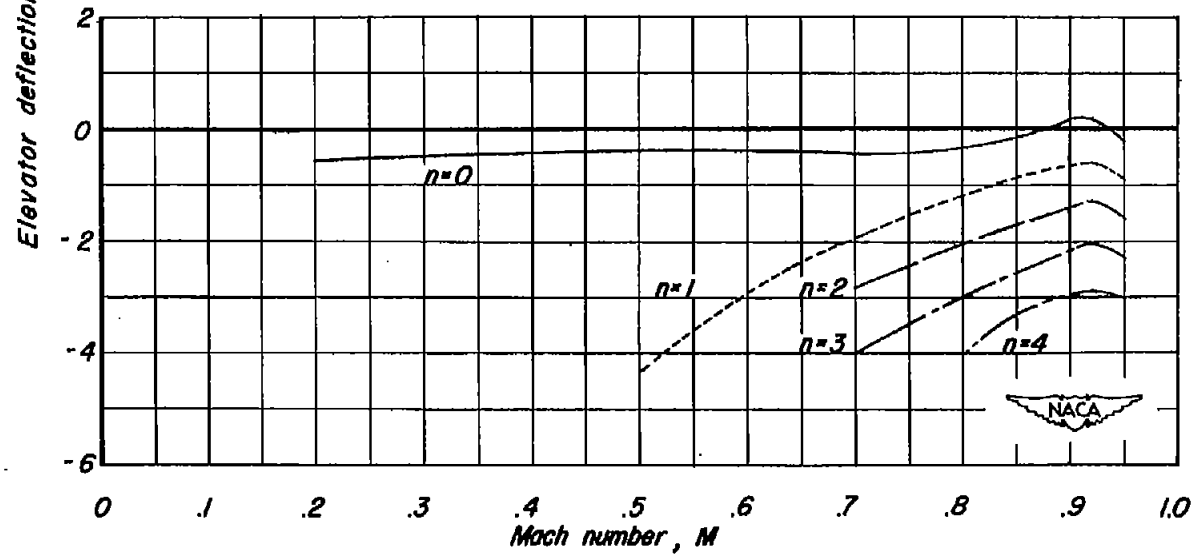

(b) Horizontal tail mounted above the fuselage. i_t, 2°.

Figure 46.- Variation with Mach number of the elevator deflection to balance an airplane in flight at 10,000 feet. Wing loading 100 pounds per square foot. Center of gravity at 0.25 c'.

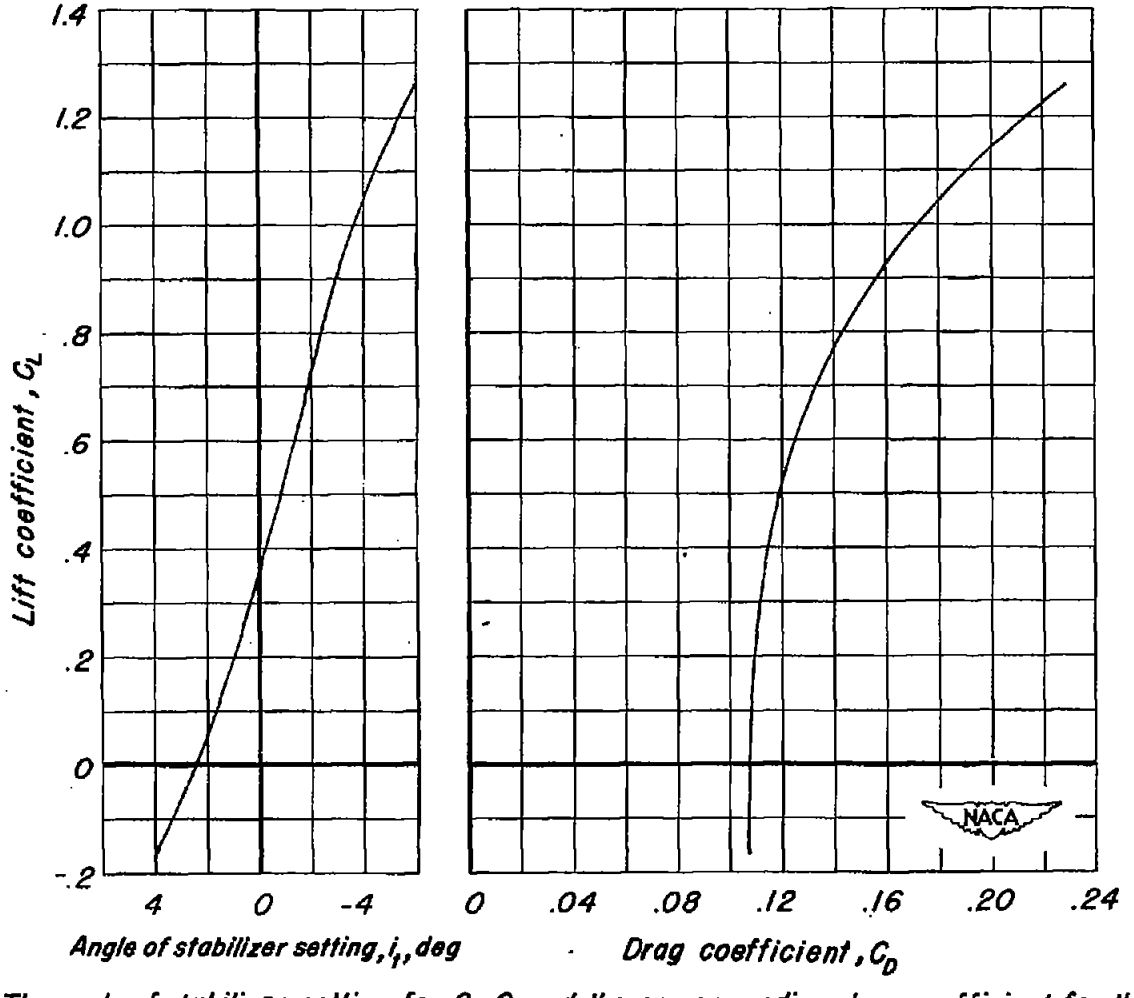

Figure 47.- The angle of stabilizer setting for $C_m = 0$ and the corresponding drag coefficient for the airplane model with the horizontal tail mounted in the extended wing-chord plane and the flaps deflected. δ_n, 30°; δ_f, 50°; M, 0.20.

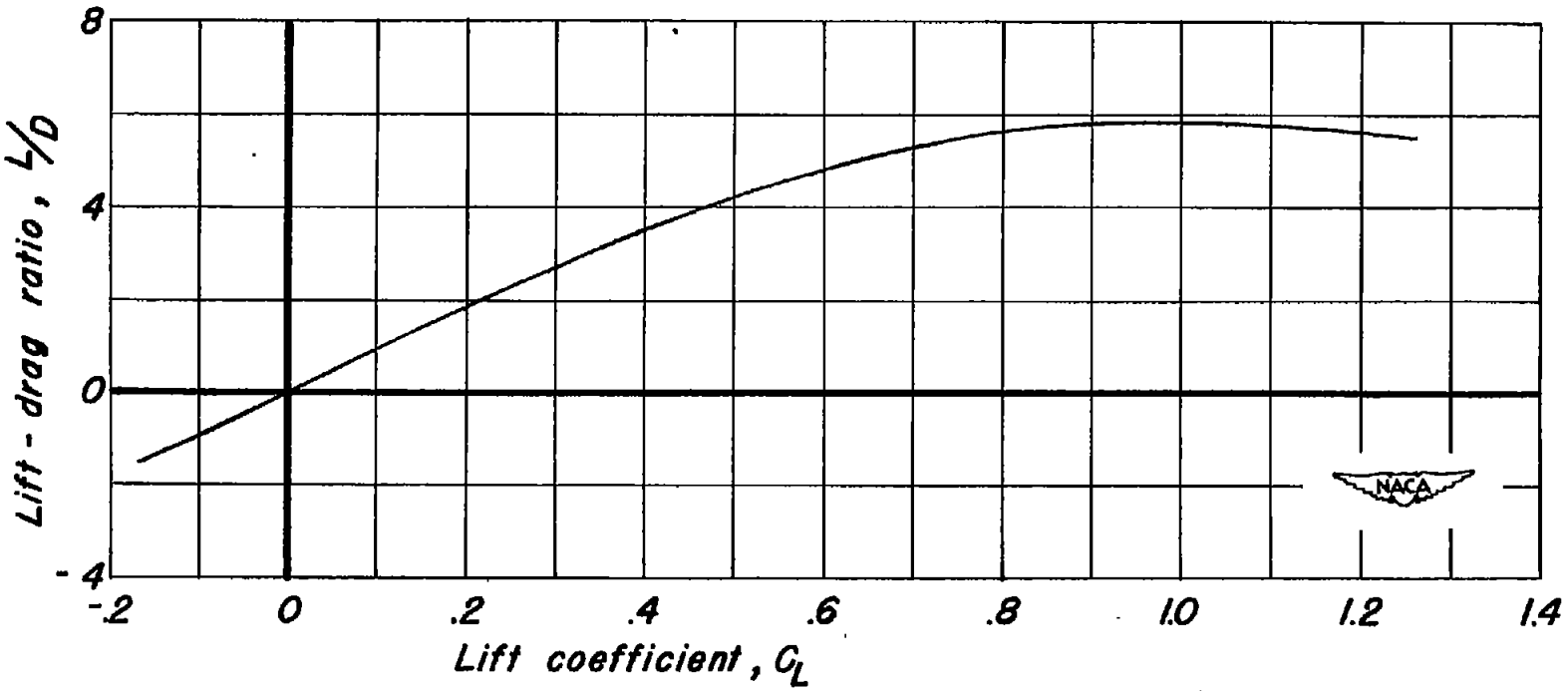

Figure 48.— The lift-drag ratio of the airplane model with the horizontal tail mounted in the extended wing-chord plane. δ_n, 30°; δ_f, 50°; C_m, 0 ; M, 0.20.

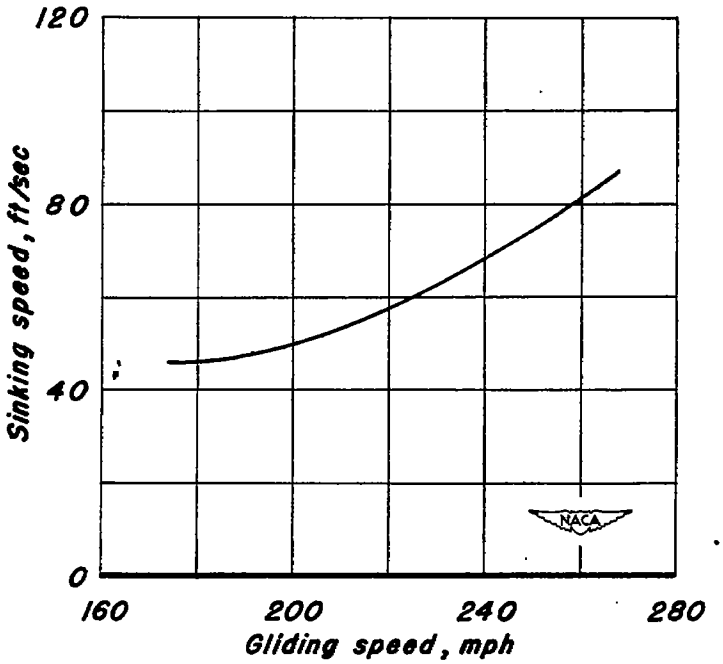

Figure 49.- Variation with gliding speed of the sinking speed of an airplane in power-off flight at sea level. Wing loading 100 pounds per square foot. Center of gravity at 0.25c'.

NACA-Langley - 12-8-49 - 375